

Constraining the Passive to Active Margin Tectonics of the Internal Central Apennines: Insights from Biostratigraphy, Structural, and Seismic Analysis

Original

Constraining the Passive to Active Margin Tectonics of the Internal Central Apennines: Insights from Biostratigraphy, Structural, and Seismic Analysis / Luca Cardello, Giovanni; Vico, Giuseppe; Consorti, Lorenzo; Sabbatino, Monia; Carminati, Eugenio; Doglioni, Carlo. - In: GEOSCIENCES. - ISSN 2076-3263. - ELETTRONICO. - 11:4(2021), pp. 1-50. [10.3390/geosciences11040160]

Availability:

This version is available at: 11583/2937474 since: 2021-11-12T18:33:26Z

Publisher:

MDPI

Published

DOI:10.3390/geosciences11040160

Terms of use:

This article is made available under terms and conditions as specified in the corresponding bibliographic description in the repository

Publisher copyright

(Article begins on next page)

Article

Constraining the Passive to Active Margin Tectonics of the Internal Central Apennines: Insights from Biostratigraphy, Structural, and Seismic Analysis

Giovanni Luca Cardello ^{1,2,*} , Giuseppe Vico ³, Lorenzo Consorti ^{4,5}, Monia Sabbatino ⁶ , Eugenio Carminati ¹ and Carlo Doglioni ^{1,7} 

¹ Department of Earth Sciences, Sapienza University of Rome, 00185 Rome, Italy; eugenio.carminati@uniroma1.it (E.C.); carlo.doglioni@uniroma1.it (C.D.)

² Department of Chemistry and Pharmacy, University of Sassari, 07100 Sassari, Italy

³ Department of Land, Environmental and Infrastructure Engineering (DIATI), Polytechnic of Turin, 10129 Turin, Italy; giuseppe.vico@polito.it

⁴ Department of Mathematics and Geosciences, University of Trieste, 34128 Trieste, Italy; lorenzo.consorti@isprambiente.it

⁵ Geological Survey of Italy (ISPRA), 00144 Rome, Italy

⁶ Department of Earth, Environmental and Resources Sciences (DISTAR), Federico II University of Naples, 80126 Naples, Italy; monia.sabbatino@unina.it

⁷ Istituto Nazionale di Geofisica e Vulcanologia, 00143 Rome, Italy

* Correspondence: glcardello@uniroma1.it



Citation: Cardello, G.L.; Vico, G.; Consorti, L.; Sabbatino, M.; Carminati, E.; Doglioni, C. Constraining the Passive to Active Margin Tectonics of the Internal Central Apennines: Insights from Biostratigraphy, Structural, and Seismic Analysis. *Geosciences* **2021**, *11*, 160. <https://doi.org/10.3390/geosciences11040160>

Academic Editors: Domenico Liotta, Giancarlo Molli and Angelo Cipriani

Received: 1 February 2021

Accepted: 28 March 2021

Published: 1 April 2021

Publisher's Note: MDPI stays neutral with regard to jurisdictional claims in published maps and institutional affiliations.



Copyright: © 2021 by the authors. Licensee MDPI, Basel, Switzerland. This article is an open access article distributed under the terms and conditions of the Creative Commons Attribution (CC BY) license (<https://creativecommons.org/licenses/by/4.0/>).

Abstract: The polyphase structural evolution of a sector of the internal Central Apennines, where the significance of pelagic deposits atop neritic carbonate platform and active margin sediments has been long debated, is here documented. The results of a new geological survey in the Volsci Range, supported by new stratigraphic constraints from the syn-orogenic deposits, are integrated with the analysis of 2D seismic reflection lines and available wells in the adjacent Latin Valley. Late Cretaceous syn-sedimentary faults are documented and interpreted as steps linking a carbonate platform to the adjacent pelagic basin, located to the west. During Tortonian time, the pelagic deposits were squeezed off and juxtaposed as mélangé units on top of the carbonate platform. Subsurface data highlighted stacked thrust sheets that were first involved into an initial in-sequence propagation with top-to-the-ENE, synchronous to late Tortonian foredeep to wedge-top sedimentation. We distinguish up to four groups of thrust faults that occurred during in-sequence shortening (thrusts 1–3; about 55–60 km) and backthrusting (thrust 4). During Pliocene to recent times, the area has been uplifted and subsequently extended by normal faults cross-cutting the accretionary wedge. Beside regional interest, our findings bear implications on the kinematic evolution of an orogenic wedge affected by far-traveled units.

Keywords: Central Apennines; passive margin inversion; mélangé; pelagic deposits; thrust sheets; backthrust; cretaceous; Miocene; nannoplankton

1. Introduction

Carbonate platforms are a type of passive margin sedimentary succession that can be commonly involved in the thrust-sheet imbrication of an orogenic wedge [1–3]. During in-sequence ongoing deformation, the wedge propagates by incorporating new portions of the foreland, which is commonly made up of crystalline basement, clastic and/or carbonatic successions, and overriding foredeep/foreland clastics with variable thickness and composition [4–6]. The so formed fold-and-thrust belt, incorporating distinctive tectono-stratigraphic units, is the combined product of inherited syn-sedimentary structures and orogenic dynamics [7,8]. Thus, the wedge-related deformation style may strongly depend on the stratigraphic architecture and in particular on the presence and depth of décollement

layers within the stratigraphic successions (i.e., salt [9]). In this sense, thick-skinned deformation (see, e.g., in [10]) can dominate when there is no suitable detachment horizon. On the contrary, when preferred slip-levels occur, thin-skinned tectonics develop, generating flat-ramp-flat geometries and disharmonic folding, which, for example, can occur within base-of-slope to pelagic successions [11,12]. At the transition between such structural domains, strain localization can occur, nucleating thrusts by inverting previous listric boundary extensional faults (see, e.g., in [13]).

During inversion of hyperextended passive margins, orogenesis forms far-traveled units that can reach a high-degree of internal deformation [14–16]. The chaotic structure of these so-formed *mélange* units is the result of the superposition of tectonic, sedimentary, and mud-diapiric processes [17], to which gravitative processes add, by incorporating both allochthonous and autochthonous blocks [18]. Despite the subsequent orogenic deformation overprint, occurring within far-traveled thrust-sheets, the structural heritage may be preserved and studied (see, e.g., in [19–22]).

The Apennines are a fold-and-thrust belt involving basinal and platform-derived thrust sheets and *mélange* units (Figure 1) that offer well-outcropping structures representative of inverted hyperextended passive margins. The present-day deep structure of the Apennines has been a long matter of debate, as the amount of thrust allochthony and the involvement of the crystalline basement are widely discussed (see, e.g., in [23–29]). In this frame, the recognition of inherited structures also bears implications on the reconstructions of the pre- to syn-orogenic evolution [30–33]. For the Central Apennines, timing of deformation and shortening rates through time were reconstructed by coupling kinematic reconstructions with dating of the deposits overlying the forebulge unconformity [34] or, more classically, by dating the siliciclastic syn-orogenic deposits of the foredeep and wedge-top basins by using biostratigraphy (see, e.g., in [35–38]). However, controversial age interpretations may be derived due to the occurrence of few index fossils or reworked specimens from cannibalized foredeep and wedge-top deposits (see, e.g., in [34–39]). Recently, thermo-chronological studies have provided absolute dating of calcite and fault-gouge that have supported the reconstruction of regional thrust evolution [40–43].

Considering that the central Apennines represent an orogen that involves large volumes of the Adriatic plate, identification and description of the most internal thrust sheets are fundamental to highlight the role of inherited structures in determining the dynamics of far-traveled thrusting. In particular, one of the most crucial problems is deciphering the degree of distance covered by the units after detachment within foreland, foredeep, and wedge-top basins during shortening. In this paper, we provide (i) a review of the existing literature of the Volsci Range (VR; Figure 1) and of the adjacent Latin Valley; (ii) a comprehensive stratigraphic and structural analysis based on new age determinations of the syn-orogenic deposits; and (iii) a reinterpretation of a composite dataset of public well data and seismic lines, integrated by unpublished data provided by Pentex Italia Limited. We recognize a polyphase structural evolution based on the documentation of the characteristic *mélange* structures in the Chaotic complex and the distinction of foreland-directed thrusts cross-cut by younger hinterland-directed reverse faults. As a brand-new outcome, the reconstruction of the pre-orogenic heritage and the syn-orogenic Miocene structures allows us to constrain a previously unpublished regional inversion tectonic process and its peculiar evolution of thrusting. In this frame, the internal Central Apennines represent an example of the kinematic evolution of platform and basin-derived thrust sheets. Our study can help unravel the evolution of similar belts worldwide, and more specifically contributes to the understanding of far-traveled thrust sheets.

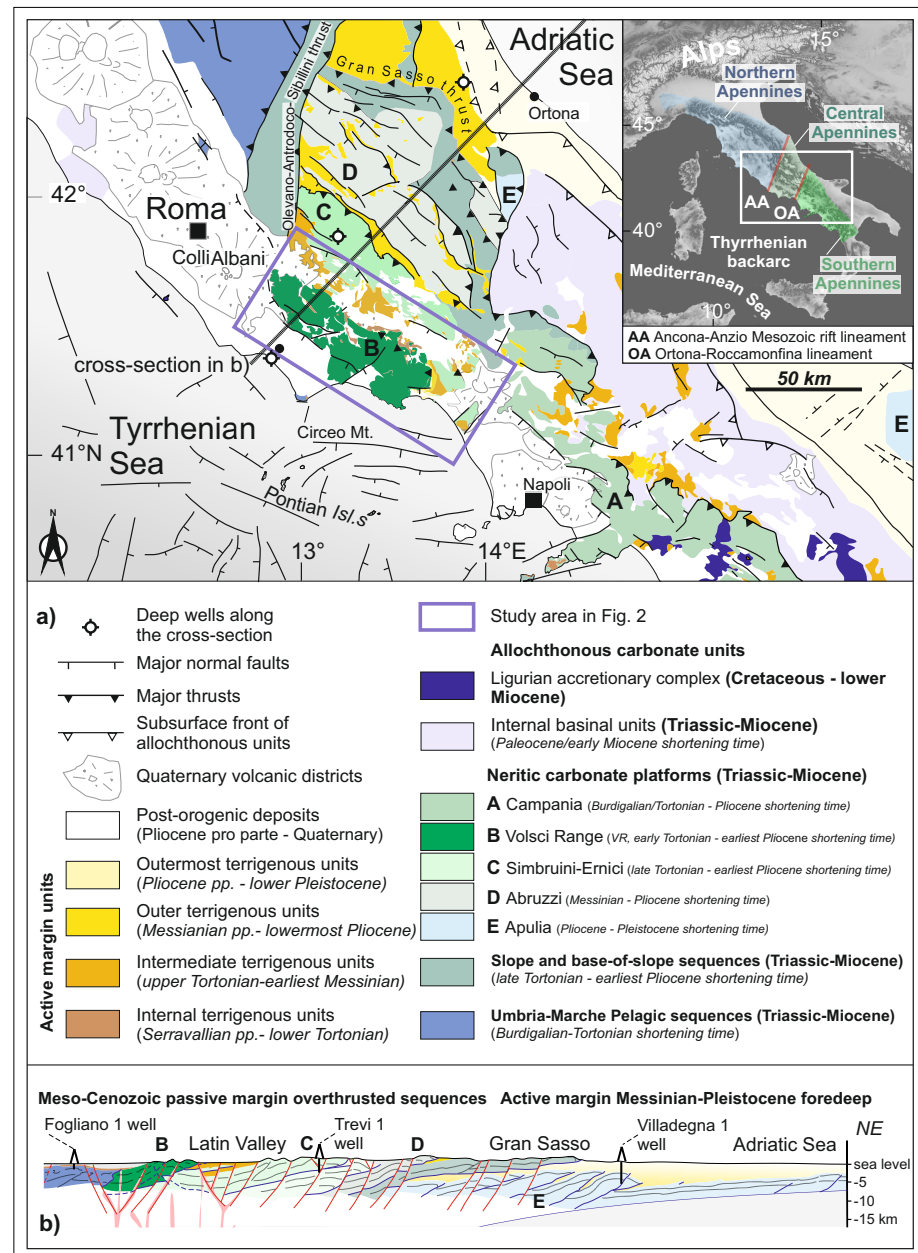


Figure 1. (a) Simplified Tectonic map of Central Italy (modified from the works in [30,38,44]), showing the active margin units and the Mesozoic passive margin units. The shortening time is in italic. (b) Crustal cross-section (modified after the work in [45]). Deep well location is taken from in [23].

2. Geological Setting

2.1. The Central Apennines

The Apennines (Figure 1) are a ~1500 km long accretionary wedge made of different pre-orogenic and syn-orogenic units accreted together during the progressive E/NE-ward migration of leading-edge frontal thrusts and associated active margin units deposited within foredeep and wedge-top basins (see, e.g., in [46–50]). From Miocene time, the Apennine foreland became progressively involved in pre-thrusting bulging, uplift, and erosion resulting from the wedge migration [51–56]. Since Tortonian time (~11 Ma), the west-directed subduction of the Adriatic slab drove the development of the accretionary wedge now exposed in the central sector of the Apennine belt [49,54]. Subsequently, the fold-and-thrust belt underwent severe crustal stretching, related to back-arc extension that progressively migrated from the Sardinian margin to the axial part of the central

Apennines [49,57]. The chain is now uplifted and cross-cut by Quaternary normal faults and also affected by several volcanic centers along the Tyrrhenian margin [45,47,49,58,59].

The central Apennines constitute a mountain chain sector bounded by two major NNE-trending tectonic lines (Figure 1), comprised between two arcs with polyphase activity: the Ortona–Roccamonfina and the Olevano–Antrodoco–Sibillini lines [60,61]. The latter can be considered as the positive transpressive reactivation (see in [7] and the references therein) of a Mesozoic extensional fault system associated with continental rifting, the Ancona–Anzio line [62] (Figure 1).

The Mesozoic paleogeography was characterized by different domains defined by peculiar stratigraphic successions. West of the Olevano–Antrodoco–Sibillini line, Meso-Cenozoic pelagic sequences occur in the northern Apennines. East of the Ancona–Anzio line, the central Apennines are mainly formed by neritic carbonate platform units that are bounded by base-of-slope to basinal domains (e.g., Gran Sasso [30]). According to the works in [63,64], drowning of the Mesozoic carbonate platform of the VR occurred during the latest Cretaceous or Cenozoic times and is testified by basinal deposits lying on top of platform carbonates. More internal basinal/oceanic units, referred to the Sicilide and Ligurian Accretionary Complex, crop out both in the southern Apennines [44] and along the coast west of Rome (i.e., Tolfa region [65,66]; Figure 1). These units are traditionally recognized as allochthonous units that were involved into the wedge in Miocene time. The occurrence of similar internal allochthonous units in the central Apennines is still debated. A stratigraphic correlation between the deposits atop the neritic carbonates of the VR and the Ligurian-Sicilian basinal units of Sicily and southern Apennines was first made by [67]. A different interpretation was proposed by the authors of [65,66], who recognized the marly-terrigenous terrains atop the VR carbonates as the remobilization of the Cenozoic basinal succession.

The terrigenous units cropping out in the central Apennines mostly occur in NW-striking valleys (e.g., Latin Valley [68]; Figure 2). These units are representative of foreland basin deposits, whose formation nomenclature varies from region to region, i.e., the Frosinone Formation [64] shares similar timing and facies with the Termini and Pietraraja formations of the southern Apennines [69,70]. To harmonize their occurrence throughout the central and southern Apennines, we have grouped them in four different units, representative of progressively more external and younger stages of the wedge accretion towards the east (Figure 1a). To the south, as shown by well logs and outcrops in the Pontian islands and at Circeo Mt., Mesozoic basinal units overthrust Oligocene to early Miocene flysch units [42,71]. South of Naples (Figure 1), Serravallian to lower Tortonian flysch represent internal terrigenous foredeep units [44]. Serravallian syn-orogenic units, indicative of plate flexuration, were recognized as well in more internal positions within the Volsci Range [72]. Such flexural deposits rejuvenate towards the east suggesting a progressive shift of the wedge towards the outer portions of the arc. Intermediate terrigenous units of late Tortonian–earliest Messinian age occur in the Latin Valley and underneath the overthrust platform carbonates of Campanian age.

North of the Latin Valley, the Simbruini-Ernicci Mts are built up of NW-striking imbricate carbonate thrust sheets that overthrust onto the outer terrigenous units of Messinian age (e.g., within the Latin valley, Figure 1 [73,74]). This is well evidenced by the Trevi well that shows the juxtaposition, at considerable depths (3000 m), of Triassic terrains onto Cretaceous and Miocene carbonates, testifying for the doubling of the Mesozoic succession [75]. A horizontal displacement in the order of 30 km and vertical offset of about 5 km has been proposed for this thrust [76,77], although field evidence from the Simbruini thrust front is at odds with this interpretation [49]. These ridges constitute the backbone of the internal sectors of the Central Apennines (internal Central Apennines), which first overthrust onto the outer active margin deposits and, during late Messinian time, were involved into renewed shortening [43]. Differently from the Internal Apennines, the axial and external parts of the chain, that occur more to the northeast, were involved into the wedge respectively during Messinian (Abruzzi) and Pliocene (Majella Mountain deformed Apulian terrains; Figure 1; see in [78]) times. During middle Pliocene time, the outermost terrigenous units experienced compression, while back-arc extension was affecting the internal part of the chain.

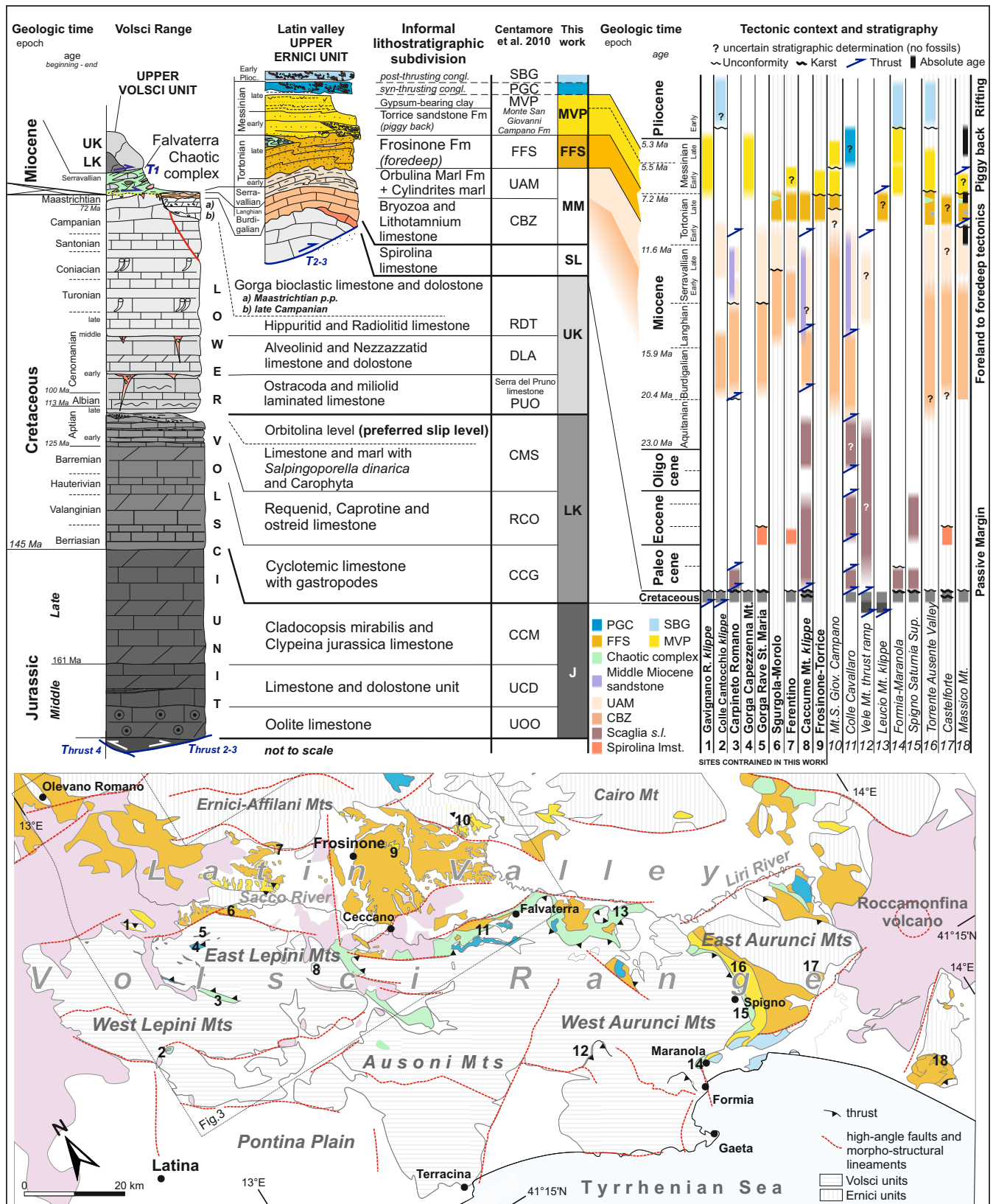


Figure 2. Simplified stratigraphic columns of the Volsci Range and the adjacent Latin Valley correlated, on the left, with the official cartography [64]. On the right, tectonic context and stratigraphy of basin deposits is reported from the literature (see Appendix A) and original data at representative localities. Localities from the Ernici unit are highlighted by vertical gray stripes. Below, the geological map of the study area with the studied locations and their respective numbers.

2.2. The Volsci Range and the Latin Valley

The VR is traditionally subdivided into major mountain groups, i.e., West Lepini, East Lepini, Ausoni, and West and East Aurunci Mts (Figure 2), that are separated by major valleys or mountain passes. More to the SW, the Mount Massico structural high occurs. These groups share a similar tectonic and stratigraphic evolution. The VR is mostly composed of passive margin Mesozoic neritic carbonates belonging to the Latium and Abruzzi platform or Apennine carbonate platform (see, e.g., in [79–81]). The Mesozoic dominant facies are representative of inner to rim carbonate platform environments (see, e.g., in [63,64,82,83]).

A compilation of the Mesozoic lithostratigraphic units cropping out in the Lepini sectors is presented in Figure 2. The Upper and Lower Volsci thrust sheets differ from the Upper Ernici unit on the basis of the Cenozoic stratigraphy. Of note, the VR succession generally bears a thin and incomplete succession of Paleocene to Miocene deposits [84] atop late Cretaceous formations of different ages, possibly due to progressive drowning of some sectors of the platform during Late Cretaceous time [63]. On the other hand, in the Latin Valley, the Ernici unit is thicker and also contains Eocene to early Tortonian foreland units and late Tortonian to earliest Pliocene active margin siliciclastic formations (see in [63] and the references therein).

Seismic interpretation studies in the Latin Valley, carried out by AGIP and other companies (www.videpi.com) (accessed on 20 January 2021), trace top-platform seismic horizons that allowed us to locally outline a fold-and-thrust structure [85]. According to the authors of [64,86], the VR front propagation affected the Latin Valley foredeep deposits that were doubled or even triplicated [45]. Upper and lower units in the Volsci Range and in the Ernici units of the Latin Valley were thus distinguished. As also shown in the cross sections in [64], thrusting involved the Cretaceous carbonates of the Ernici unit together with upper Tortonian foredeep sediments of the Frosinone Formation [63,64]. Finally, out-of-sequence thrusting during and after the Messinian salinity crisis was documented in [77,87], possibly related to backthrusting, like at Carpineto Romano [88]. The thrust front does not crop out, but according to the most recent reconstructions, it is offset by normal faults [45,86]. At least from Middle Pliocene time, the study area experienced regional uplift, accompanied by subaerial exposure and consequent diffuse erosional processes that generated erosional surfaces, now found at different elevations [63].

According to the authors of [89], just north of VR the uplift rate increased during the last 2.4 Myr. In the VR, no such detail was reached yet. However, early to late Pleistocene slope, river, and lacustrine paralic and continental deposits were mapped within depressions bounded by high-angle NW- and NE-striking normal faults that dissected the fold-and-thrust fabric. Further, E-striking transtensional faults contribute to generate middle Pleistocene wrench zones and basins between the Latin Valley and the Pontina Plain. Syn- to post-tectonic upper Pliocene–middle Pleistocene continental successions are preserved in the Middle Latin Valley, the Pontina Plain, and locally in the VR intermontane depressions [64]. Further, during late Pliocene to possibly Holocene times, the fold-and-thrust belt was progressively cross-cut by a system of conjugate synthetic and antithetic normal faults determining the formation of the coastal plain and intra-mountain depressions [64,90,91]. The VR hosts volcanic terrains of Pleistocene age from both nearby volcanic districts and local eruptive centers belonging to the Volsci Volcanic Field (VVF; Figure 1 [64,92]).

3. Materials and Methods

3.1. Stratigraphic Review and New Paleontological Determinations

The lithostratigraphic architecture of the Meso-Cenozoic carbonate platform succession has been reviewed, following the scheme in [45], and it has been integrated with a stratigraphic chart that compares eighteen different key localities representative of pre-orogenic passive margin to syn-orogenic foreland basin lithostratigraphic units throughout the study area (Figure 2). Erosive submarine and karst-related unconformities are re-

ported to support the regional review of the syn-orogenic evolution, also constrained by the absolute ages provided in [43] for the Massico Mt ridge. The overall stratigraphic setting allowed us to correlate diachronous events among different structural units from the Volsci Range and Latin Valley. Lithologies not constrained by biomarkers are traced by a question mark, whereas lithologic and biostratigraphic information coming from the review of the existing literature is resumed in the table of Appendix A. We have harmonized the stratigraphic information published in the 1:100,000 maps (i.e., Latina, Frosinone, and Alatri; <https://www.isprambiente.gov.it/>) (accessed on 20 January 2021), and in the more recent and detailed 1:50,000 maps (i.e., Anagni, Ceccano, and Velletri; <https://www.isprambiente.gov.it/>) (accessed on 20 January 2021) as well as and in other papers (i.e., in [72,84,86–88,93,94] and, using the stratigraphic nomenclature after that in [64], then grouped the deposits into the broader informal lithostratigraphic subdivision of Figure 2.

New biostratigraphic information was acquired by studying Upper Cretaceous–Miocene to early Pliocene samples collected from fifteen localities at Colle Cantocchio, Gorga, Gavignano, Carpineto Romano, Caccume Mt., and Siserno Mt. (Figure 2). Further sampling through the Latin Valley at Morolo, Ferentino, and Frosinone localities was performed in order to determine facies and fossil content of syn-orogenic deposits. Hard rock samples have been prepared for thin sections analysis, which provided thirty-three new age determinations. Further, we collected seventeen samples for nannoplankton using samples prepared under smear slide technique, and following the procedures described in [95]. We observed the nannoplankton content through the polarized light microscope Zeiss Axioscop equipped with an $\times 100$ oil immersion objective lens. We performed a qualitative evaluation of the assemblages on all the samples, but only twelve of them proved to be fossiliferous, while five other ones are barren or poorly fossiliferous. Important time maker nannoplankton taxa were identified up to species level, as presented in Supplementary Material. We base our time determination on the micro-biostratigraphic frames in [82,96–98] for the shallow-water carbonate assemblage and the biostratigraphic scale in [99–101] for the nannoplankton.

3.2. Structural Analysis

A new structural-geological survey of the carbonate and siliciclastic succession integrates previous work of the Geological Survey of Italy (ISPRA) (i.e., in [64,102,103] and the references therein). The resulting new geological map is built also considering a specific review of the 1:50,000 geological sheets “Anagni” and “Ceccano” in order to avoid lithostratigraphic synonymy (see Appendix A) [64,103].

Bedding attitude was retrieved from existing map sheet tables at the scale 1:25,000 on a stripe of about one kilometer to each side of the main cross section (Figure 3). In order to constrain fault kinematics, field measurements of faults, fractures, and slicken-fibers were collected at key localities and plotted by means of TectonicsFP software [104] with lower-hemisphere projections and rose diagrams. In particular, at each locality eigen vectors are calculated from the bedding and are indicative of the orientation of the axes of deformation, where the gray circles are representative of the plane between the principal and minimal eigenvector. In general, an eigenvector is a vector which gets stretched, but not rotated, when operated on by the matrix. Considering that eigenvectors have corresponding eigenvalues, the amount of squeezing or stretching (the strain) is called the eigenvalue. Eigenvectors from key localities are reported in Table S1 (Supplementary material).

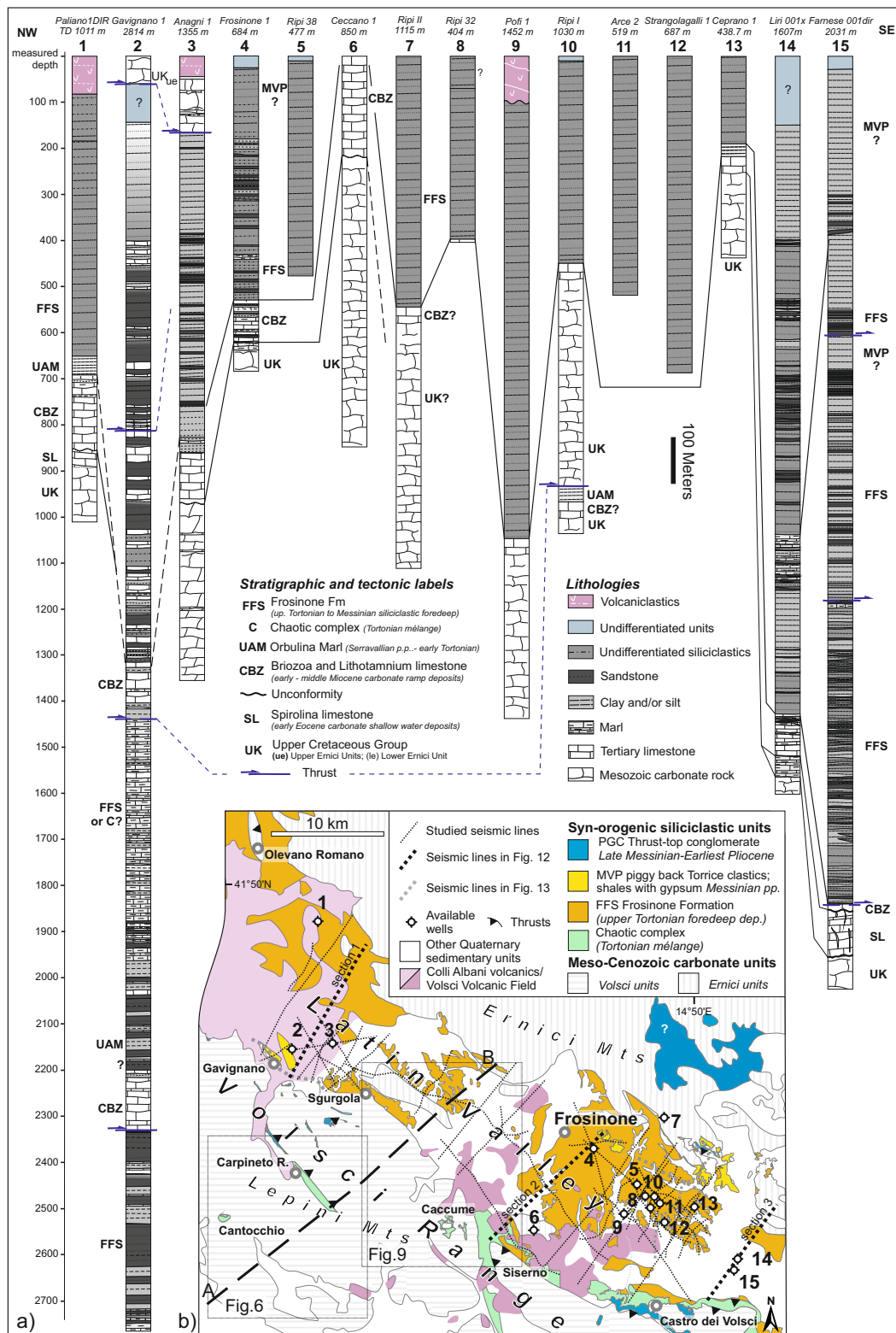


Figure 3. (a) Comparison among lithostratigraphic data from wells in the Latin Valley. (b) Sketched geological map with the location of the studied wells and seismic lines. Wells 1, 2, and 4 are from a public dataset (www.videpi.com) (accessed on 20 January 2021). Wells 3, 5, 8, 11, 12, and 13 are provided by Pentex Limited Italia (see Acknowledgments). Wells 6, 7, 9, and 10 are reported in [105]. Full lines are stratigraphic correlations within the same structural unit. Black dashed lines are uncertain stratigraphic and tectonic correlations (blue lines). Regional cross section AB (Figure 6) and the detailed structural maps of the Figures 6 and 9 are also shown.

3.3. Borehole Data from the Latin Valley

Composite well log data from the exploration and production of hydrocarbon activity were used to calibrate the seismic lines (Figure 3). Fifteen wells were drilled through the syn-orogenic lithologies, and they provide insights on late Miocene siliciclastic deposits. Four wells are from a public database (www.videpi.com) (accessed on 20 January 2021), the others were extrapolated from the literature [64,106,107] or confidential reports provided by Pentex Italia Ltd. The stratigraphic calibration of the seismic profiles was performed by using (i) the Frosinone 1 well, which is located within a relatively dense network of seismic lines and drilled at total depth of 684 m, reaching the Orbulina Marl Fm at 526 m and the CBZ at 551 m, while the Cretaceous carbonate platform top was encountered at 620 m, and (ii) the Anagni 1 well, which encountered mesozoic platform carbonates between 47 and 162 m and reached again the carbonate top at 862 m after having crossed a thick siliciclastic succession (Figures 2 and 3). Three wells were characterized by velocity data that allowed us to calibrate seismic data and/or calculate average and interval velocity for the identified macro-units. Where velocity logs were not available, an average interval velocity based on our calculations was applied to fit with the correspondent lithology and reflector detected on seismic profile. In few cases, velocity logs were available for a direct local time-depth chart; in the other cases, average velocity obtained by the analysis of the available logs and from literature was used. These two velocity laws were used to depth-convert the two-way-time interpretation on seismic dataset, in order to define thickness and depth of the main top interpreted horizons to set the geological cross section (Figure 14). Biostratigraphic data are available only for a few key wells (i.e., Paliano 1, Gavignano 1, Anagni 1, Frosinone 1, Liri 1, and Farnese 1) and have been anchored using the regional scale in [96].

3.4. Seismic Dataset

The structural setting of the Latin Valley presented in this study largely relies on thirty-eight 2D seismic reflection profiles irregularly arranged (map view Figure 3b). In the north, some seismic lines gather around the Gavignano 1 and the Anagni 1 wells, while in the south they occur together with different wells (Figure 3). The seismic sections originate from different acquisition campaigns carried out in the 1980s and 1990s for the exploration of hydrocarbons by AGIP and recently by Sovereign and Pentex. Most seismic lines are part of a public dataset (ViDEPI Project. Available online: <https://www.videpi.com> accessed on: 20 January 2021). This public network has been integrated by a few other seismic lines from different surveys, to better constrain the structural setting of the Latin Valley. The interpreted seismic dataset was a stack version. Public data were in raster format, so we produced segy files for each raster seismic line in order to be able to import all the dataset into the interpretation software (OpendTect). This was achieved using Kogeo© 2.7, a free and open software for 2D/3D seismic data analysis that allows to create a geo referenced seg-y file from a scanned seismic image (<http://www.kogeo.de/index.htm>) (accessed on 20 January 2021). Seismic quality is good to poor, probably due to a lack of reprocessing and therefore interpretation may be inaccurate in some points. In those cases, we have integrated the outcropping geological information to reconstruct a geological model along the seismic profile, identifying when possible the main reflectors.

The most evident reflectors are the unconformities at the top of the upper Cretaceous carbonates (Figure 4), and of the Orbulina Marl Fm. (UAM; Figure 2). To calibrate and detect the main reflectors/markers in the Latin Valley, a synthetic seismogram was created for the Anagni-1 well (Figure 4) by focusing on the following formation discontinuities (from the bottom to the top): at the top of the Cretaceous limestones (UK), at the top of the Bryozoa and Lithothamnium limestone (CBZ), and at the base of the Frosinone Formation (FFS). For the interpretation of the seismic profiles, we identified the top-CBZ as the key reflector with the strongest acoustic impedance contrast observed over the entire Latin Valley. This often corresponds to the UAM lithostratigraphic unit (Figure 2), which at the basin scale corresponds with one of the most used reflectors that tie wells with seismic

lines [108–110]. Miocene and Cretaceous near-top reflectors are well recognizable because of the characteristic geometry and energy picks that are stronger than the adjacent reflectors. In particular, the marly layers reflect most of the down-going seismic energy, obscuring the siliciclastic sequence or the underthrust carbonate units. Despite the limited thickness of UAM, this reflector was followed also on the poorer quality seismic lines.

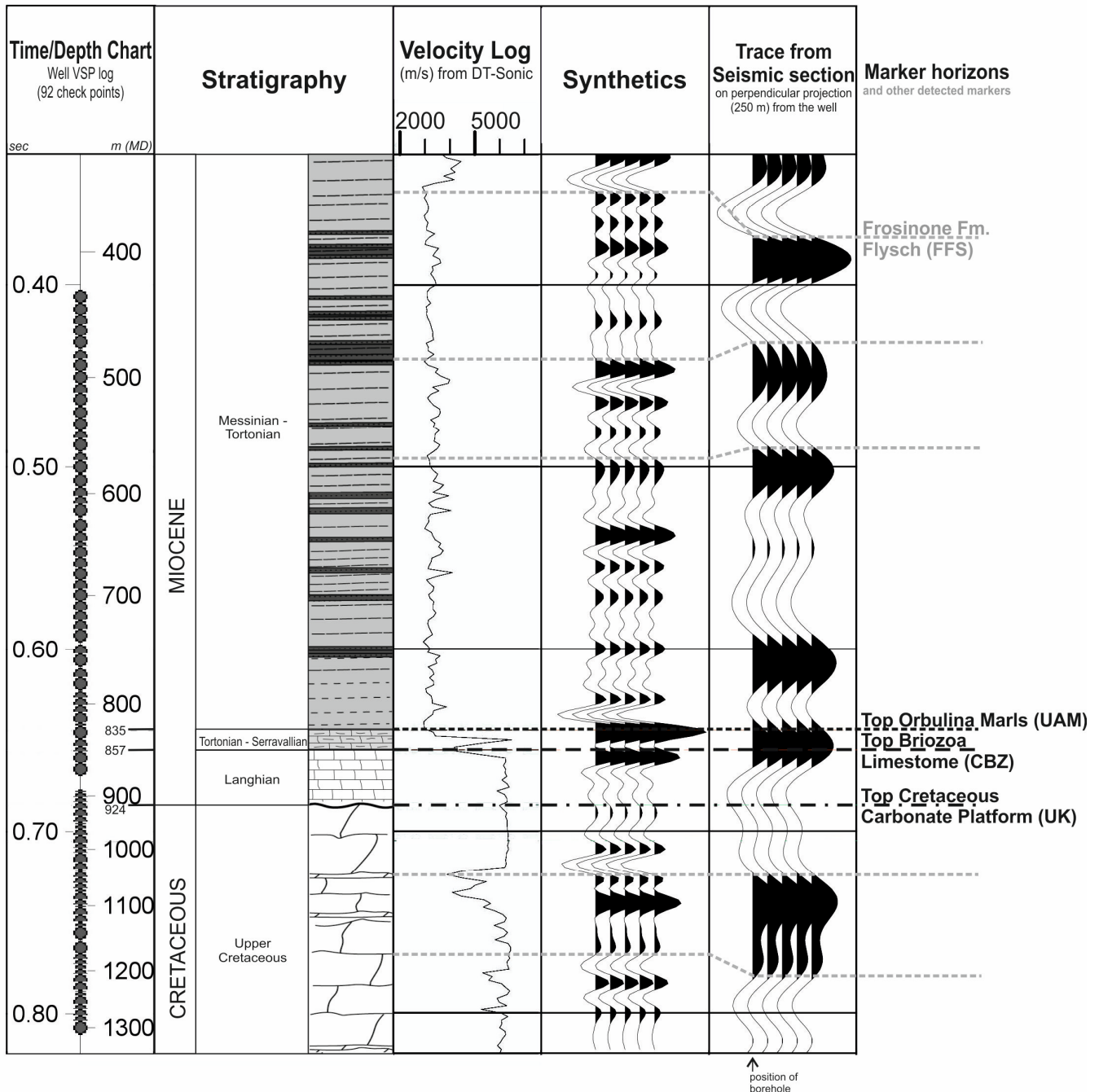


Figure 4. Simplified stratigraphic column of the Anagni 1 borehole with velocity log, synthetic seismogram, and an extract of a seismic section passing by the well (location in Figure 3). The seismic marker horizons and additional stratigraphic horizons interpreted in this study are also shown.

4. Results

4.1. Stratigraphic Constraints

4.1.1. Stratigraphic Review

The stratigraphy of the study area is schematically reported from the literature in Figure 2, where the lithostratigraphic units are anchored to the exposed sections at each of the eighteen localities presented in the map. The basics of the different tectonic units are exposed in Section 2.2. A new set of ages is proposed for the succession cropping out at the northern Volsci Range, as shown in the next section.

The Upper Campanian to Eocene carbonate platform succession that rest on the Hippuritid and Radiolitid limestone is generally missing [64], possibly due to a widespread depositional hiatus, although it locally crops out (e.g., at Gorga [103,111]). Note that the shallow-water *Spirolina* limestone (lower to mid-Eocene [112]), which crops out only in rare patches comprised between two unconformities—probably related to emersion events—was found at Gorga [112], Ferentino, and Castelforte (Figure 2; see also in [96,113], while it was recognized in well logs of Paliano 1 DIR and Farnese 001dir (Figure 3). In the Volsci Range, the Bryozoa and Lithothamnium limestone (CBZ) was dated as middle Miocene (see, e.g., in [64,87]). However, our data from the Volsci Range show that at least the CBZ base is early Miocene in age (see Section 4.1.2). Locally in the Volsci Range (e.g., Carpineto Romano, Figure 2), the CBZ lithotype is reported to occur within and beneath the allochthonous sub-Ligurian units [72], that can be compared with the Falvaterra Chaotic complex in [63].

Overall, the Falvaterra Chaotic complex is an ensemble of Paleocene to middle Miocene lithoclasts (from dm to decametric) wrapped within a matrix, whose best age constraints were provided mostly from the outcrops of Colle Cavallaro [114]. The basal contact of the Chaotic complex, although tectonically overprinted [63], is often marked by a ferruginous-limonitic veneer that occurs as a calcareous-detrital iron-oxide cruston. Differently from the classical carbonate hardgrounds, that are surfaces of syndimentarily cemented carbonate layers that have been exposed on the seafloor under an extremely low sedimentation rate, the crustons of the Volsci Range could be either of karstic origin and/or the product of fluids involved into thrust faulting. Near Formia these crustons occur on top of peritidal limestones with benthic foraminifera (redetermined after the work in [63]) including *Spirolina* sp. [115], which can be possibly attributed to the early Eocene [111]. In particular, the foraminifera shown in [63] (their Figure 4) appear closer to some shallow-water discorbidae rather than planktonic forams. However, this need to be verified with new determinations. Our data constrain the top platform units providing new insights on the correlation, envisaged in [63], between these crustons and the Upper Cretaceous–lower Miocene succession preserved in the Chaotic complex (cf. Section 5.1 on the basis of the new stratigraphic constraints presented in Section 4.1.2.). Concerning the stratigraphic evidence from the Paleogene-early Aquitanian pelagic terms atop (Figure 2), they are mostly represented by Scaglia lithotypes (e.g., Formia and Spigno Saturnia, Figure 2). These lithotypes also crop out beneath the thrust south of Carpineto Romano, and beneath the Caccume Mt. and Colle Cavallaro klippen (Figure 2). Further, Scaglia *sensu lato* lithotypes were found as blocks of various dimensions wrapped in clayey matrix together with: early-middle Miocene lithoclasts (Figure 2; Appendix A), upper Serravallian cherty marl, and massive to laminated arcose greywackes with mica [103]. The latter resulted sterile at the Caccume Mt. [84]. Lithologies of clasts involved into the Chaotic complex belong to a wide chronostratigraphic interval (i.e., Paleogene-Serravallian pro parte; Figure 2). More to the south, beneath the Vele Mt. thrust, siliciclastic marly deposits, mapped as Chaotic complex equivalent units, occur. Our data provide age constraints for the northern Volsci Range, see Section 4.1.2, and provide insights on the stratigraphic development of the sedimentary succession later deformed as Chaotic complex.

In the Latin Valley, the Frosinone Fm. was homogeneously attributed to late Tortonian time, while on the northeastern edge of the valley the base seems to be younger (i.e., uppermost Tortonian [87]). The upper part of the Frosinone Fm. unit bears olistoliths and

olistostromes [115], from Mesozoic platform and Chaotic complex equivalent lithologies. They are reported at Sgurgola [35] and in the Torre Ausente Valley [64,116], although not as nicely cropping out as at the Massico Mt. [37].

Well data show a highly variable facies pattern of the siliciclastic units that include carbonate intercalations and thick marly successions with minor to rare sandstone horizons (Gavignano 1; Anagni 1; Frosinone 01; Farnese 001 wells; Figure 3). Due to tectonic juxtaposition, these successions may appear repeated at least twice and thus also reaching a total thickness of about 1.8 to 2.5 km at Gavignano and Liri and Farnese wells. Single thrust-bounded siliciclastic units are up to some 0.7 km thick.

In particular, the Gavignano 1 well hits four repeated siliciclastic-marly sequences bounded by thrust faults juxtaposing older terrains above younger ones. The uppermost unit is constituted of Upper Cretaceous (UK) limestones (cf. Anagni 1 well). The deeper fault-bounded units are about 600–900 m thick. Their siliciclastic sequence is defined by different lithofacies associations including alternations of sandstone, marl, and limestone. By correlating the wells providing detailed biostratigraphic information (e.g., Paliano, Gavignano, and Frosinone), we have correlated similar lithostratigraphic units, thus providing a formation identification. Biostratigraphic data from wells do not report Messinian taxa. Thus, we consider the Messinian Monte San Giovanni Campano unit (MVP) following the work in [63] and composed of wedge-top clastics [87], including other formally defined lithostratigraphic units (i.e., Torrice Sandstone Fm, Figure 2). Despite this lack of subsurface biostratigraphic information, its occurrence at depth cannot be excluded. Further, the correlation among conglomerates bearing exotic clasts of granitoids (SBG) is not clear as not supported by resolute available stratigraphic information. However, their occurrence is of regional relevance as they could be representative of the transition from late orogenic [117] to backarc settings (i.e., Formia; Figure 2).

4.1.2. New Stratigraphic Constraints

New stratigraphic data from the northern Volsci Range and Latin Valley constrain the age of sedimentary units (Appendix B). The uppermost Cretaceous carbonate units were studied at different localities to reconstruct the tectono-stratigraphic setting of the top of the platform before thrusting. This information is provided by the variable thickness and facies distribution of the carbonate units between the Hippuritid and Radiolitid limestone and the ferruginous cruston on top, which usually marks the top of the platform. East of Gorga (Figure 2), the Hippuritid and Radiolitid limestone is overlain by some decameters of Maastrichtian bioclastic limestone and dolostone. This unit is truncated at the top by breccias, indicating an unconformity on the Upper Cretaceous succession. Those breccias are intercalated with a middle Burdigalian shallow-water marly level (Lep 12c, Appendix B) passing upward to typical CBZ limestone.

The Mesozoic platform top was found on top of the Lower Volsci Unit at the Caccume Mt., where it occurs as an encrusted breccia. At Carpineto Romano (Figure 5), atop of the platform succession of the Lower Volsci Unit, when preserved, discontinuous thin patches of proximal early Miocene CBZ limestone and middle Miocene *Orbulina* Marl formations occur (cf. Cosentino et al., 2002). At Colle Cantocchio (Figure 2; Appendix B), the early Miocene CBZ limestone was found disconformable on the Jurassic-Cretaceous limestone, which is marked by a hardground (structural details in Section 4.2.1).

Atop the Meso-Cenozoic carbonate units, the Chaotic complex occurs as a *mélange* that contains both native and exotic blocks, the latter being Cretaceous to Miocene basinal to distal ramp deposits that are coeval with the *in situ* formerly described proximal succession (Figure 5). Both block types are internally folded. South of Carpineto Romano (Figure 3), the deformed platform blocks involved within the Chaotic complex are stratigraphically comparable with the encrusted carbonates that are preserved at the top of the Lower Volsci Unit (cf. Figure 2). In particular, within the Chaotic complex, we have mapped several lenses of Cenomanian to early Campanian limestones covered by middle Campanian karstic breccias and ferruginous to limonitic cruston (Figure 5; structural details in Section 4.2.2).

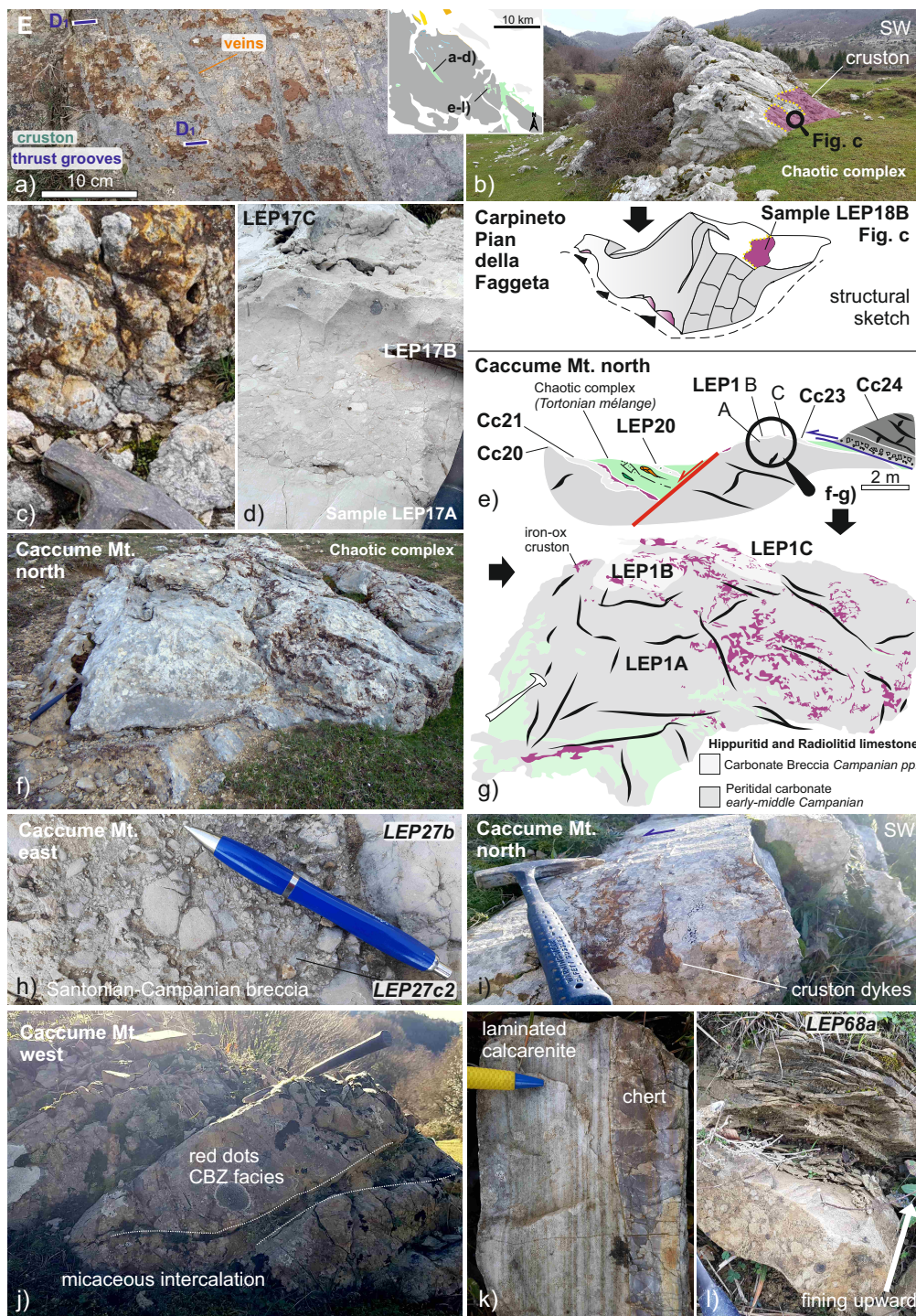


Figure 5. Sampled lithologies of the top of the platform and Chaotic complex. (a) Carpineto Romano (Pian della Faggeta; cf. Figures 6–8), encrusted top of platform crossed by E-trending thrust grooves and later veins having growth-fiber lineations plunging towards the NE (corresponding to plot 3 in Figure 8; $41^{\circ}34'51''$ N/ $13^{\circ}6'30''$ E); (b–c) encrusted native block within the Chaotic complex; (d) Campanian breccia beneath cruston; (e) Sampling site of the top of the Lower Volsci Unit north of Caccume Mt. and inherited paleo-topographic reconstruction; (f–g) outcrop detail of the cruston and underneath discordant units. (h) example of discordant Santonian-Campanian breccia beneath Chaotic complex. (i) Small-scale dykes of the grooved top platform cruston ($41^{\circ}34'32''$ N/ $13^{\circ}14'5''$ E); (j,k) lower Miocene blocks $41^{\circ}34'33''$ N/ $13^{\circ}13'20''$ E; (l) Tortonian turbidites from Caccume Mt. north.

Differently from the native blocks, the Scaglia-type pelagic to hemipelagic limestones (with rare planktonic foraminifera and iron oxides) occur as exotic inclusions. In this

category, at Carpineto Romano and Caccume Mt. (Figures 2 and 5; Appendix B), we have found CBZ blocks of early Miocene age represented by red dots (iron oxide spherules) glauconitic calcarenite associated with micaceous intercalations and chert (Figure 5). Minor lenses of hemipelagic middle Miocene marl and sandstone occur as well. Overall, the blocks are wrapped within a sandy-clayey matrix that is alternated with shales, foliated brownish marl, greenish arenaceous beds with exotic lithic, and coarse-grained micro-conglomerate with carbonatic and crystalline elements.

The matrix of the Chaotic complex at the base of the Caccume and Siserno mounts, includes Paleocene-Eocene, Oligocene-early Miocene, middle Miocene, and perhaps also late Tortonian-Messinian nannofossil assemblages (Appendix B). A similar wide span of ages was obtained from the shaly units of Colle Cantocchio (Figure 2), where Mesozoic to Tortonian nannoplankton reworked specimens were found beneath a major thrust (Appendix B; see also Section 4.2.1).

In the Latin Valley, the nannoplankton from the Frosinone Fm. can be referred, although rare or hardly diagnostic, to late Tortonian time. Wedge-top conglomerate deposits were studied at two key localities. At Gavignano (Figure 3), folded calcareous conglomerate occurs atop karstified Cenomanian limestones that according to the well data are juxtaposed on arenaceous deposits (cf. Figure 3). The clasts of mixed origin are from the Upper Cretaceous carbonates (i.e., Coniacian-Campanian and Albian-Cenomanian; see also Farinacci, 1965) and from the Tortonian Orbulina Marl Fm. The embedding matrix is made of abundant quartz grains along with reworked *Amphistegina* and *Elphidium* that make it possible to refer the whole Gavignano clastic deposit to the MVP unit. In particular, the fining upward series with rare sandy matrix at the base (LEP10L) are dated to the latest Tortonian-earliest Zanclean and the clay marl at the top (LEP10M) to the Messinian. Thus, we consider this topmost constrain as indicative of the Messinian age of the MVP unit in the Latin Valley.

Within the eastern Lepini backbone, the conglomerates of Gorga are composed of pebbles and rounded blocks of reworked conglomerates whose clayey matrix and a bioturbated marly pebble were investigated. The age of these samples is late Tortonian for the marly pebble due to the presence of the coccolithophore *Discoaster surculus*, and top Tortonian-earliest Zanclean for the clay matrix bearing the marker *Amaurolithus primus*.

4.2. Structural Analysis of the Volsci Range

In this section, we document the field data used to reconstruct a geological cross section across the northern Volsci Range. The Western Lepini Mounts essentially consist of a 3 km thick Jurassic to Cretaceous carbonates dipping to (E)NE, whose local variations are shown in the stereoplots from 1 to 6 in Figure 6. The Neogene lithostratigraphic units atop are locally preserved beneath a few klippen structures that we document in detail in the next paragraphs. In the map and in the cross section of Figure 6, two areas are highlighted and described in detail as they preserve novel insights about pre-orogenic and syn-orogenic tectonics, which are presented from the oldest to the youngest event.

Near the western edge of the Western Lepini Mounts, a detailed survey performed at Colle Cantocchio allowed us to update the previous work by providing details on the stratigraphic contacts and fault kinematics (Figure 7). In particular, we integrate the data from in [93] by describing the pre-orogenic contacts and the low-angle fault juxtaposing Cretaceous rocks onto the Orbulina Marl Fm. As we can see from the panoramic view and cross section (Figure 7), lower Cretaceous calcareous dolostones (LK) are juxtaposed to a thick Jurassic-Cretaceous succession. The LK unit is downthrown towards the WSW and it overall consists of a striated proto-cataclasis of a normal fault (in orange). The fault has a cut off angle of about 40° with the footwall bedding. On top of this fault (paleofault, orange line in Figure 7), patches of lower Miocene CBZ occur sealing the contact (see Section 4.1.2). At the contact, an oxidized bluish rim of Mesozoic limestones marks the paleoescarpment (yellow dotted line in Figure 7), which is surrounded by altered shales (late Serravallian-Tortonian pp. Orbulina Marl Fm).

Such an inherited tectono-stratigraphic setting is preserved at the footwall of a thrust, whose hanging wall consists of a one-hundred-meter-thick pile of Upper Cretaceous (early-mid Campanian) limestone, and whose base constitutes the roof of a cave. The cave is defined by an iron oxide-rich striated principal slip surface. In the hanging wall, cataclastic bands are crosscut by minor mirror-like faults.

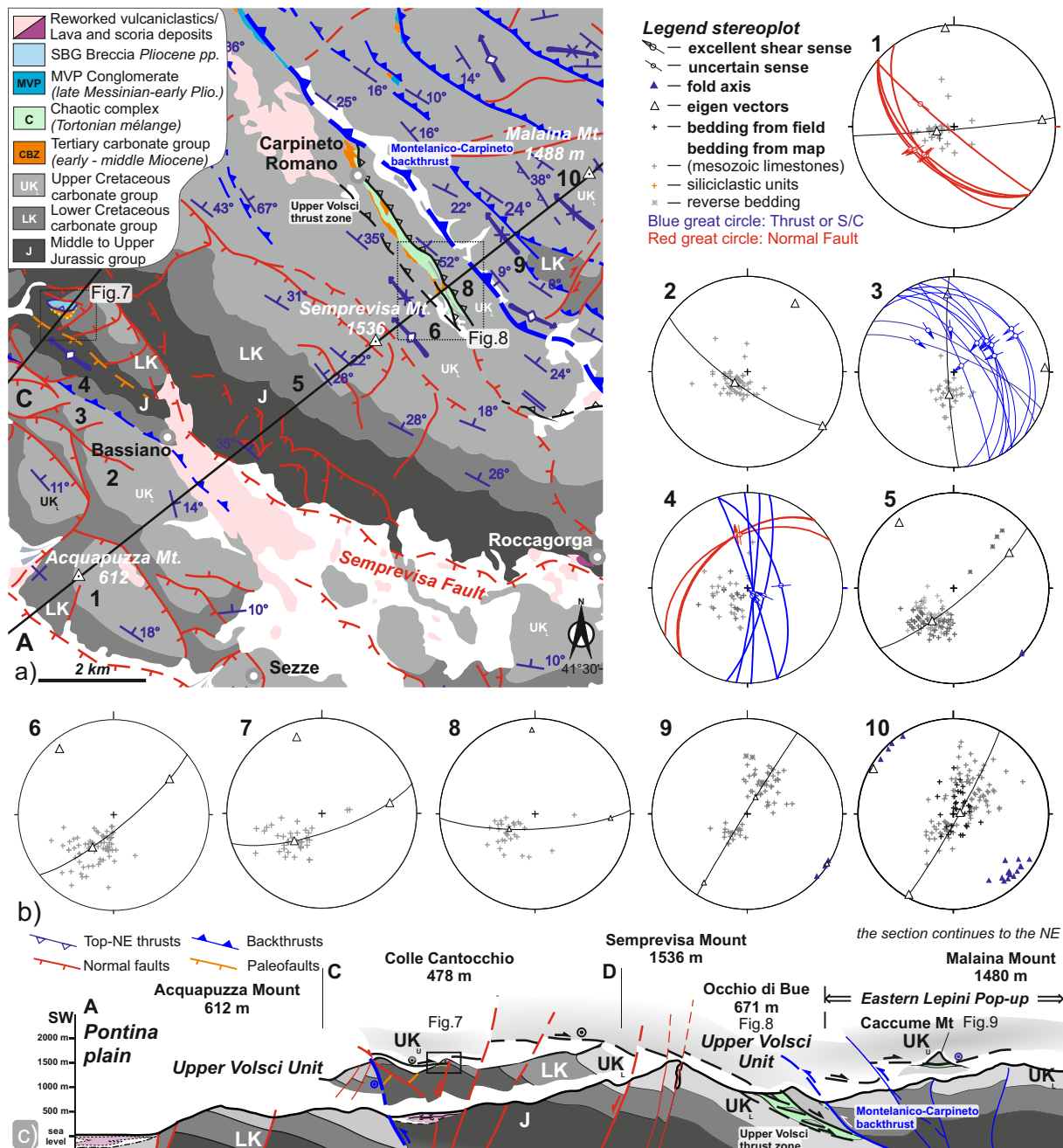


Figure 6. (a) Geological map of the western Lepini sector. (b) Stereoplots (lower hemisphere projection, equal area) summarizing orientation data for the structural elements representative of the subdivided areas in panel (a). Eigen vectors are indicative of the orientation of the axes of deformation calculated from the bedding, where the gray circles represent planes that contain the intermediate and maximum eigenvectors, as shown also by the data reported in the supplementary material. (c) Cross-section of the Volsci Range limited to the Malaina Mount to the northeast.

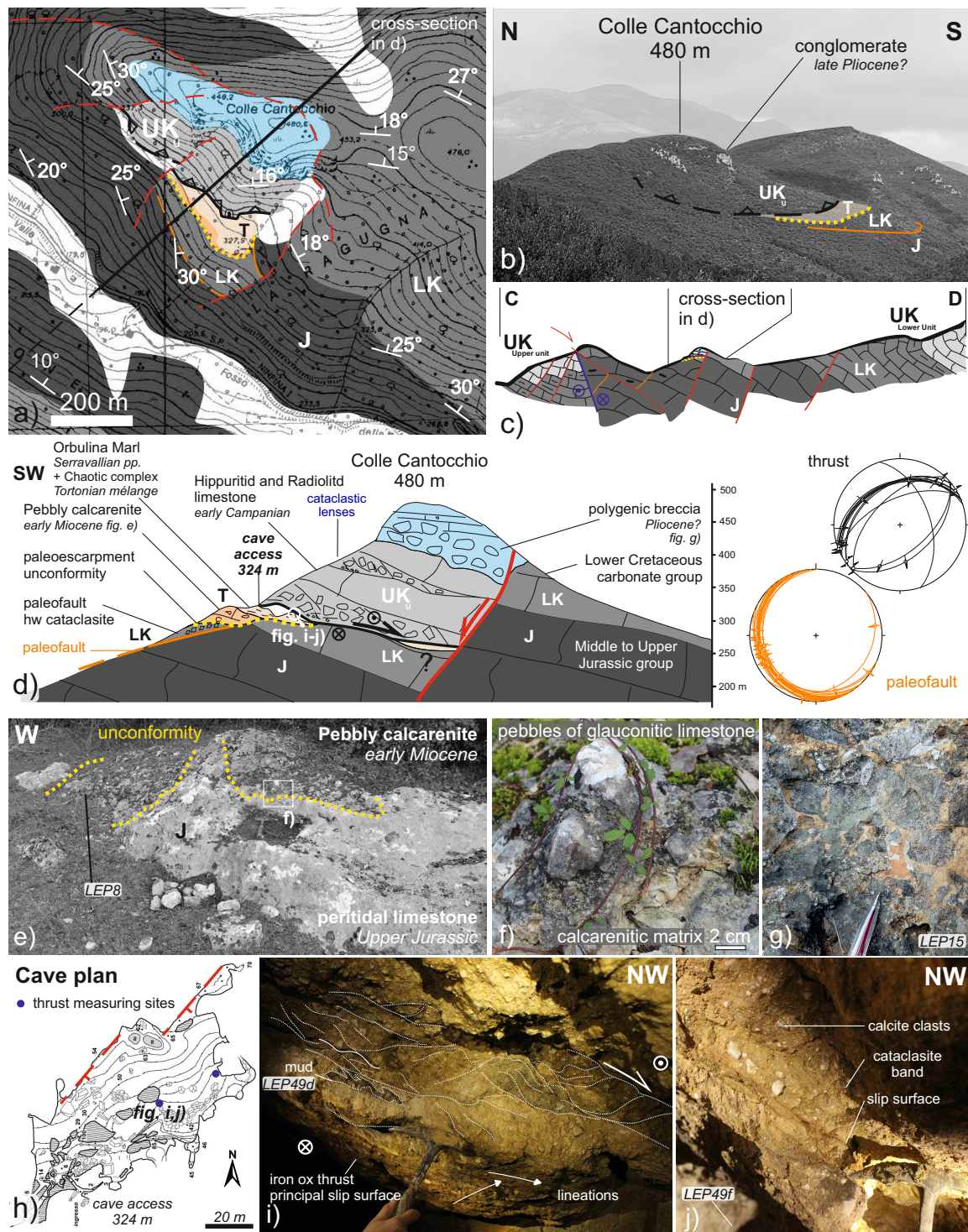
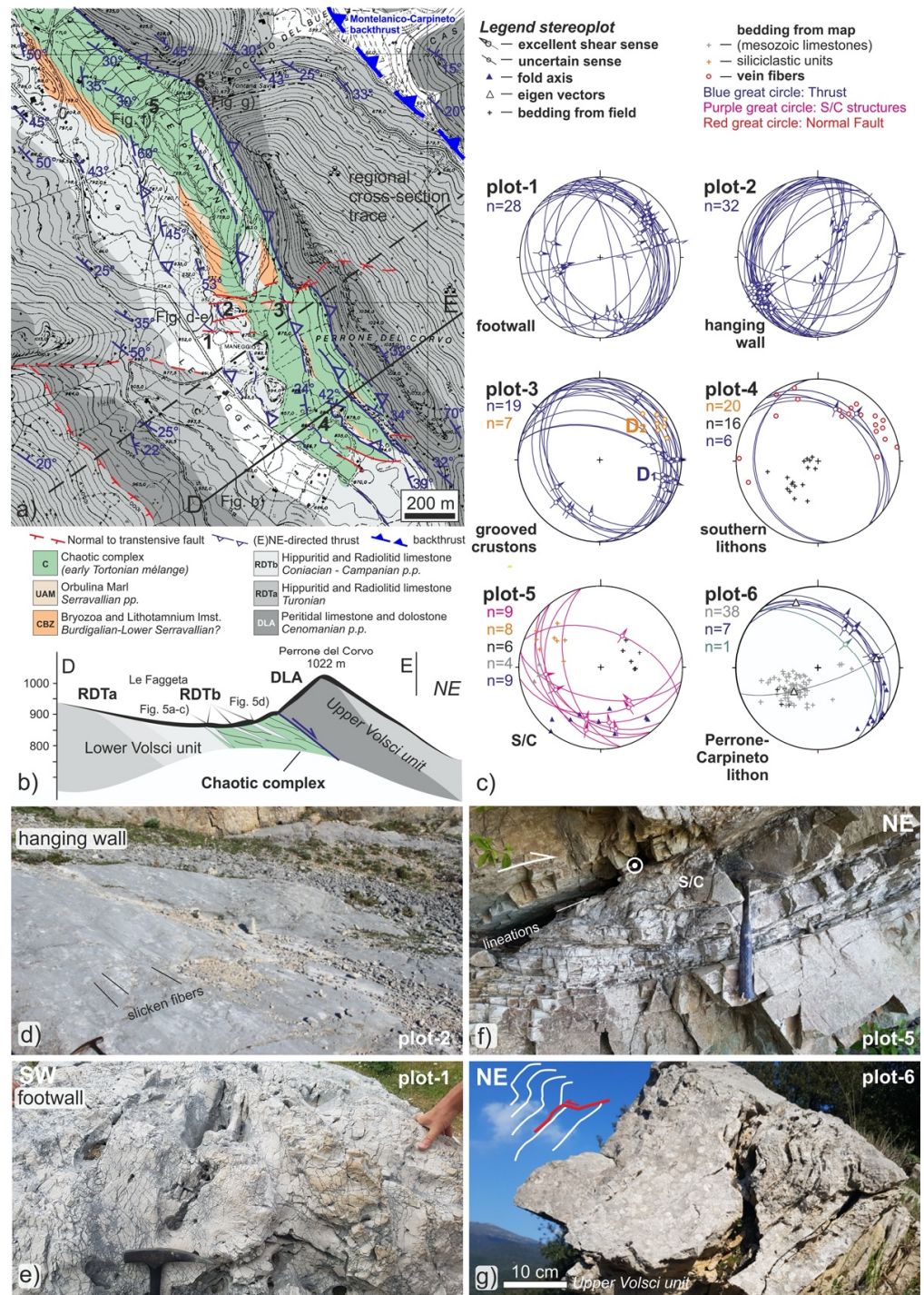


Figure 7. (a) Geological map of Colle Cantocchio modified after Cocozza and Praturon (location in Figure 6 [93]). (b) Structural overview looking eastward. Blue line: thrusts and transpressive faults; yellow dotted line: paleoescarpment unconformity below Middle Miocene terrains (T); orange line (paleofault). (c) Larger geological cross section from Figure 6 and detailed (d) cross section (bold line traced in panel (a)) with stereoplots (lower hemisphere projection, equal area) of faults with slickenlines measured at the paleofault and in the roof of the cave. (e) Detail of the paleoescarpment contact of the pebbly calcarenite (f) over the hardground composed of oxidized Upper Jurassic peritidal limestones (41°34'29" N/13°0'9" E); (g) Polygenic breccia composed by Miocene and Cretaceous calcareous clasts with a reddish cement and calcareous matrix. (h) Cave details, grooved-base thrust fault zone constituted by foliated cataclasite bands (i,j). Sampling sites are referred to Appendix B.



As constrained by nannoplankton analysis on samples from the fault core, both clasts and matrix (see Appendix B) are representative of different levels of a basinal sedimentary succession. The cataclasite also includes fragments of calcite mineralizations. The internal fabric is marked by the occurrence of slip surfaces associated with transpressive S/C structures indicating top-to-the-NE thrusting. Overall, the thrust seems to cut up-section although bounded and possibly tilted by later normal faults. The NW edge of the cave is bounded by a NE-striking normal fault with a displacement in the order of 20–40 of meters (red line in Figure 7h). At the top of the hill, the overall structure is topped by transgressive polygenic marine breccia composed by Miocene and Cretaceous calcareous clasts with a reddish cement and calcareous matrix, possibly crosscut by a SW-dipping normal fault with a displacement in the order of 150 m.

4.2.1. Thrusting at the top of Lower Volsci Unit

Figure 8 summarizes the kinematic indicators affecting the top of the Mesozoic platform and the Chaotic complex in six localities at the top of the Mesozoic succession of the Lower Volsci Unit in the Western Lepini Mounts.

Starting from the base of this deformed area, the Hippuritid and Radiolitid limestone (Campanian RDTb; Appendix B) of the Lower Volsci Unit is affected by bedding-parallel proto-cataclasite bands crossed at low-angle by striated curvy fault mirrors with dm² to m² dimensions (Figure 8). Across the most evident fault mirror (Figure 8), both footwall (plot-1) and hanging wall (plot-2) are characterized by top-to-the-NE slicken fibers, measured also on smaller fault mirrors. Crustons are disconformably topped by veined and laminated beige sandy calcarenites (plot-3). The thin carbonate blocks embedded in the Chaotic complex at Pian della Faggeta (plot-4) have variable thickness (up a few meters thick) and limited lateral extent (up to some dozens of meters). The native carbonate lithons are internally deformed and in places, display a sharp contact at their base with the siliciclastic units, and can be internally affected by top-to-the-(E)NE asymmetric folding. On the top of some of these slices, E-trending thrust grooves are cross-cut by NE-stretching mode-I veins. Beside the dominant NE-stretching, provided by the fiber direction of veins, more to the south (plot-4, Figure 8), veins crossing carbonate slices in similar structural positions also show NW-directed stretching.

At Occhio di bue locality (plot-5), a block of middle Miocene limestones and marls with chert topped by light green clay of late Serravallian age (c.f., Cosentino et al., 2003) is affected by S/C structures indicating top-to-the NE shear. Coherently, at the contact with the Cenomanian limestone on top, 1–2 m of foliated proto-cataclasite bands are topped by (E)NE verging folds (plot-6; Figure 8). In the same plot, top-to-the-NE striated bedding is reported as it crops out more to the north at the top of the same lithon. While bedding is folded around N- to NNW-striking axes (cf. stereoplots 7–8; Figure 6), northeast of a major backthrust it is folded around NW-striking axes of folds (stereoplots 9–10).

As the Chaotic complex is concerned, field data from the Eastern Lepini Mounts highlight the top-to-the-ENE juxtaposition of the Upper Volsci unit above the Chaotic complex (i.e., Caccume Mt., Siserno Mt.), which in the Volsci Range is preserved in a few klippen atop the Lower Volsci Unit, whereas in the Latin Valley it is found on top of the Frosinone Formation (Figures 9a and 10a). At the Caccume Mt., we report structural information from the juxtaposition of folded Cenomanian Lower Cretaceous limestone on the Chaotic complex. The regional folding affecting the Lower Volsci Unit defines a well-marked NW-striking open fold while the Upper Volsci unit of the Caccume Mt. displays rather dipping beds folded around an NNW-striking axis. The basal contact of the Chaotic complex is marked by thrust grooves and ferruginous faint slicken lines along the crustons, while at the top of the Chaotic complex, S/C and C' structures display top-to-(E)NE shearing. Cross-cutting field relationships show that thrust grooves are further cross-cut by high-angle en-échelon shear zones and normal faults.

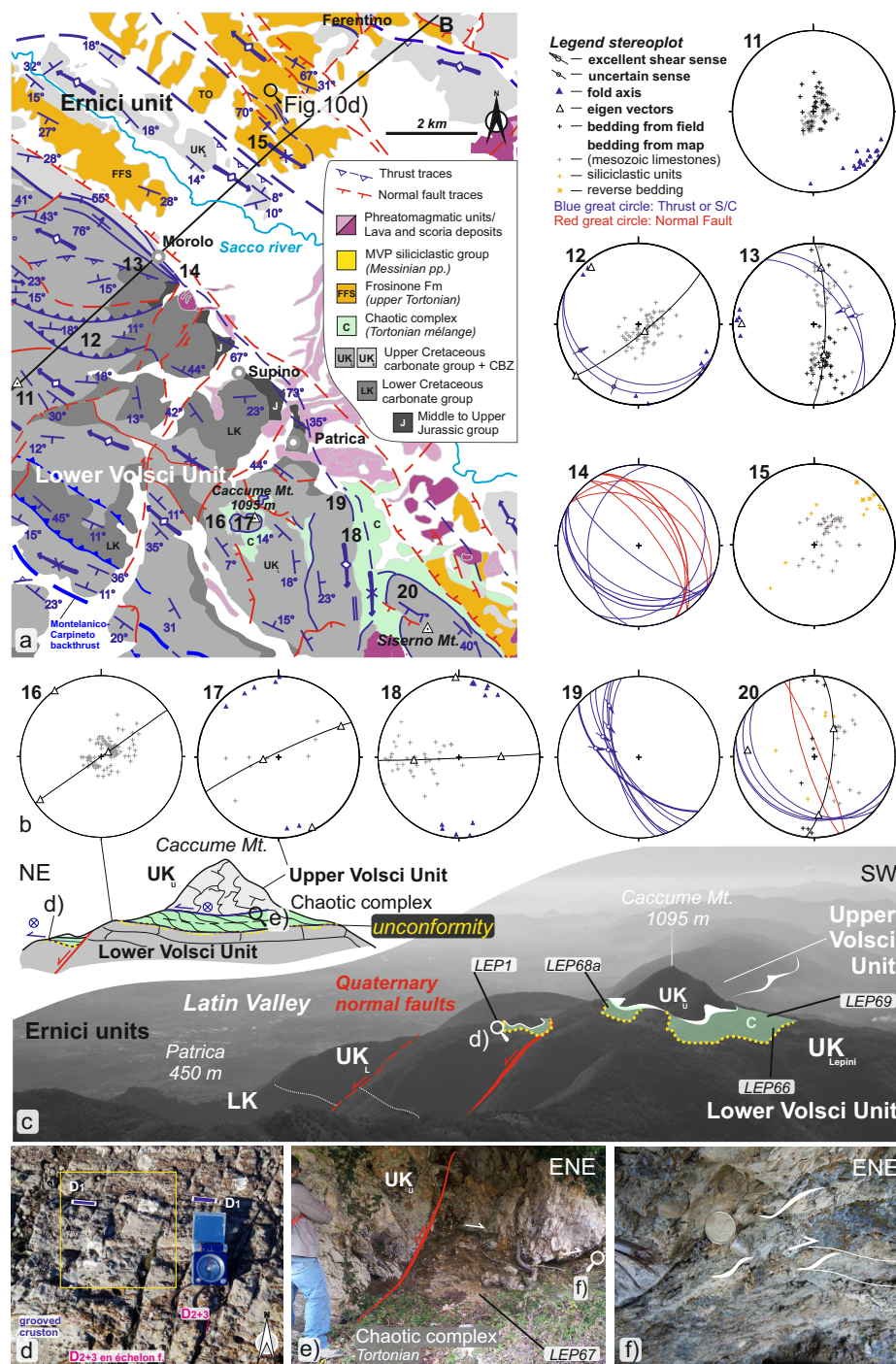


Figure 9. (a) Geological map of the Eastern Lepini sector and part of the Latin Valley. (b) Stereoplots (lower hemisphere projection, equal area for locations 11–20; numbering following after Figure 6) summarizing orientation data for the structural elements representative of the areas in panel a). Plot-13 shows E-striking folds interposed in the frontal thrust zone near Morolo, while plot-18 represents the N-S trending flank of a salient associated with transpressive S/C structures of Plot-19. (c) Sketched geological cross section and structural overview of the Volsci Range front (Caccume Mt. lower and upper unit, respectively, correspond to plots 16 and 17). Normal faults dip towards the NE, crosscut the Upper thrust. Sampling sites are reported in Appendix B. (d) Caccume Mt. front, detail of the encrusted top of the platform affected by E-trending D1 grooves and later crossed by oxides-rich (D₂₊₃) en-echelon fractures and later NW-striking oxides-free and cemented veins; 41°34′46″ N/13°13′60″ E). (e) Upper thrust juxtaposing the Cenomanian neritic limestone over the Chaotic complex (41°34′15.00″ N/13°13′55.13″ E), which, as shown as the sampling site of LEP67 on a lithotype that in panel (f), is affected by top-to-the-(E)NE S/C structures.

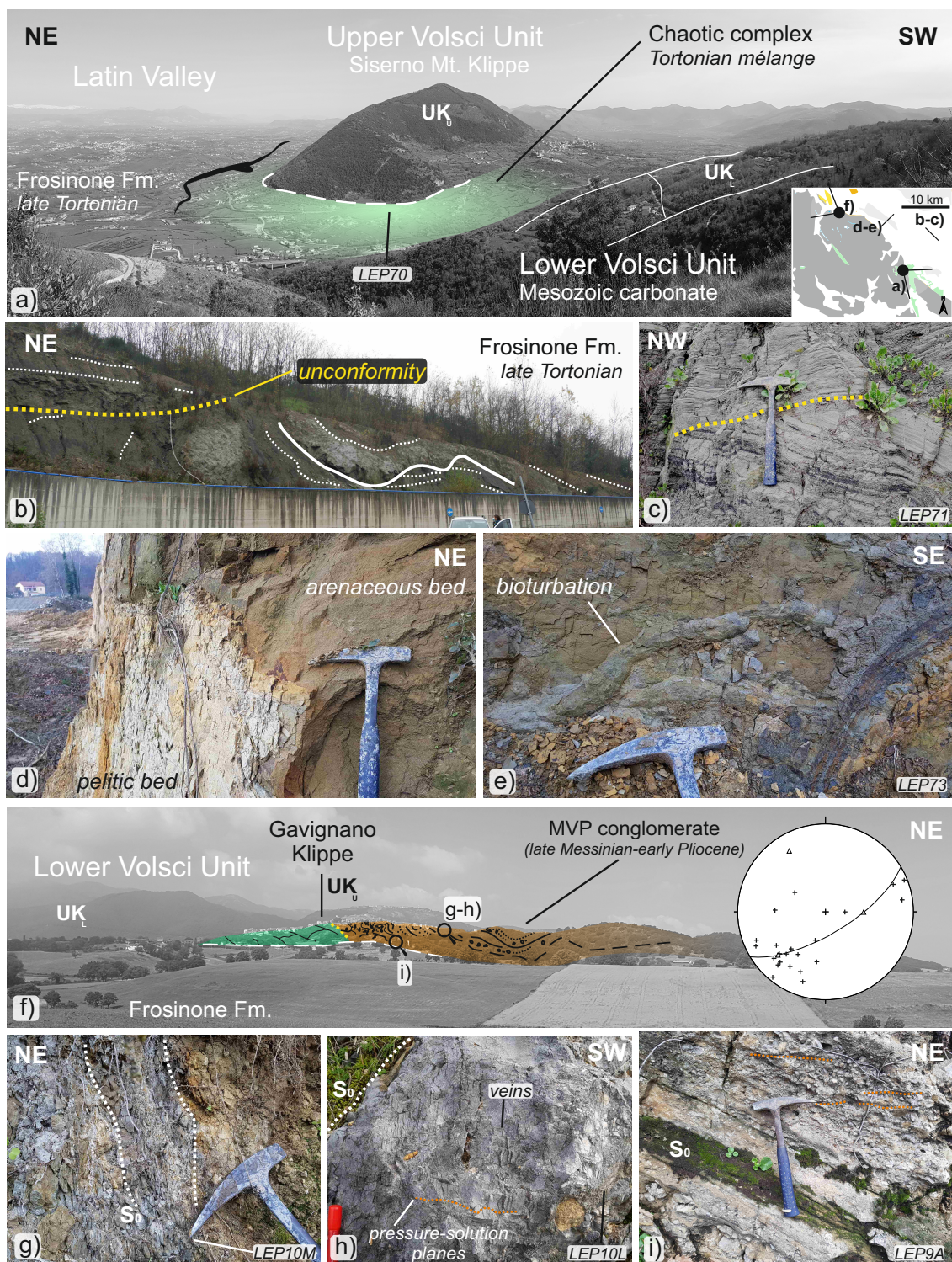


Figure 10. (a) Structural overview over two frontal klippen of the Latin Valley cropping out at Siserno Mt. where the Chaotic complex is juxtaposed to the Frosinone Fm. (b) Near Frosinone, an unconformity subdivides folded FFS units from the channelized facies on top. (c) Detail of the unconformity. (d) Vertical pelitic-arenaceous succession with (e) bioturbated levels. (f) Structural overview of the Gavignano area with stereoplotted (lower hemisphere projection, equal area) of bedding and eigenvectors, that are indicative of the orientation of the axes of deformation related to the MVP thrust top conglomerates of Gavignano with (g–i) location of sampling localities. Conglomerates at the base are affected by pressure solutions and in the most calcareous beds also by veins. Sampling sites are referred to the Table in Appendix B.

4.2.2. The Volsci Range Thrust Front and the Latin Valley Structures

The geometries of the frontal part of the Volsci Range and Latin Valley are shown from the SW to the NE (stereoplots 11–15, Figure 9). The thrust front between the Ernici and Lower Volsci units occurs as a series of imbricates of overturned Cretaceous to CBZ layers (i.e., NW of Morolo; Figure 9). New data allowed us to recognize a salient at the front of the Eastern Lepini Mounts. This structure is accompanied by a change in the fold trend from NW to W (plots 12 and 13; Figure 9) and by transpressive top-to-the-NE kinematics. The frontal part is defined by a large-scale anticline in the west and a syncline in the east (Figure 9). The two folds are separated by a series of NNW-striking tear faults with inferred right-lateral kinematics (Figure 9). More to the east (plot-18), the N-S trending flank of the salient is associated with transpressive S/C structures in Cretaceous limestones (plot 19). Overall, the fold-and-thrust fabric is cross-cut by NE-dipping normal faults at the northeastern VR edge. As it is downfaulted, the thrust front does not outcrop further north. In the VR, a salient has been mapped between Morolo and Patrica (Figure 9), its most external point being characterized by the outcrop of Jurassic limestones. Upper Cretaceous units occur as klippe above the imbricated Chaotic complex juxtaposed to the foredeep deposits of the Frosinone Fm.

At the southern edge of the studied area of the Latin Valley (Figure 10a), the Chaotic complex was mapped as juxtaposed on the Frosinone Fm., and it reaches its maximum thickness west of the Siserno Mt. (about 250 m).

There (Figure 10a), we identify two thrusts: one juxtaposing the Upper Volsci Unit on the Chaotic complex (white dashed line) and the other juxtaposing the Chaotic complex onto the Frosinone Formation (black thrust). At Frosinone, a new road cut exposes a major intraformational unconformity within the Frosinone Fm. (yellow dotted line, Figure 10b, c) between folded layers beneath and sub-horizontal channelized deposits atop.

The channelized facies is made of arenaceous-pelitic associations with sets of thin pelitic-arenaceous and marly beds intercalated in thick massive arenaceous-pelitic layers. Southwest of Ferentino, paleocurrents are marked by a NW–SE direction, whereas the Frosinone formation is internally deformed and displays verticalized to overturned successions (Figures 9 and 10). There, the facies consists of an arenaceous association of amalgamated massive beds with arenaceous-pelitic and pelitic-arenaceous sets. As shown on the map (Figure 3), north of Sgurgola and north of the Siserno Mt., an anticline with upper Cretaceous and CBZ limestone belonging to the Ernici Unit emerges from the Latin Valley siliciclastics, which are locally bioturbated. In the syncline between this ridge and the Volsci Range, pelitic facies of the Frosinone Fm. occur.

At Gavignano (Figure 10f), the MVP Messinian calcareous conglomerate occurring on top of the Upper Volsci Unit overthrusting the Frosinone Formation is folded along an NNW-striking axis and is near vertical in places. In the most calcareous layers, pressure solution seams and veins crosscut the pebbles as typical of load-driven compaction.

4.2.3. Backthrusts and Normal Faults

Backthrusts best crop out in the northwestern part of the VR, where their presence is highlighted by some pockets of Messinian-earliest Pliocene heterogeneous conglomerate (Figure 11). Transpressive kinematics associated with a general top-to-the-(E)SE sense of thrusting was observed on the reverse faults along the Montelanico-Carpineto Backthrust. As typical of cannibalized wedge-top basins, blocks of conglomerates occur within a marly-conglomeratic matrix near Gorga (Figure 11).

In Figure 11, we sketch the structural setting related to the backthrusts, which cross-cut and preserve the top-to-the-(E)NE Chaotic complex at the footwall of the Montelanico-Carpineto Backthrust. This major backthrust (i.e., Montelanico-Carpineto Backthrust) bounds the East Lepini structure, a large-scale anticline with its culmination at the Malaina Mt. (Figures 6 and 11). The backthrust is accompanied by recumbent folds and minor high-angle reverse faults. In the southwestern sectors of the VR (Figure 11), normal faults cross-cut older contractional structures. More to the SW, another high-angle backthrust

was mapped west of Bassiano (Figure 6). This structure allows the juxtaposition of the Jurassic and Early Cretaceous carbonate onto the upper Cretaceous and it is defined by transpressive kinematics (stereoplots in Figure 6).

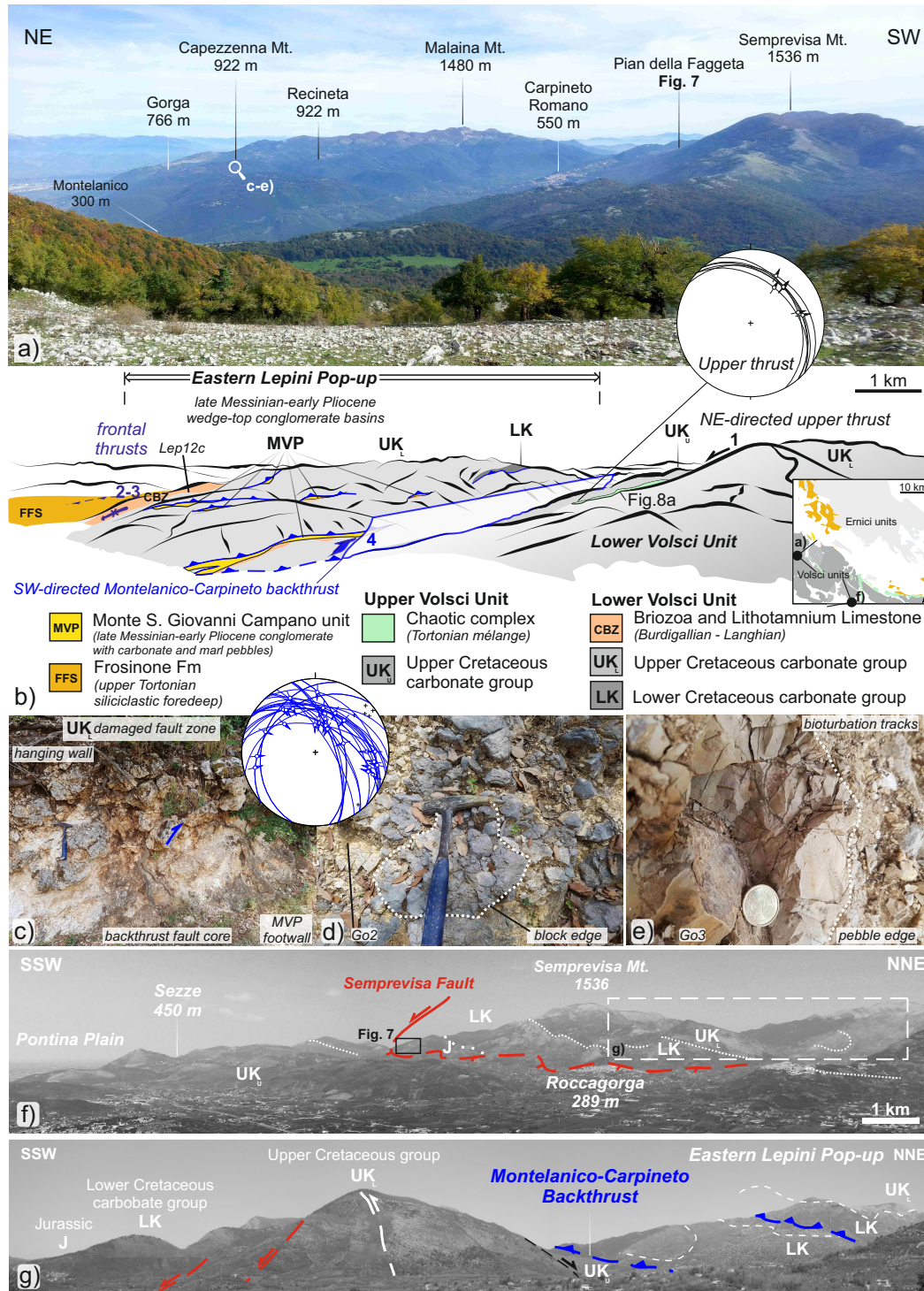


Figure 11. (a,b) Structural overview of the backthrusts in the northern Volsci Range with sampling sites (see Appendix B) and stereoplot (lower hemisphere projection, equal area) of bedding and backthrusts. (c) Thrust zone detail. (d) Block of conglomerate within conglomerate with clayish marly matrix. (e) Pebble of bioturbated marl with chondrites. (f,g) Structural overview of the Lepini sector and the Montelanico-Carpineto backthrust continuation towards the south beneath the Eastern Lepini Pop-up.

Along the southern slope of Semprevisa Mt. (i.e., the Semprevisa Fault), a major normal fault dissects the whole Jurassic-Upper Cretaceous succession, while along the northern slope, the top of the Mesozoic succession is overthrust by Upper Cretaceous units (documented in depth in the following sections). To the southwest, stepwise segments of normal faults bound the Pontina Plain (Figure 2). Further to the northeast, domino-like blocks are bounded by 2–3 km spaced faults, each with about 0.5 km downdip offset. More details on the Quaternary fault system are in [45].

4.3. Seismic Interpretation of the Latin Valley

By tracing the reflectors of the unconformable contact between the Meso-Cenozoic carbonates and the upper Miocene siliciclastic deposits on top (cf. Section 3.4), two major seismic units were recognized in the subsurface of the Latin Valley: (i) the Upper Ernici unit and (ii) the Lower Ernici unit.

The Upper Ernici unit crops out at Ceccano (Figure 2), and northwest of Morolo (Figure 9), where it constitutes a carbonate ridge in the middle of the Latin Valley. Coupled seismic and field geological evidence shows that the ridge is represented by detached Upper Cretaceous carbonates topped by a thick CBZ succession sealed by UAM and FFS units. The Upper Ernici Unit was drilled by the Frosinone 1, Ripi I, Ripi II, Pofi 1, and Ceprano 1 wells (Figure 3). This thrust-bounded unit is composed of a stratigraphic succession that can be correlated with the upper units of the Gavignano-1 well.

The Lower Ernici unit, apart from the distinctive near-top reflections, displays a variable amplitude and frequency with a discontinuous and chaotic pattern of reflectors that generally is characterized by noisy seismic facies. We exclude that this reflector is a coherent noise (multiple) as it can be followed over the entire study area and it displaces geometries that roughly differ from the above reflectors. Due to the scarce penetration of the seismic signal, this unit can be considered as the acoustic substratum of the area. No boreholes reached this unit. By comparison due to our reconstruction of the thrust geometry, the top of the Lower Ernici seismic unit is possibly represented by the Meso-Cenozoic carbonates that crop out northeast of the Latin Valley (Figure 2). Due to the above reported uncertainty, marks indicate the less-constrained portions of the interpreted cross sections.

Within the Latin Valley, minor thickness changes of the carbonate tectonic units occur. Due to the repetition of the top-CBZ reflector accompanied by underlying top-UK reflectors, we have recognized multiple repetitions of the Upper Ernici unit due to the occurrence of several thrust faults. The Ripi I well [106]), although crossing a major thrust zone, shows no siliciclastic deposits under the Mesozoic carbonates, but rocks of the *Orbulina* Marl and CBZ formations.

To show the general structural trend of the research area, we present three representative seismic lines (Figure 12), constrained by field and borehole data, showing thrust sheets characterized by a general top-to-the-NE sense of shear. Major thrusts, although occurring in all of the seismic lines, are well evident but discontinuous in number and distribution from line to line. Four major groups of thrusts form before the occurrence of normal faulting (Figure 13). From the most internal to the outermost we describe them as (1) the first group (thrust-1) marks the juxtaposition of the Chaotic complex on top of the FFS units and it can be correlated with the Upper Volsci thrust. (2) Thrust-2 marks the translation and doubling of the Upper Ernici unit within the Frosinone foredeep domain. No clear indication of the front could be recognized in the study area, possibly due to subsequent erosion. This structure is also represented by a series of thrust splays that cross-cut the formerly formed the fold-and-thrust fabric. Carbonate thrust-sheet units as thick as 0.6–0.8 s intervals have undergone significant translation in the order of 20–25 km. Considering that no thrust ramp could be observed toward the SE, this is a minimum estimate calculated on the hanging wall flat. (3) Thrust-3 is a group of reverse faults with flat-ramp-flat geometries that involve both the Upper and Lower Ernici units. The thrust-3 records a minimum offset in the range of 5 to 8.5 km. (4) The latest reverse faults belonging to the thrust-4 include the backthrusts at the northern edge of the Latin Valley.

Such backthrusts cross-cut the previous 1–3 thrust faults and allow the formation of a triangle structure, during the deposition of the MVP deposits in the structural lows. In the southernmost section (Figure 12; Section 3), the cut-off relationships provided by the latest thrusts may have allowed the exposure of Thrust-2.

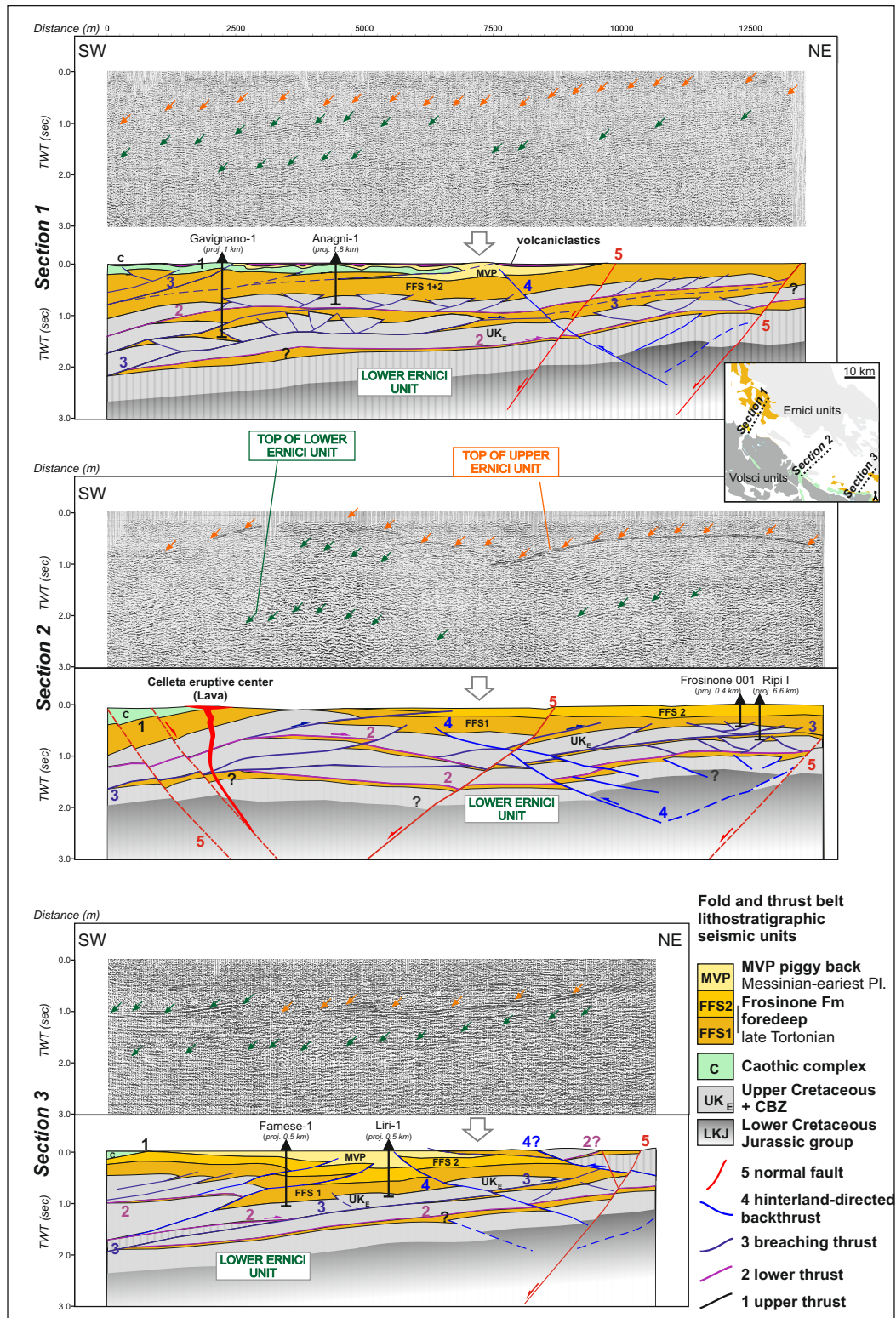


Figure 12. Two-times travel (TWT) seismic lines (from www.videpi.com (accessed on 20 January 2021); below, interpreted), also showing the projection of the wells. The location of both wells and seismic line traces of Section 1 (line label FR-309-80), Section 2 (FR-306-82), and Section 3 (FR-302-80) are in Figure 3. The vertical gray stripes highlight the Lower Ernici Unital.

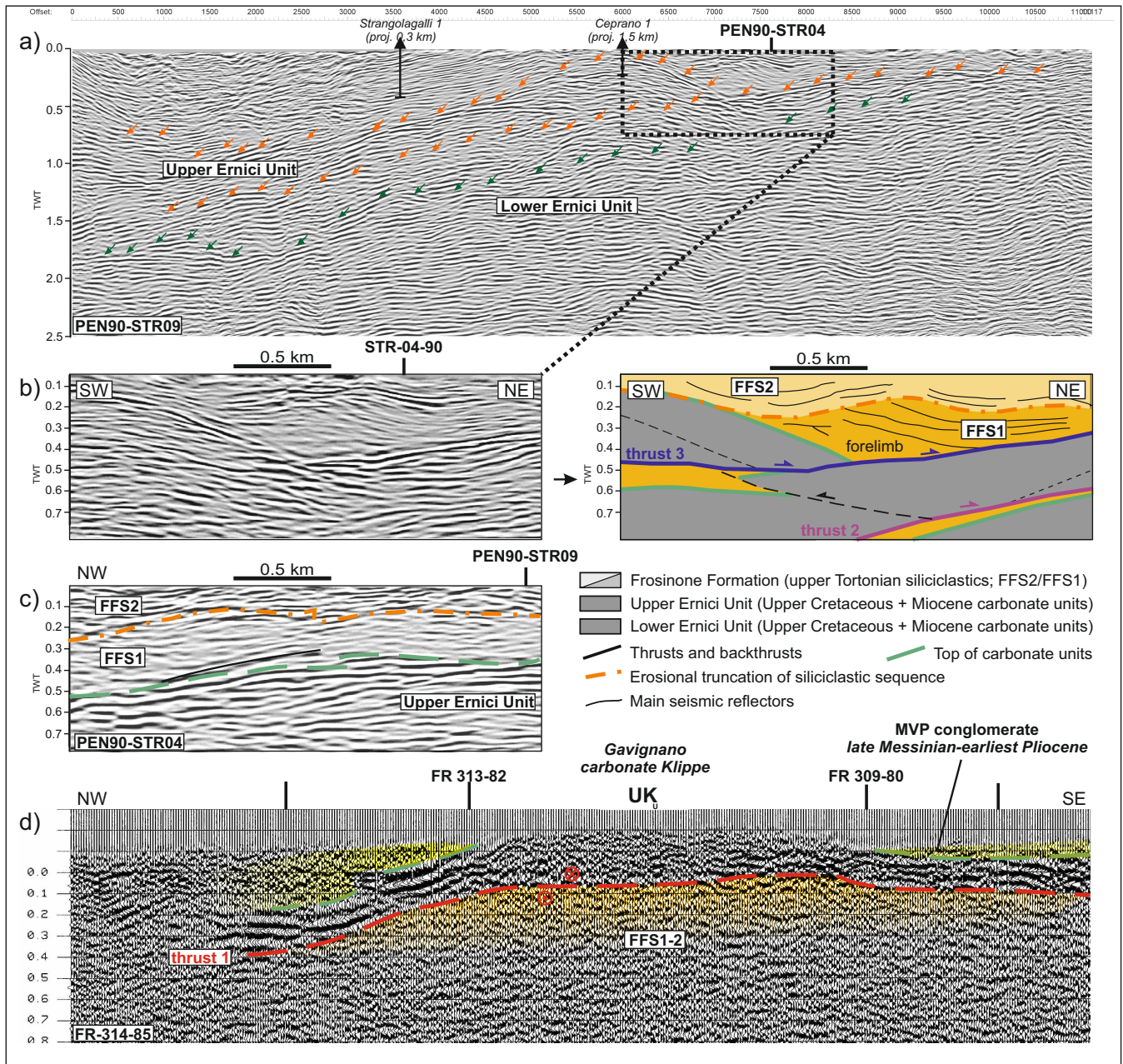


Figure 13. (a) Top-platform unconformities related to the upper (orange arrows) and lower Ernici units (green arrows) (Dip seismic line); (b) detail (right, interpreted) showing the angular unconformity between the Lower Frosinone seismic subunit (FFS1) and the Upper Frosinone seismic subunit (FFS2); (c) W-E view (Strike seismic line), showing the lateral variability of seismic facies FF1 and FFS2. (d) FR-314-82. Strike view of the Gavignano klippe, the purple dashed line marks the thrust onto the Frosinone Formation (transparent facies FFS), while the yellow dotted line highlights the top reflectors of the carbonates with the MVP conglomerate atop. Seismic line traces and well location in Figure 3.

The most prominent of this group of thrusts generates the outcrop of basal platform at the foothill of the VR Front. A few backthrusts were recognized at depth, with vertical displacement up to 1–2 km. In Figure 12, normal faults with appreciable offset were identified (labeled with number 5). NE-striking faults concentrate at the Latin Valley edges and do not clearly show in seismic lines. NW-striking faults bound Quaternary graben, where travertine, continental, and volcanoclastic deposits were cumulated. The normal fault trace in seismic lines was drawn when it is anchored to the outcrop evidence. In

these cases, we have extended the minimum offset recognized at surface to the deeper structural levels.

The most distinctive unconformities occur at the top of the Mesozoic carbonate succession and above the Middle Miocene CBZ Fm., overlapped by late Serravallian-early Tortonian UAM horizons (Section 3 in Figures 12 and 13). At the borehole scale this contact may appear as a paraconformity but the discontinuous and variable thickness of both CBZ and UAM suggest that this is actually an unconformity with an irregular erosional surface. Three subunits, divided by two major unconformities, can be observed within the siliciclastics deposits and labeled as Lower Frosinone seismic subunit (FFS1), Upper Frosinone seismic subunit (FFS2), and Monte San Giovanni Campano seismic unit (MVP); the first two are made by the late Tortonian Frosinone Fm., while MVP is formed by the Messinian piggyback deposits (Monte San Giovanni Campano unit; see MVP in Figures 2 and 12).

The thickness of the syn-orogenic units varies depending on the fold-and-thrust belt structure, being the siliciclastic deposits thicker to the south and to the north (up to 0.600 sec) and thinner in the central part (usually limited to 0.180 sec). As shown in Figure 13, Subunit FFS1 is folded together with the underlying carbonates, showing a transparent seismic facies, while Subunit FFS2 is thicker in the syncline and thinner towards the anticline and it is possibly related to Thrust-2. In FFS2, minor internal unconformities, typical of syn-depositional antiforms in foredeep basins, are here expressed by lobate-type seismic facies. In detail, the antiformal-growth geometries are crestal erosional truncations and diverging/converging reflection patterns around the hinge of the anticlines. In the piggyback basins, the FFS2 is defined by well-reflecting horizons and is marked by an erosive unconformity that at Ceprano cross-cuts both FFS1 at anticline culminations (Figure 13). This anticline is sealed by FFS2 and is formed on top of Thrust-3. As shown by the strike section in Figure 13, the thrust-and-fold geometry changes laterally as also reported for the Gavignano klippe more to the north.

5. Discussion

The tectono-stratigraphic analysis of field and subsurface data enabled us to define different thrust units, providing insights for a time-deformation analysis of one of the innermost portions of the Central Apennines. Hereby, we present a geological cross section, interpretative of the deep structures produced after the integration of field and subsurface structures (Figure 14), that includes pre-orogenic passive margin deposits, mélangé units, foredeep, and wedge-top deposits. In the following, we discuss the main novel features of the geologic history that led to the development of the geological setting of Figure 14. In the cross section, we correlate the Upper Volsci Unit remnants of the Colle Cantocchio, Carpineto Romano, and Caccume Mt klippen. Based on the mixed exotic-native composition of the blocks of the Chaotic complex, we recognize that they were overthrust together with the Upper Volsci Unit on top of the Lower Volsci Unit. As shown in the cross section, the Lower Volsci Unit of the Western Lepini Mountains is a monocline essentially composed of Jurassic to Cretaceous carbonates dipping to (E)NE, that together with the remnants of the upper units was further crossed by high-angle faults. In detail, the Montelanico-Carpineto backthrust, bounds the Eastern Lepini pop-up that is affected by small-scale folds and reverse faults, whose geometry suggests positive reactivation of pre-orogenic normal faults during shortening. The wedge-top pockets preserved by the backthrusts are infilled by MVP Messinian conglomerate that was deposited directly on the Lower Volsci Unit, when the Upper Volsci unit was already dismantled. Thrusts and folds are mostly evident in the Latin Valley (Figure 12), whose substrate has been reconstructed by applying a depth conversion on a structural model published in [45].

By studying the top of the Mesozoic carbonate platform both in the Lower Volsci Unit and in the blocks embedded in the Chaotic complex (Appendix B; Figure S1), we have reported the occurrence of an irregular surface at the top of the platform. Such a paleotopography was likely the result of Late Cretaceous syn-sedimentary tectonics. In such scenario, the most elevated structures might have been affected by karstism (possibly with

the formation of ferruginous crustons) during the latest Cretaceous (see Section 4.1). The occurrence of a Late Cretaceous tectonics is supported by the lithostratigraphic unit we refer to the “Gorga bioclastic limestone and dolostone” upper Campanian to Maastrichtian in age, whose lateral change and abrupt facies shift points to syn-depositional tectonics (Figure 2). At Gorga (Figure 3), this unit is represented by about 250 m thick rock volume [112], that thins rapidly towards the west, whereas it lacks in the rest of the Volsci Range. In particular, as recognized at Caccume Mt. and near Carpineto Romano (Figure 5), the unconformity occurring at the top of the platform is marked by a very thin younger breccia partially overprinted by a dolomitic and ferrous cruston (cf. Figures 5 and 9), whose age and origin need to be further constrained.

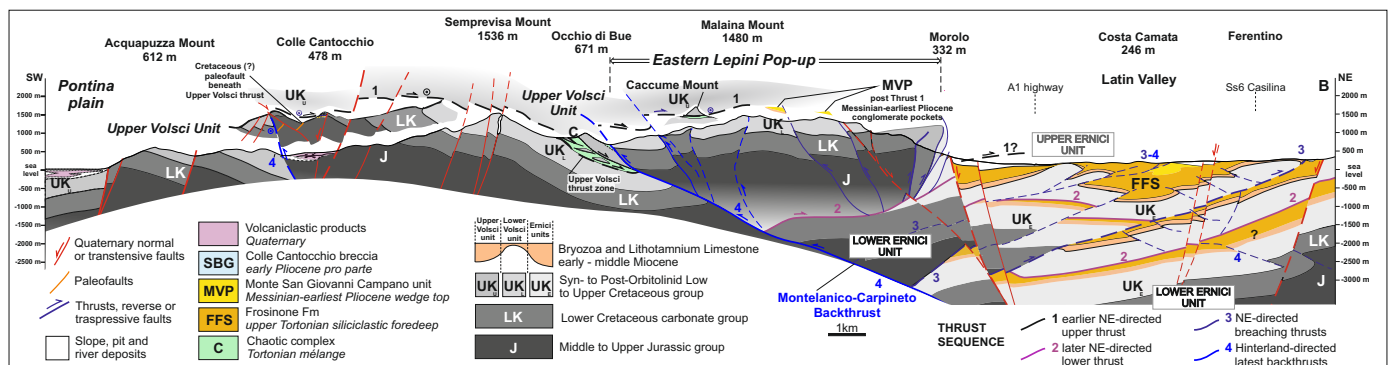


Figure 14. Geological cross section AB (trace in Figure 3) interpretative of both field and subsurface data converted to depth (see methods). Numbers related to the group of faults are disposed as in Figure 12. In the Volsci Range, the Upper Volsci Unit experiences about 25 km of thrusting (Thrust-1) towards the ENE. Thrust-2 accommodated the overthrust of the Volsci Range and Upper Ernici Unit on top of the Frosinone Formation. In Latin Valley, the Upper Ernici unit is doubled by the breaching of Thrust-3. Late reverse faults (Thrust-3 and -4) contribute to forming a triangle zone in the Latin Valley and backthrusts in the rear. Normal faults generate a graben in the Latin valley and SW dipping faults towards the Pontina Plain.

In the Apennine platform, the transition from the Upper Cretaceous carbonates to Paleocene–Eocene margin, slope, and Scaglia-type basin deposits was guided by a synchronous regional extension during Maastrichtian–Eocene time that affected both the Jurassic base-of-slope domains [30] and the demised sectors of the neritic platforms [118]. We recognize that the discordant stratigraphic contacts of Colle Cantocchio are due to the development of a submarine paleoescarpment, guided by normal faults down-stepping towards the WSW. The bluish hardground (highlighted by yellow dots Figure 15) can be interpreted as a submarine unconformity marking the onlap (escarpment contact) of the lower Miocene intraformational pebbly calcarenite on the Mesozoic carbonates. Similar facies have been reported elsewhere by the authors of [119] and are here interpreted as a diagenetic effect on the articulated inherited physiography of the previously unedited fault escarpment described in Figure 6. A simplified back-restoration of section C-D (Figure 7c) is attempted in Figure 15, where a fault step occurred to the south with an offset in the order of 700–1000 m due to the exposure of the Jurassic terrains and the downthrowing of the Cretaceous units in the hanging wall. The Semprevisa Fault can be still recognized laterally for over 10 km, although overprinted by later Pliocene–Quaternary tectonics, and possibly remarks at least part of this inherited structure. In our interpretation, as shown by the stratigraphic contacts, the Jurassic units of the southwestern slope of the Semprevisa Mt. were already exposed in early Miocene time (Figure 15). As suggested by the clasts within the Chaotic complex, coeval basinal sedimentation occurred more to the WSW [120]. In particular, the recognition of Cretaceous–Paleogene Scaglia lithotypes and of distal early Miocene CBZ limestones in the exotic blocks of the Chaotic complex (see Figures 7, 9 and 10) suggest that sedimentation occurred in a bypass slope setting during Paleogene–Neogene time. In particular, the Paleogene is recorded by a condensed to hemipelagic sedimentation, evolving during the Miocene to mixed calcareous-siliciclastic turbidites with chert. The *Orbulina* Marl Fm. (Serravallian pp.) sealed the pre-orogenic early Miocene topography.

The Colle Cantocchio pre-orogenic fault is a part of the normal fault system that produced the steps from the exposed Jurassic carbonates to the basin and is here proposed to be at least Eocene in age, although older ages cannot be excluded. Synthetizing, according to the new data, we propose a provenance of the Chaotic complex (i.e., including the exotic blocks) from a hemipelagic paleogeographic domain with slow depositional rates placed to the WSW of the present-day Volsci Range.

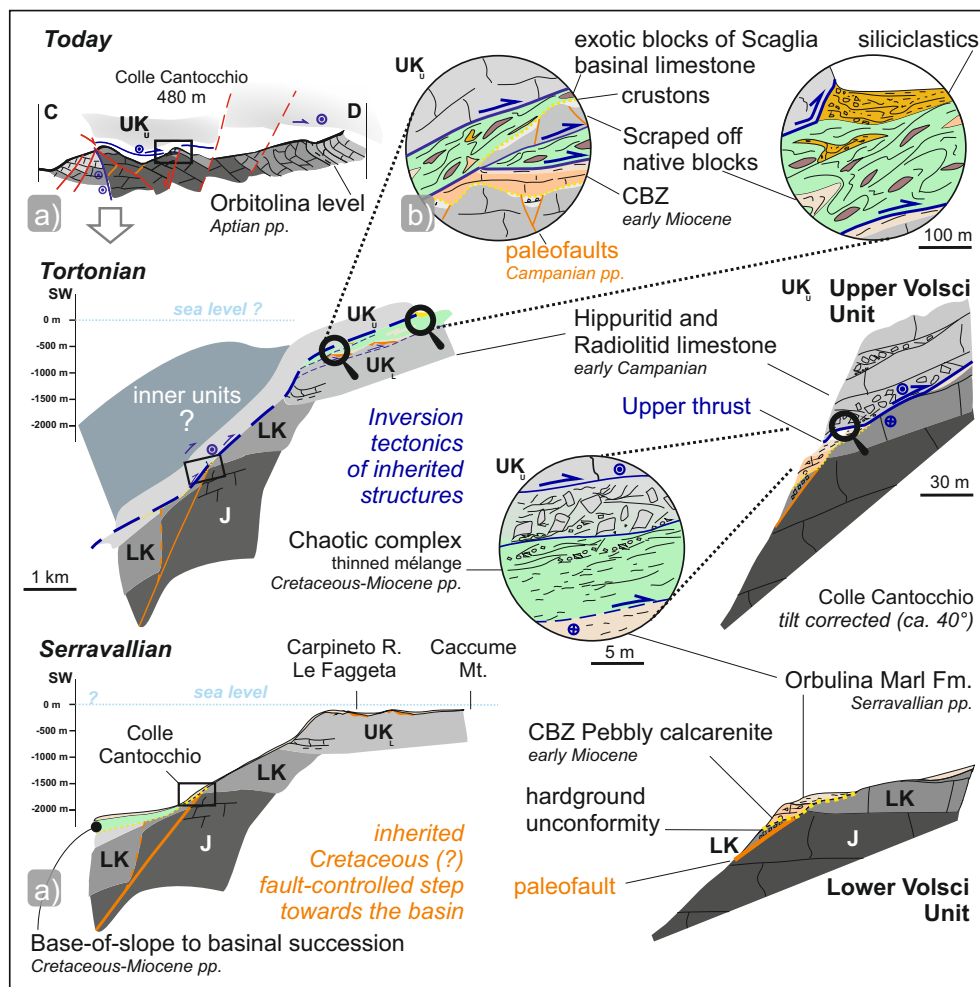


Figure 15. Reconstruction of the ramp-flat geometry of the upper thrust after restoration of section C-D by removing late backthrusts and normal faults. During Tortonian time, inversion tectonics of inherited structures occurred on a ramp by the overthrusting of the Upper Volsci Unit. At the transition from ramp to flat, native blocks were scraped off from the Lower Volsci Unit. On the right, peculiar settings inspired by field examples are contextualized to understand the mélangé formation. During Serravallian time, the inherited structure was sealed by Orbulina Marl hemipelagic deposits. To the southwest, base-of-slope to basinal Cretaceous-Miocene deposits occurred on a fault-controlled step of the platform. On the right, a detail of the paleoscarpment setting prior to thrusting.

The ongoing research in the southern Volsci Range, is providing constraints for the determination of the age of the encrusted normal faults bounding the Formia plain and Spigno Saturnia areas, whose data from the literature are reinterpreted above (cf. Figure 2). A comparable syn-sedimentary setting, leading to the deposition of Scaglia deposits has been recorded nearby the VR [8,121] and documented at the western tip of the Volsci Range [122]. Of note, at Colle Cantocchio (Figure 5), the early Miocene transgression over the Jurassic-Lower Cretaceous rocks occurred on a step of the escarpment, where there was no record of Paleogene basinal sedimentation. In alternative, this sector could be associated with renewed normal faulting activity along a pre-existing Cretaceous-Paleogene normal

fault, which may have further exposed the Mesozoic rocks with its reactivation and allowed the CBZ-UAM units to settle on top prior to the Tortonian onset of thrusting.

5.1. Chaotic Complex Emplacement and Thrust Propagation

To define the overthrusting towards the (E)NE of the Upper Volsci Unit and to understand the evolution of the Chaotic complex, we correlated the carbonate klippen by documenting the stratigraphic and structural elements of the syn-orogenic deposits. This correlation was initially proposed by Accordi [71], but inherited structures, thrust kinematics, and age of the syn-orogenic deposits needed to be better constrained. With the degree of allochthony and origin of the Chaotic complex being long debated [45,64,67,86,123], in this section we discuss the Chaotic complex origin and the role of the thrust propagation towards the foreland into the late Miocene wedge growth.

Starting from the southwest, the Colle Cantocchio cataclasite and shale preserved underneath the Upper Volsci Thrust can be interpreted as a thin Chaotic complex unit juxtaposed on the paleo escarpment setting (c.f. Section 5.1). In this frame, the inherited topography produced a ramp in the upper thrust during shortening. A comparable setting occurs more to the south at the Vele Mt. (Figure 2), where the siliciclastic deposits underneath the thrust could be correlated with the Chaotic complex sliver of Colle Cantocchio (Figure 15). As commonly occurring in mélangé complexes [124,125], the Chaotic complex formed at the expenses of the Lower Volsci Unit, whose inherited and articulated top was scraped off and grooved (see Figures 7–9). The Chaotic complex is a combination of (i) autochthonous “native” and (ii) allochthonous “exotic” blocks (Figure 15). The latter derive from a discontinuous series of Paleogene-Burdigalian pelagic deposits deposited more to the south and progressively mixed with lower Serravallian to upper Tortonian siliciclastic units bearing also crystalline clasts.

In particular, the matrix of the Chaotic complex shows the same composition of the embedded blocks, but it also shows the occurrence of late Tortonian-Messinian microfossil assemblages, which may have deposited during the final stage of thrusting related to the Upper Volsci Thrust. Further, we are able to further narrow this time range to the late Tortonian, considering also the absence of *Amaurolithus* sp., typical marker of top Tortonian-Messinian. Provided that the overthrust of the pelagic elements of the Chaotic complex is due to the juxtaposition of the Upper Volsci Unit, which squeezed them out towards the foredeep, they must have originated from about the same distance reached by the Upper Volsci Thrust front (Thrust-1).

In this frame, the SE-ward termination of the Chaotic complex and the lens-like shape of the outcrop at Carpineto Romano (Figure 6) provide an example of interaction between inherited top-platform physiography and thrust geometry. In our interpretation, this structure is an inherited depression at the top of the platform that was later crosscut by the Upper Volsci Thrust. At its southern tip, as demonstrated by Accordi [71], this thrust still occurs as it doubles of the upper Cretaceous units although not involving anymore the Chaotic complex, whereas, as shown on the map (Figure 6), at the northern of the Upper Volsci Thrust, the younger Montelanico-Carpineto backthrust cross-cut it (Figure 11).

The Upper Volsci Unit is mainly composed by Upper Cretaceous neritic carbonates (e.g., Carpineto Romano, Figure 8), implying that this unit detached essentially above the uppermost Lower Cretaceous Orbitolina Marl level during shortening. However, although rare, older Mesozoic rocks can also be found. A second detachment level, highlighted by subsurface data, corresponds with the Orbitolina Marl Fm, which allowed the doubling. The chronological relationship between Thrust-1 (marking the overthrust of the Upper Volsci Unit on to the Upper Ernici unit) and Thrust-2 (between the Ernici Units of the Latin Valley) is beneath the resolution of our data. However, provided their geometrical distribution, these thrusts are likely to represent a classical thrust propagation towards more external and lower structural levels through time (i.e., towards the foreland). The minimal shortening associated with Thrust-1 is of about 25–30 km, which corresponds with the approximated present-day distance between Colle Cantocchio and the frontal klippe

along the ENE-directed Thrust-1; while Thrust-2 ranges about 20 to 25 km as shown by the thrust-2 structures in Figure 14. These amounts are comparable with the shortening estimated at the thrust fronts of the Gran Sasso Massif (>20 km [30]) and of the Apennine platform in the southern Apennines (>60 km [126]), while it is significantly lower than the translation that affected the Ligurian Accretionary Complex onto the foredeep units (> 100 km [127]). In this frame, the Tortonian southern Apennine platform thrusting [28] matches our thrust dynamics (Figure 15). As also typical of the far-traveled Sicilian platform units [128], the thrust geometry is characterized by long flats (10–15 km) and thin thrust-sheets, that in our case can be as thin as about 0.7 km near the front. This implies that the Orbitolina level and Orbitolina Marl Fm preferred slip levels were very efficient in allowing far-traveled thrusting.

As shown by thickness and facies variations of the siliciclastic deposits of the Latin Valley, the Thrust-2 shortening stage was accompanied by syn-sedimentary folding of the deposits of the FFS2 seismic unit (Figure 13). In our interpretation, while the unconformable FFS1 contact with the CBZ limestone marks the flexuration of the foredeep, the unconformable contact associated with wedge shape and channelized FFS2 facies marks the growth of pop-up anticlines, thus being representative of wedge-top settings initially developed during Thrust-2.

The channelized facies may be, respectively, representative of syn-tectonic fringe and lobe deposits and of inner channelized sand bodies, while pelitic facies are rather typical of outer fans [129]. In particular, the observed syn-sedimentary folded channelized structures (Figure 10b), show that, the deposition of the Frosinone Fm. thus encompassed an increasing input (mostly during the FFS1 stage), later followed by a progressive channelization of turbidity flows onto the synclines during the FFS2 stage. As already suggested in [130] for the Latin Valley on the channelization of the foredeep to wedge-top sediments, the active margin possibly followed a comparable evolution similar to what elsewhere envisaged in the southern Apennines by Casciano et al. [131].

At the front of our study area, a transition between the *mélange* and the flysch units occurs. Based on published maps [64], wells, and seismic lines on the southwestern edge of the Latin Valley, we also confirm that the Chaotic complex is juxtaposed to the Frosinone Fm. of the upper Ernici unit (cf. Gavignano; Figures 10 and 13). For this feature, the authors of [132] proposed an olistostrome origin, while Centamore et al. (2007) proposed gravitational sliding of the Chaotic complex off the Volsci Upper UnItal. Further, this level can correlate with the *mélange* levels of the Massico Mt. [43,133].

To explain the abrupt thickening of the Chaotic complex east of the Caccume Mt. (Figure 10), we suggest that a growth structure was forming during the initial uplift of the Volsci Range front as testified by fault-propagation fold (Figure 14) at the hanging wall of thicker FFS units with syn-sedimentary folds (Figures 10 and 12). This generated the glide of the Chaotic complex on top of the FFS units. Similar contexts were reconstructed for other *mélange* units at thrust fronts, where the remobilization of the formerly emplaced thrust sheets, allows the incorporation of the extrabasinal (exotic) lithologies within the foredeep [18,134]. An alternative possible explanation to allow the juxtaposition of the Upper Volsci unit onto the FFS units, would envisage thrusting to occur during the uppermost Tortonian-earliest Messinian.

5.2. The Late Stages of Shortening

As observed in seismic lines (Figures 12 and 13), thrust-3 produced the doubling of the flat of the far-traveled Thrust-2, by involving deeper carbonates in the thrust ramps. We have also shown that in the area break back thrusting occurred [135] (Figure 16). As shown near Ceprano well (Figure 13), MVP wedge-top deposits that include calcareous pebbles from the CBZ unit [87] were directly deposited on Mesozoic carbonates deformed by an anticline. This contact is representative of a wedge with regional subsidence slower than local antiformal growth [136]. Nannoplankton determination finally allowed constraining the age of the folded conglomerates and atop marls of Gavignano, thus allowing a correlation

with the MVP stratigraphic unit (Figure 10). This unit represents a folded Messinian thrust top deposit and this constraint attributes this late folding stage to late Messinian–earliest Pliocene time. As supported by subsurface data (Figures 3 and 13) the Gavignano klippe was involved into the renewed deformation of the VR front, which would correspond with the latest stage of thrusting and veining dated in [43] at the late Messinian on the Massico Mt. (cf. Figure 2). Those absolute constraints can be used to review the regional thrust kinematics. In this sense, the ages determined along the thrusts in areas more to the south can be compared to what provided in [114]. These authors have attributed a late Miocene–Pliocene age to the clayey matrix beneath the thrust at the front of the Siserno Mt. Similar to what reported for the Chaotic complex in this work (Appendix B), they have also reported that the exotic clasts are representative of a wide range of ages, from Late Cretaceous (including Scaglia Rossa pelagic limestone) to early–middle Miocene. The degree of fragmentation of microfauna embedded within the Chaotic complex [114] suggests active deposition during the late Miocene–Pliocene as well. Therefore, we can envisage a late involvement of Pliocene deposits into the reactivated thrust zones at the VR front. In this interpretation, the Chaotic complex was already exhumed likely after the strong erosion related to the Messinian salinity crisis [137–140], which also affected the Ernici Mts [77], implying reactivation in the rear [49].

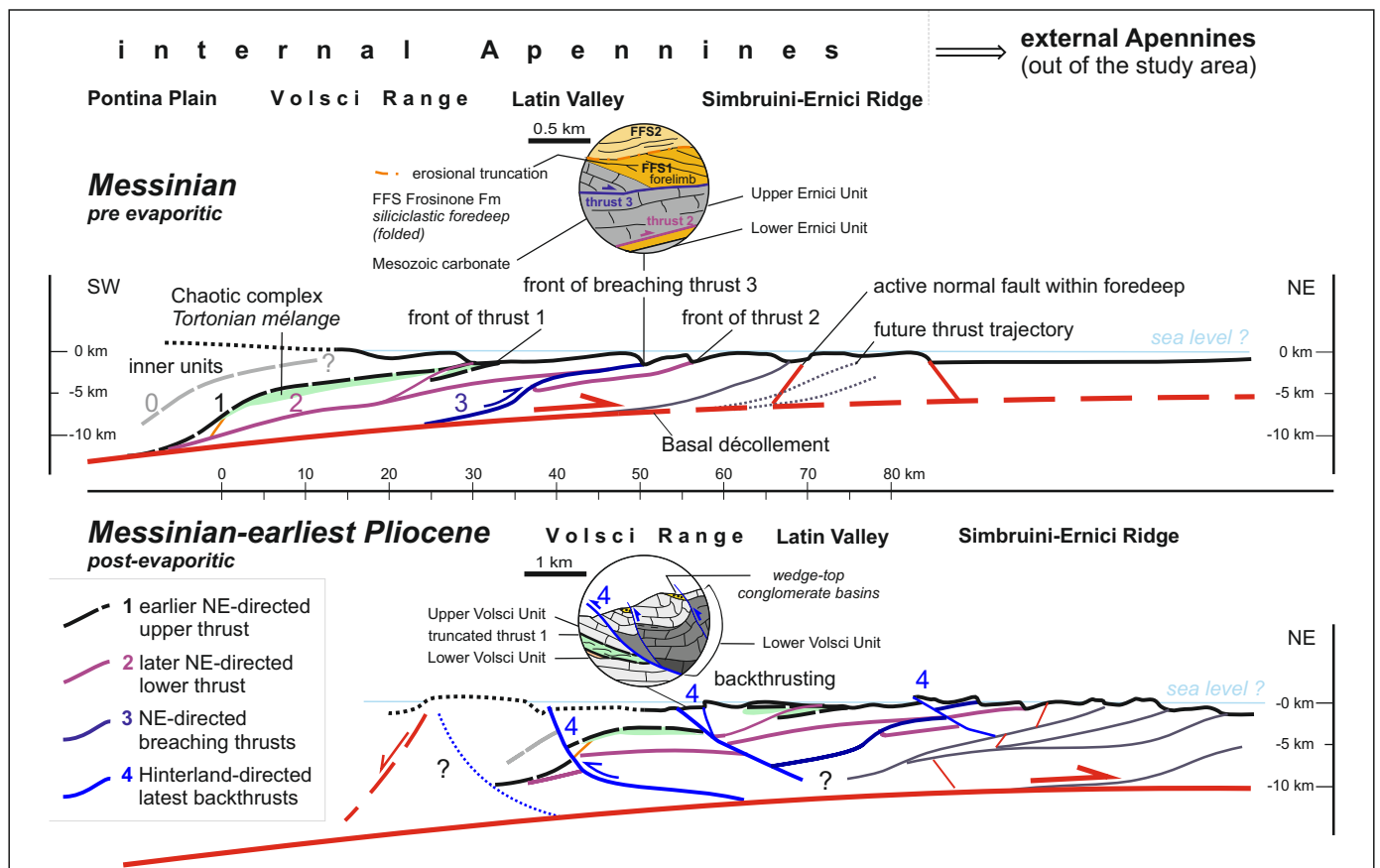


Figure 16. Sketch of relative timing and geometries of fore- and back-thrust involving different generations of thrusts (1–4) within the Apennine wedge through time. Backthrusts generate at progressively lower depths, moving towards the hinterland (to the left), due to the dip of the basal detachment.

In this context, the late Messinian shortening event could be correlated with the late orogenic structures in the northern VR that are crossed by a series of SW-directed backthrusts (Figure 11). In our interpretation, the SW-directed Montelanico-Carpineto back-thrust cross-cuts the top-to-the (E)NE older Upper Volsci Thrust. Despite the lack of valuable data from the main lineament, minor thrusts show that top to the SW-backthrusting,

could be accounted as partially reactivating the older fabric. Further, the fault strike of the backthrusts diverges about 20° from the trend of the upper Volsci Thrust that is underthrust beneath the Eastern Lepini pop-up (Figures 5 and 11).

So far, scarce constraints of top-to-the-SW shear were found, although backthrusting is possibly localized more to the NE of the studied area of Figure 11. Our stratigraphic constraints (Appendix B) from the MVP conglomerate near Gorga, document Messinian Lago-Mare conglomerates that are produced after iterative cannibalization of older wedge-top deposits. The further occurrence of upper Messinian deposits in the Pian della Faggeta area (Figure 5), is a possible clue indicating depositional activity on top of the Volsci Range during the Messinian salinity crisis (5.96–5.33 Ma). During that time, the area was exposed to linear erosion followed by the deposition of sandy gravels that Centamore et al. (2010) dated at the early Pliocene (south of Castro dei Volsci; Figure 3). This implies that the major valleys were already formed before the latest orogenic compressional events affected both the VR and Latin Valley [117]. Field evidence in the rear (Figure 5), suggests the presence of a major backthrust with transpressive kinematics further south, possibly implying that a deeper backthrust affected the southwestern slope of the VR during the early Pliocene. At that time, the Apennines experienced renewed shortening with frontal thrusting accompanied by backthrusting and tilting toward the foreland to the northeast (Figure 16).

During late orogenic deformation, thrust front migrated towards the outermost active margin units (Figure 1), and the inherited fold-and-thrust belt of the external Apennines was folded together with lower Pliocene syn-orogenic conglomerates (i.e., Rigopiano conglomerate [30,78]). Meanwhile, the previous in-sequence structure of the internal Apennines was truncated by triangle zones (Figure 12) and by more internal backthrusts (e.g., in the Volsci Range, Figures 11 and 14).

In our interpretation (Figure 16), the backthrusting roots at deeper levels, by following the dip of the basal detachment towards the backarc. In this sense, moving to the inner parts of the wedge, the inner wedge is remobilized, affecting a larger volume with respect to the external part. In the case of late orogenic deformation affecting only the sedimentary cover, shortening localizes within the weakest stratigraphic levels, possibly by reactivating the décollement of the older fore-thrusts [136,141–145], while in the rear faulting tends to broaden and possibly involve also deeper structural levels.

Finally, Pleistocene to Holocene NW- and NE-trending normal faults deeply affected the fold-and-thrust belt structure. In particular, the almost constant NE-dip shown by the bedding planes of the studied carbonates might be interpreted as the result of the activity of the major NW-striking and SW-dipping listric normal faults bordering the Pontina Plain, which were also documented at depth [146].

6. Conclusions

This study contributes to constraining the timing of initiation and progressive development of platform-derived thrust sheets, mélange units, foreland, foredeep, and wedge-top sediments of the internal Central Apennines. The main phases of the evolution of the belt are as follows:

1. Late Cretaceous extensional tectonics. The dismembering of the carbonate platform into shallower and deeper domains is constrained by the finding of crustons that may testify moments of subaerial exposure, characterizing the top of the Lower Volsci UnItal. Cave exploration and field mapping allowed us to recognize a previously unreported fault-controlled paleo-escarpment constituted by Cretaceous and Jurassic carbonates sealed by early Miocene deposits that were previously dated as middle Miocene. These units seal a hardground settling on a platform edge facing to the west, where basal to bypass slow-rate sedimentation occurred till Burdigalian time.
2. Tortonian Chaotic complex emplacement (Thrust-1) and foreland-directed (in-sequence) thrust propagation (Thrust-2). During the overthrusting of the Upper Volsci Unit, Paleogene to Neogene basal deposits were squeezed off towards the Foredeep and

juxtaposed as a *mélange* unit on top of the carbonate platform together with early to middle Miocene calcareous-cherty-siliciclastics. The Chaotic complex also bears highly deformed basinal exotic and native blocks of neritic carbonates, the latter being scrapped off by the overthrust of the embedding Chaotic complex, whose Paleogene–Miocene matrix includes up to Tortonian nannoplankton. Seismic analysis supported by well logs at the regional scale highlighted repeated carbonate thrust sheets that have first been involved into an initial in-sequence propagation towards the foreland to the ENE occurred during foredeep to wedge-top sedimentation.

3. Intra Messinian thrusting (Thrust-3) breached the thrust front by doubling the flat of previous thrust fronts. Subsurface data show that during alternated phases of wedge-top deposition and erosion, the Upper Ernici unit was shortened approximately 5–8.5 km in the Latin Valley.
4. Messinian to early Pliocene backthrusting (Thrust-4). New biostratigraphic data constrain the thrust top deposits in the Volsci Range and in the Latin Valley, where SE-directed backthrusts contributed to the tilt and cross-cut of previous Thrust-2 and -3 structures.
5. Late Pliocene to Holocene normal faulting. Post-shortening extension has determined NE- and NW-striking orthogonal normal faults or WNW–ESE-trending right-lateral transtensional faults. These faults may have locally intercepted pre-existing normal faults that had been passively transported within the thrust sheets.

Finally, our findings bear implications on platform derived thrust sheets associated with active margin successions and *mélange* units. The far-traveled thrust sheets, hereby documented both in the field and in the subsurface, constitute a key aspect for the development of the internal Apennines, whose degree of allochthony and role of inherited structures was long debated. Furthermore, at the light of our new interpretation, the deeper platform units could be a new focus for hydrocarbon accumulation and may provide targets for geothermal and/or hydrocarbon research in the area. Beside the regional geological aspects, this work bears implications on the modes of involvement of *mélange* units at the transition from passive margin to foreland basin systems.

Supplementary Materials: The following are available online at <https://www.mdpi.com/article/10.3390/geosciences11040160/s1>.

Author Contributions: Conceptualization, G.L.C., G.V., L.C., M.S., and E.C.; methodology, G.L.C., and G.V.; software, G.V.; validation, E.C. and C.D.; formal analysis, G.L.C., G.V., L.C., and M.S.; investigation, G.L.C., G.V., L.C., M.S., and E.C.; resources, E.C., L.C., and C.D.; data curation, G.L.C., G.V., L.C., and M.S.; Writing—Original draft preparation, G.L.C., G.V., and L.C., Writing—Review and editing, G.L.C., G.V., L.C., M.S., and E.C.; visualization, G.L.C., G.V., L.C., and M.S.; supervision, E.C. and C.D.; project administration, G.L.C. and E.C.; funding acquisition, E.C., L.C., and C.D. All authors have read and agreed to the published version of the manuscript.

Funding: This research was funded by Progetti di Ateneo 2016 (C. Doglioni), 2017 and 2019 (C. Doglioni and E. Carminati) and by the Spanish Ministry of ‘Economía y Competitividad’ (projects CGL2012-33160 and CGL2015-69805-P).

Data Availability Statement: Data used for seismic interpretation and model reconstruction can mainly be found in the public VIDEPI database (www.videpi.com) (accessed on 20 January 2021) and in the Pentex Ltd. database. Data available at the ENI data room were also viewed.

Acknowledgments: We gratefully acknowledge Pentex Limited Italia and Luigi Albanesi for the permission to analyze their subsurface data and publish the seismic lines of the Strangolagalli Oil Concession area. We acknowledge ENI for the permission to participate at the data room as requested in San Donato Milanese, Milan, and in particular to analyze some seismic lines on old Permit Areas. We thank the G. Wang and the D. Liotta, G. Molli and A. Cipriani for the opportunity to share our research in the Special Issue “The Apennines: Tectonics, Sedimentation, and Magmatism from the Palaeozoic to the Present”. Enrico Tavarnelli, Andrea Artoni and an anonymous reviewer are acknowledged for insightful comments and suggestions. We are grateful to “Gruppo Grotte Castelli

Romani”, “Federazione Speleologica del Lazio”, Andrea Cesaretti, Piero Ciccaglione, Pio Di Manna, Simone Fabbi, Luca Forti, Angelo Giuliani, Domenico Mannetta and Anne Mérienne for their support.

Conflicts of Interest: The authors declare no conflict of interest. The funders had no role in the design of the study; in the collection, analyses, or interpretation of data; in the writing of the manuscript; or in the decision to publish the results.

Appendix A

In the following, we report the Biostratigraphic and lithostratigraphic data of outcrops and stratigraphic units available from the literature related to syn-orogenic deposits shown in the representative stratigraphic logs of Figure 2 in the main manuscript. The formation labels are also related to Figure 2.

Site n°	Group of Localities	Latitude	Longitude	Tectonic Unit	Formation	Lithology	Biomarkers	Age Range	Comments	Author
1	Gavignano R. klippe	41°42'9.16" N	13°20'38.15" E	Upper Volsci unit	DLA	limestone	<i>Cisalveolina fraasi</i>	Cenomanian	in situ	[147]
		41°42'9.16" N	13°20'38.15" E	Upper Volsci unit	MVP	calcareous conglomerate	<i>Globorotalia apertura</i> , <i>G. involuta</i> , <i>G. concinna</i> , <i>Globigerina falconensis</i>	uppermost Tortonian-lowermost Zanclean	reworked	[103], this work
		41°42'9.16" N	13°20'38.15" E	Upper Volsci unit	PGC	polygenic conglomerate	no data	upper Messinian (?)		[103]
2	Colle Cantocchio klippe	41°34'29.48" N	13°0'1.49" E	lower Volsci unit	RDT	limestone	<i>Dicyclina schlumbergeri</i> , <i>Accordiella conica</i> , <i>Orbitoides</i>	Campanian	in situ	[93]
		41°34'29.48" N	13°0'1.49" E	lower Volsci unit	CBZ	calcareous	echinid, <i>Ditrupea</i> , <i>Elphidium</i> , bryozoa, <i>Miogyospina</i> , <i>Amphistegina</i> , <i>Operculina</i> , <i>Heterostegina</i> , <i>Lepidocyclus</i>	Burdigalian	in situ	[93]; this work
		41°34'29.48" N	13°0'1.49" E	lower Volsci unit	UAM	gray-yellowish clay	<i>Orbulina universa</i> , <i>O. suturalis</i> , <i>O. bilobata</i> , <i>Globorotalia</i> aff. <i>Menardii</i> , <i>Globorotalia opima</i> , <i>Globorotalia scitula ventriosa</i> , <i>Globigerinoides trilobus</i> , <i>Globigerina eggeri</i> , <i>Globigerina</i> cf. <i>Bulloides</i> , <i>Globigerina concinna</i> , <i>Globoquadrina dehiscens</i> , <i>Globoquadrina altispira</i> , <i>Bolivinoidea miocenica</i> , <i>Valvulina pennatula italica</i> .	upper Serravallian—Tortonian P-P.	reworked	[93]
		41°34'29.48" N	13°0'1.49" E	Upper Volsci unit	SBG?	polygenic breccia	no data	Pliocene-Pleistocene (?)	reworked	[93]
3	Carpinetto Romano	41°35'17.12" N	13°06'15.66" E	lower Volsci unit	RDT	limestone	rudist, <i>Dicyclina schlumbergeri</i> , <i>Rotalispira</i>	Coniacian-Campanian	in situ	[103]
		41°35'17.12" N	13°06'15.66" E	lower Volsci unit	CBZ	limestone	<i>Amphistegina</i> , <i>Heterostegina</i> , bryozoa, <i>Operculina</i> , <i>Miogyospina globulina</i>	Burdigalian—Langhian	in situ?	[103]
		41°35'17.12" N	13°06'15.66" E	Upper Volsci unit	RDT	limestone	<i>Rotalispira maxima</i>	lower Campanian	native block within C	this work—sample LEP 17C

Site n°	Group of Localities	Latitude	Longitude	Tectonic Unit	Formation	Lithology	Biomarkers	Age Range	Comments	Author
		41°35'17.12" N	13°06'15.66" E	Upper Volsci unit	RDT	limestone with iron crust (ancient karstification ?)	<i>Decastronema, ostracodae, discorbidae</i>	Campanian	native block within C	this work—sample LEP 18B
		41°35'17.12" N	13°06'15.66" E	Upper Volsci unit	Scaglia s.l.	limestone	Heteroelcidae, Hantkeninidae, <i>Schackoia, Guembelina, Clavhedbergella, Globorotalia</i>	Albian?; Maastrichtian-early Eocene	exotic block within C	[71,148]
		41°35'17.12" N	13°06'15.66" E	Upper Volsci unit	C	glauconitic calcarenite	<i>Orbulina, Globigerinoides sacculiferus, Globoquadrina altispira, Globigerina paraboloides, Bigenerina nodosaria</i>	upper Serravallian-Tortonian P-P.	reworked	This work; [103]
		41°35'17.12" N	13°06'15.66" E	Upper Volsci unit	UAM	marl with cylindrites and calcarenite	<i>Sphenolithus heteromorphus, Cyclicargolithus floridanus, Reticulofenestra pseudoumbilicus, Coccolithus miopelagicus, Helicosphaera walbersdorfensis, Calcidiscus premacintyreii, Neogloboquadrina continuosa, Neogloboquadrina acostaensis.</i>	upper Serravallian	exotic block?	[72]
4	Gorga, Capezzenna Mt.	41°37'38.45" N	13°08'32.37" E	lower Volsci unit	RDT	limestone	<i>Rotalispira maxima, Dicyclina schlumbergeri</i>	Santonian-Campanian	in situ	[103]
		41°37'38.45" N	13°08'32.37" E	lower Volsci unit	MVP	marl pebble in conglomerate	<i>Amaurolithus primus</i>	uppermost Tortonian—basal Pliocene	in situ	this work—GO2
		41°37'38.45" N	13°08'32.37" E	lower Volsci unit	MVP	bioturbated marl pebble in conglomerate	<i>Discoaster surculus, Helicosphaera wallichii, Calcidiscus leptoporus, C. macintyreii, Coccolithus pelagicus, Discoaster multiradiatus, Helicosphaera carteri, Reticulofenestra minuta, R. pseudoumbilicus, Sphenolithus moriformis, S. radians, Zygrhablithus bijugatus</i>	uppermost Tortonian—basal Pliocene	in situ	this work—GO3
5	Gorga, Rave St. Marie	41°39'36.01" N	13°07'9.51" E	lower Volsci unit	RDT	limestone	<i>Orbitoides medius, Sivasella monolateralis</i>	Maastrichtian	in situ	[111]
		41°39'36.01" N	13°07'9.51" E	lower Volsci unit	Spirolina lmst.	limestone	<i>Spirolina, carofita</i>	lower Eocene	in situ	[111]
		41°39'36.01" N	13°07'9.51" E	lower Volsci unit	CBZ	limestone and marl	<i>Cyclicargolithus floridanus, Sphenolithus conicus, Miogyopsina cf. globulina</i>	lower Miocene (not younger than middle Burdigalian)	in situ	This work—LEP12C
		41°39'36.01" N	13°07'9.51" E	lower Volsci unit	UAM	marl with cylindrites	<i>Globorotalia menardii, Globorotalia ventriosa, Globigerina nepenthes</i>	lower Tortonian	in situ	[103]

Site n°	Group of Localities	Latitude	Longitude	Tectonic Unit	Formation	Lithology	Biomarkers	Age Range	Comments	Author
6	Sgurgola	41°40'38.97" N	13°9'34.03" E	upper Ernici unit	CBZ	limestone	<i>Amphistegina</i> , <i>Heterostegina</i> , briozoa, <i>Operculina</i> , <i>Miogypsina globulina</i> , <i>Cycloclypeus</i> , <i>Globorotalia scitula</i> , <i>Globigerinoides trilobus</i> , <i>G. sacculifer</i> , <i>G. bisphaericus</i> , <i>Orbulina universa</i> , <i>Orbulina suturalis</i> , <i>Globoquadrina dehiscens</i> , <i>Globorotalia mayeri</i>	Langhian—lower Serravallian	in situ	[103]
		41°40'38.97" N	13°9'34.03" E	upper Ernici unit	UAM	marl with cyndrites	<i>Globorotalia menardii</i> , <i>Globigerina nepenthes</i> , <i>Globorotalia ventriosa</i> , <i>Globorotalia acostaensis</i> , <i>G. bulloides</i> , <i>G. paraboloides</i> , <i>G. pseudopachyderma</i> , <i>G. apertura</i> , <i>Globigerinoides obliquus</i> , <i>Globoquadrina globosa</i> , <i>Orbulina universa</i>	upper Serravallian—Tortonian P-P.	in situ	[103]
		41°40'38.97" N	13°9'34.03" E	upper Ernici unit	FFS	arenaceous-argillous turbidite	<i>Globorotalia menardii</i> , <i>Globigerina nepenthes</i> , <i>Globorotalia ventriosa</i>	upper Tortonian	in situ	[103]
7	Ferentino	41°41'22.95" N	13°14'41.78" E	upper Ernici unit	RDT	limestone	<i>Rotalispira scarsellai</i> , <i>Accordiella conica</i> , <i>Cuvillierinella salentina</i>	middle Campanian	in situ	[103]
		41°41'22.95" N	13°14'41.78" E	upper Ernici unit	Spirolina lmst.	limestone	<i>Spirolina</i> , carofita, discorbidae	lower Eocene	in situ	[103]
		41°41'22.95" N	13°14'41.78" E	upper Ernici unit	CBZ	limestone	<i>Amphistegina</i> , <i>Heterostegina</i> , briozoa, <i>Operculina</i> , <i>Miogypsina globulina</i> , <i>Cycloclypeus</i> , <i>Globorotalia scitula</i> , <i>Globigerinoides trilobus</i> , <i>G. sacculifer</i> , <i>G. bisphaericus</i> , <i>Orbulina universa</i> , <i>Orbulina suturalis</i> , <i>Globoquadrina dehiscens</i> , <i>Globorotalia mayeri</i>	upper Langhian—upper Serravallian	in situ	[103]
		41°41'22.95" N	13°14'41.78" E	upper Ernici unit	UAM	marl with cyndrites	<i>Globorotalia menardii</i> , <i>Globigerina nepenthes</i> , <i>Globorotalia ventriosa</i> , <i>Globorotalia acostaensis</i> , <i>G. bulloides</i> , <i>G. paraboloides</i> , <i>G. pseudopachyderma</i> , <i>G. apertura</i> , <i>Globigerinoides obliquus</i> , <i>Globoquadrina globosa</i> , <i>Orbulina universa</i>	upper Serravallian—Tortonian P-P.	in situ	[103]
		41°41'22.95" N	13°14'41.78" E	upper Ernici unit	FFS	arenaceous-pelitic turbidite	no data	upper Tortonian		[103]
8	Caccume Mt. klippe	41°34'46.13" N	13°14'0.62" E	lower Volsci unit	RDT	limestone	<i>Rotalispira scarsellai</i> , <i>Accordiella conica</i> , <i>Thaumatoporella</i> , <i>Nezzazatinella</i>	Santonian—Campanian	in situ	this work—LEP1A-C; LEP27
		41°34'46.13" N	13°14'0.62" E	lower Volsci unit	RDT	limestone with iron cruston	<i>Rotalispira scarsellai</i> , <i>Accordiella conica</i> , <i>Thaumatoporella</i> , <i>Nezzazatinella</i>	Santonian—Campanian	in situ	this work—LEP1A-C; LEP28
		41°34'46.13" N	13°14'0.62" E	upper Volsci unit	RDT	rudstone	<i>Rotalispira maxima</i> , <i>Accordiella conica</i>	Campanian	native block within C	this work LEP20

Site n°	Group of Localities	Latitude	Longitude	Tectonic Unit	Formation	Lithology	Biomarkers	Age Range	Comments	Author
		41°30'53.47" N	13°26'25.33" E	Volsci Thrust Front	C	marl, sandstone, greenish clay (matrix)	<i>Racemiguembelina fructicosa</i>	Maastrichtian	reworked	[114]
		41°30'53.47" N	13°26'25.33" E	Volsci Thrust Front	C	marl, sandstone, greenish clay (matrix)	<i>Globigeraspis</i> sp., <i>Globigerina</i> cfr. <i>dissimilis</i> , <i>Globorotalia aequa</i> , <i>Globorotalia quetra</i>	middle-upper Eocene	reworked	[114]
		41°30'53.47" N	13°26'25.33" E	Volsci Thrust Front	C	marl, sandstone, greenish clay (matrix)	<i>Cassidulina subglobosa horizontalis</i> , <i>Globoquadrina dehiscens</i> , <i>Globoquadrina</i> cfr. <i>quadraria</i> , <i>Globigerinoides bisphaericus</i>	early Miocene	reworked	[114]
		41°30'53.47" N	13°26'25.33" E	Volsci Thrust Front	C	marl, sandstone, greenish clay (matrix)	<i>Haplophragmoides</i> sp., <i>Eggerella bradyi</i> , <i>Nodosaria ovicula</i> , <i>Elphidium complanatum</i> , <i>Elphidium macellum</i> , <i>Nonion boueanum</i> , <i>Nonion umbilicatum</i> , <i>Pullenia bulloides</i> , <i>Plectofrondicularia diversicostata</i> , <i>Plectofrondicularia semicosta</i> , <i>Orthomorphina</i> cfr. <i>proxima</i> , <i>Robertina bradyi</i> , <i>Bulimina aculeata</i> , <i>Bulimina costata</i> , <i>Bulimina fusiformis</i> , <i>Bulimina inflata</i> , <i>Bolivina arta</i> , <i>Bolivina cistina</i> , <i>Bolivina punctata</i> , <i>Bolivinoidea miocenica</i> , <i>Uvigerina canariensis</i> , <i>Uvigerina laviculata</i> , <i>Uvigerina peregrina</i> , <i>Uvigerina rutila</i> , <i>Angulogenerina angulosa</i> , <i>Valvulineria bradyana</i> , <i>Valvulineria complanata</i> , <i>Gyroidina longispira</i> , <i>Gyroidina longispira miocenica</i> , <i>Gyroidina soldanii</i> , <i>Gyroidina soldanii altiformis</i> , <i>Eponides haidingeri</i> , <i>Eponides umbonatus stellatus</i> , <i>Rotalia beccarii inflata</i> , <i>Siphonina reticulata</i> , <i>Cassidulina laevigata carinata</i> , <i>Cassidulina oblonga</i> , <i>Cassidulina subglobosa</i> , <i>Sphaeroidina bulloides</i> , <i>Globigerina bulloides</i> , <i>Globigerina concinna</i> , <i>Globigerina eggeri</i> , <i>Sphaeroidinella</i> cfr. <i>dehiscens</i> , <i>Globigerinoides trilobus</i> , <i>Globigerinoides rubra</i> , <i>Orbulina suturalis</i> , <i>Catapsidrax unicavus</i> , <i>Globigerinita naparimaensis</i> , <i>Globorotalia</i> cfr. <i>bononiensis</i> , <i>Globorotalia scitula</i> , <i>Globorotalia aff. scitula</i> , <i>Globorotalia mayeri</i>	Pliocene?	Not reworked	[114]
12	Vele Mt. Thrust ramp	41°21'12.97" N	13°31'7.49" E	Upper Volsci unit	LK	limestone	<i>Cladocoropsis mirabilis</i> , <i>Salpingoporella dinarica</i> , <i>Orbitolina lenticularis</i> , <i>Cuneolina laurentii</i> , <i>C. camposauri</i> , <i>Salpingoporella annulata</i>	uppermost Jurassic—lower Cretaceous	in situ	[102]

Site n°	Group of Localities	Latitude	Longitude	Tectonic Unit	Formation	Lithology	Biomarkers	Age Range	Comments	Author
		41°21'12.97" N	13°31'7.49" E	Upper Volsci unit	UK	limestone	<i>Accordiella conica</i> , <i>Dicyclina schlumbergeri</i> , <i>Sellialveolina viallii</i>	Cenomanian- Santonian	in situ	[102]
		41°21'12.97" N	13°31'7.49" E	Upper Volsci unit	C	clay mélange	no data		reworked	[102]
13	Leucio Mt. klippe	41°28'0.12" N	13°37'5.79" E	Upper Volsci unit	LK	limestone	<i>Cladocoropsis mirabilis</i> , <i>Salpingoporella dinarica</i> , <i>Orbitolina lenticularis</i> , <i>Cuneolina laurentii</i> , <i>C. camposauri</i> , <i>Salpingoporella annulata</i>	Uppermost Jurassic— lower Cretaceous	in situ	[102]
		41°28'0.12" N	13°37'5.79" E	Upper Volsci unit	C	clay mélange	no data	upper Tortonian— lower Messinian		[102]
14	Formia-Maranola	41°17'23.93" N	13°36'35.81" E	lower Volsci unit	UK	limestone	<i>Accordiella conica</i> , <i>Rotalispira scarsellai</i> , <i>Dicyclina schlumbergeri</i> , <i>Moncharmontia apenninica</i>	Santonian— Campanian	in situ	[115]
		41°17'23.93" N	13°36'35.81" E	lower Volsci unit	UK	limestone with iron crust	<i>Scandonea</i> ; <i>Ticinella sp.</i> , <i>Hedbergella sp.</i>	Campanian?— early Eocene?		[63,115]
		41°17'23.93" N	13°36'35.81" E	lower Volsci unit	C	silty clays, marls and sandstone; Pietra paesina; Scaglia-type limestone; marly limestones and Mg-bearing sandstones	radiolarians, heterohelicidae, <i>Globotruncana</i> , <i>Hedbergella</i> , <i>Globigerinoides sp.</i> lagenidae, globigerinidae		exotic blocks	[115]
		41°17'23.93" N	13°36'35.81" E	lower Volsci unit	MVP	mica-rich silty clays and argillous sands with gypsum	<i>Glorotalia</i> , <i>globorotaloidea</i> , <i>Globorotalia incompta</i> , <i>G. mayeri</i> , <i>G. obesa</i> , <i>G. pseudopachyderma</i> , <i>G. scitula</i> , <i>Globigerinoides spp.</i> , <i>Globigerina quinqueloba</i> , <i>Orbulina sp.</i>	middle to upper Messinian	in situ	[115]
		41°17'23.93" N	13°36'35.81" E		SBG	polygenic breccia	<i>Bolivina leonardi</i> , <i>Cibicides italicus</i> , <i>Elphidium complanatum</i> , <i>lenticulina clerici</i> , <i>Marginulina costata</i> , <i>Nodosaria pentecostata</i> , <i>Glorotalia puncticulata</i> , <i>G. bononiensis</i>	uppermost Messinian— lower Pliocene	in situ	[115]
15	Spigno Saturnia	41°18'45.84" N	13°41'59.17" E	lower Volsci unit	RDT	limestone	<i>Rotorbinella scarsellai</i> , <i>Accordiella conica</i>	Aptian-Turonian	in situ	[96]
		41°18'45.84" N	13°41'59.17" E	lower Volsci unit	RDT	limestone with iron crust	no data			[115]
		41°18'45.84" N	13°41'59.17" E	lower Volsci unit	C	silty clay, marl and sandstone; Pietra paesina; Scaglia-type limestone; marly limestones and Mg-bearing sandstones	radiolarians, heterohelicidae, <i>Globotruncana</i> , <i>Hedbergella</i> , <i>Globigerinoides sp.</i> lagenidae, globigerinidae		exotic blocks	[115]

Site n°	Group of Localities	Latitude	Longitude	Tectonic Unit	Formation	Lithology	Biomarkers	Age Range	Comments	Author
16	Torrente ausente Valley	41°21'53.62" N	13°43'55.16" E	upper Ernici unit	CBZ	limestone	<i>Amphistegina</i> , <i>Elphidium</i> , <i>Heterostegina</i> , <i>Gypsina</i>	lower Aquitanian—lower Serravallian (?)	in situ	[149]
		41°21'53.62" N	13°43'55.16" E	upper Ernici unit	UAM	marl with cylindrites	<i>Orbulina universa</i> , <i>O. suturalis</i> , <i>Globorotalia menardii</i> , <i>Globorotalia scitula ventriosa</i> , <i>Globigerinoides trilobus</i> , <i>Globigerina</i> cf. <i>bulloides</i> , <i>Globigerina concinna</i> , <i>Globoquadrina dehiscens</i>	Serravallian p.p.—Tortonian p.p.	in situ	[115]
		41°21'53.62" N	13°43'55.16" E	upper Ernici unit	FFS	sandstone with olistolites and olistostromes	<i>Globorotalia menardii</i> , <i>Globigerina nepenthes</i> , <i>Globorotalia ventriosa</i> , <i>G. parabulloides</i> , <i>Globigerinoides obliquus</i> , <i>Globoquadrina globosa</i>	upper Tortonian	in situ with native blocks	[115]
		41°21'53.62" N	13°43'55.16" E	upper Ernici unit	MVP	calcarenite and conglomerate with quartz grains	<i>Amphistegina</i> , <i>Elphidium</i> , <i>Textularidae</i> , <i>Miliolidae</i> , <i>Globigerinidae</i> , <i>Globotruncane</i> , <i>Nummulites</i>	lower Messinian	reworked	[115,116,150]
		41°21'53.62" N	13°43'55.16" E	upper Ernici unit	MVP	subordianate marl and gypsum towards the top	<i>Globorotalia acostaensis</i> , <i>Globigerina bulloides</i> , <i>Globigerina vanazuelana</i> , <i>Orbulina bilobata</i> , <i>Orbulina suturalis</i> , <i>Orbulina universa</i>	lower Messinian	in situ	[115]
17	Castelforte	41°17'55.49" N	13°49'54.89" E	upper Ernici unit	RDT	limestone	<i>Accordiella conica</i> , <i>Rotalispira scarsellai</i> , <i>Dicyclina schlumbergeri</i> , <i>Moncharmontia apenninica</i> , <i>Laffitteina</i>	Santonian-Maastrichtian	in situ	[113]
		41°17'55.49" N	13°49'54.89" E	upper Ernici unit	Spirolina <i>lmst.</i>	limestone	<i>Spirolina</i> , <i>Coskinolina liburnica</i> , <i>Alveolina ellipsoidalis</i>	upper Paleocene—lower Eocene	in situ	[113]
		41°17'55.49" N	13°49'54.89" E	upper Ernici unit	CBZ	limestone	<i>Amphistegina</i> , <i>Cibicides</i> , <i>Operculina</i> , <i>Eponides</i>	Langhian (?)—Serravallian p.p.	in situ	[115]
		41°17'55.49" N	13°49'54.89" E	upper Ernici unit	UAM	marl and sandstone	<i>Orbulina universa</i> , <i>O. suturalis</i> , <i>Globorotalia menardii</i> , <i>Globorotalia scitula ventriosa</i> , <i>Globigerinoides trilobus</i> , <i>Globigerina</i> cf. <i>bulloides</i> , <i>Globigerina concinna</i> , <i>Globoquadrina dehiscens</i>	Serravallian p.p.—Tortonian p.p.	in situ	[115]
		41°17'55.49" N	13°49'54.89" E	upper Ernici unit	FFS	arenaceous-siltous clay turbidite	no data	Tortonian		[115]
18	Massico Mt.	41°9'39.27" N	13°54'16.24" E	upper Ernici unit ?	RDT	limestone	<i>Dicyclina schlumbergeri</i> , <i>Accordiella conica</i> , <i>rudist</i>	Campanian	in situ	[37]
		41°9'39.27" N	13°54'16.24" E	upper Ernici unit ?	CBZ	limestone	<i>Amphistegina</i> , <i>bryozoa</i> , <i>Ditrupea</i> , <i>ostreidae</i>	Burdigalian—Langhian	in situ	[37]
		41°9'39.27" N	13°54'16.24" E	upper Ernici unit ?	UAM	marls and sandstone	<i>Orbulina</i> , <i>Globorotalia menardii</i>	Serravallian—lower Tortonian p.p.	in situ	[37,115]
		41°9'39.27" N	13°54'16.24" E	upper Ernici unit ?	FFS	clay and sandstone with olistolithes	<i>Globorotalia mayeri</i> , <i>G. scitula</i> , <i>Globigerinoides trilobus</i> , <i>Bolivina</i> sp., <i>Discoaster brouweri</i> , <i>D. variabilis</i> , <i>D. surculus</i> , <i>Helicosphaera wallichii</i> , <i>Sphenolithus abies</i>	upper Tortonian—lower Messinian(?)	in situ	[37,115]

Appendix B

In the following, we report the new Stratigraphic constraints and age determination of the samples collected from twenty-five different localities in the study area representative stratigraphic logs of Figure 2 in the main manuscript.

Sampling Locality	Latitude	Longitude	Sample	Fm	Lithology	Texture and Components	Biomarker	Age Range
Gavignano, Contrada Fornarelli	41°41'54" N	13°3'30" E	LEP9A	MVP	Calcarenic/arenitic matrix with abundant quartz grains	<i>Elphidium</i> and <i>Amphistegina</i> ; clasts of Cretaceous age (with <i>Rotalispira</i>) and clasts with <i>Orbulina</i> reworked <i>Elphidium</i> e <i>Amphistegina</i> and clasts with planktonic forams		Late Miocene
	41°41'54" N	13°3'30" E	LEP9A2	MVP	Calcarenic/arenitic matrix with abundant quartz grains			Late Miocene
Gavignano, promenade	41°42'10" N	13°2'39" E	LEP10B	MVP	Lithoclast of Rudist (radiolites) limestone with benthic foraminifera	Peloidal packstone with <i>Rotalispira</i>	<i>Moncharmontia apenninica</i> , <i>Rotalispira</i>	Coniacian-Campanian
	41°42'10" N	13°2'39" E	LEP10A	MVP	Calcarenic/arenitic matrix with abundant quartz grains	reworked <i>Elphidium</i> e <i>Amphistegina</i> and clasts with planktonic forams		Late Miocene
	41°42'10" N	13°2'39" E	LEP10	MVP	Lithoclast wackestone with planktonic foraminifera	<i>Orbulina</i>	<i>Orbulina</i>	Serravallian-Tortonian
	41°42'8.67" N	13°2'38.40" E	LEP10L	MVP	Calcarenic/arenitic matrix		<i>Coccolithus pelagicus</i> , <i>Discoaster surculus</i> , <i>Helicosphaera wallichii</i> , <i>Reticulofenestra bisecta</i> , <i>Reticulofenestra minuta</i> , <i>Amaurolithus primus</i> , <i>Coccolithus pelagicus</i> , <i>Discoaster surculus</i> , <i>Discoaster variabilis</i> , <i>Nicklithus amplificus</i> , <i>Sphenolithus abies</i>	uppermost Tortonian—lowermost Zanclean
	41°42'11.18" N	13°2'42.66" E	LEP10M	MVP	Marl and clay			Messinian
Bassiano, Colle Cantocchio	41°34'28.33" N	13°0'02.26" E	LEP8A	CBZ	Conglomerate of calcarenitic pebbles with glauconite	Pebbly grainstone with echinid, ditrupae, <i>Elphidium</i> , bryozoa, <i>Miogypsina</i> , <i>Amphistegina</i> , <i>Operculina</i> , <i>Heterostegina</i> , <i>Lepidocyclus</i> matrix made up with echinoderm and ostreid fragments	<i>Miogypsina</i> , <i>Elphidium</i> , bryozoa	early Miocene
	41°34'28.33" N	13°0'02.26" E	LEP8C	CBZ	Conglomerate of calcarenitic pebbles with glauconite	and ostreid fragments with reworked Cretaceous clasts with <i>Thaumatoporella</i> orpeloidal facies Echinid, <i>Elphidium</i> , bryozoa,	Ostreid and echinoderms	early Miocene
	41°34'32" N	13°0'9" E	LEP16	CBZ	Conglomerate with Cretaceous clasts	<i>Amphistegina</i> , <i>Heterostegina</i> , <i>Lepidocyclus</i>	<i>Elphidium</i> , <i>Amphistegina</i>	early Miocene
Bassiano, Colle Cantocchio Bat Cave	41°34'31.92" N	13°0'2.08" E	LEP49d	UAM	Clay within thrust		<i>Braarudosphaera bigelowii</i> , <i>Catinaster cf. coalitus</i> , <i>C. cf. glenos</i> , <i>Coccolithus cf. eopelagicus</i> , <i>C. cf. miopelagicus</i> , <i>C. pelagicus</i> , <i>Cyclicargolithus abisectus</i> , <i>Cy. floridanus</i> , <i>Helicosphaera carteri</i> , <i>H. walberdosfensis</i> , <i>Ortorhadus cf. rugosus</i> , <i>O. serratus</i> , <i>Pontosphaera multipora</i> , <i>Reticulofenestra bisecta</i> , <i>R. cf. dictyoda</i> , <i>R. minuta</i> , <i>R. cf. pseudoumbilicus</i> , <i>Sphenolithus moriformis</i> , <i>S. radians</i> , <i>Triquetrorhabdulus carinatus</i> , <i>T. challegeri</i> , <i>Watznaueria barnesiae</i>	Mesozoic, Paleocene-Eocene; Oligocene-middle Miocene; Serravallian-Tortonian?

Sampling Locality	Latitude	Longitude	Sample	Fm	Lithology	Texture and Components	Biomarker	Age Range
	41°34'31.92" N	13°0'2.08" E	LEP49f	UAM	Clay beneath thrust		<i>Braarudosphaera bigelowii</i> , <i>Calcidiscus leptoporus</i> , <i>Catinaster</i> <i>cf. coalitus</i> , <i>C. glenos</i> , <i>Chiasmolithus sp.</i> , <i>Coccolithus cf.</i> <i>eopelagicus</i> , <i>C. cf. miopelagicus</i> , <i>C. pelagicus</i> , <i>C. tenuiforatus</i> , <i>Cruciplacolithus sp.</i> , <i>Cyclicargolithus abisectus</i> , <i>Cy.</i> <i>floridanus</i> , <i>Discoaster cf.</i> <i>deflandrei</i> , <i>D. multiradiatus gr.</i> , <i>D. sp.</i> , <i>Helicosphaera carteri</i> , <i>H.</i> <i>walberdosfensis</i> , <i>Nannotetrina</i> <i>fulgens</i> , <i>Ortorhadus serratus</i> , <i>Pontosphaera multipora</i> , <i>Reticulofenestra bisecta</i> , <i>R. cf.</i> <i>dictyoda</i> , <i>R. minuta</i> , <i>R. cf.</i> <i>pseudoumbilicus</i> , <i>Sphenolithus</i> <i>moriformis</i> , <i>S. radians</i> , <i>Triquetrorhabdulus carinatus</i> , <i>Watznaueria barnesiae</i> , <i>Zygrhablithus bijugatus</i>	Mesozoic, Paleocene- Eocene; Oligocene- middle Miocene; Serravallian- Tortonian?
Bassiano, Colle Cantocchio near top	41°34'29" N	13°0'9" E	LEP15	SBG	Breccia with Mesozoic clasts	Reddish matrix with echinoderm fragments	echinoderms	
Gorga, Rave Santa Maria	41°39'18" N	13°7'18" E	LEP 14B	UK	Grainstone/ Packstone with rudists	<i>Rotalispira</i> and ostracods	<i>Rotalispira</i>	Campanian
	41°39'35" N	13°7'8" E	LEP12A	UK	Calcarenite with resedimented rudist	bioclastic detritus (echinoderms) with <i>Orbitoides</i> and <i>Murciella</i>	<i>Orbitoides</i> and <i>Murciella</i>	Upper Campanian- lower Maastrichtian
	41°39'35" N	13°7'8" E	LEP12B	CBZ	Breccia of encrusted K pebbles, calcarenitic matrix	Bivalve, echinoid fragments and reworked Cretaceous clasts		early Miocene
	41°39'35" N	13°7'8" E	LEP12C	CBZ	Marl level with tiny limestone clasts		<i>Cyclicargolithus floridanus</i> , <i>Sphenolithus conicus</i>	not younger than middle Burdigalian
Gorga, Capezzenna Mt.	41°39'6.86" N	13°4'22.07" E	GO2	MVP	Marly lens within conglomerate		<i>Amaurolithus primus</i>	uppermost Tortonian— lowermost Zanclean
	41°39'6.86" N	13°4'22.07" E	GO3	MVP	Marly clast within conglomerate	Clast with <i>Chondrites</i> bioturbations	<i>main markers: Discoaster</i> <i>surculus</i> , <i>Helicosphaera wallichii</i> . <i>Other components: Calcidiscus</i> <i>leptoporus</i> , <i>C. macintyreii</i> , <i>Coccolithus pelagicus</i> , <i>Discoaster</i> <i>multiradiatus</i> , <i>Helicosphaera</i> <i>carteri</i> , <i>Reticulofenestra minuta</i> , <i>R. pseudoumbilicus</i> , <i>Sphenolithus</i> <i>moriformis</i> , <i>S. radians</i> , <i>Zygrhablithus bijugatus</i>	upper Tortonian
Marroni, Morolo	41°39'38.68" N	13°10'27.54" E	LEP72	FFS	Marl and clay		<i>Discoaster variabilis</i> , <i>Helicosphaera carteri</i> , <i>Reticulofenestra bisecta</i> , <i>R.</i> <i>minuta</i> , <i>Sphenolithus procerus</i> , <i>Zygrhablithus bijugatus</i>	not older than upper Tortonian
Colle Fatuccio, Ferentino	41°40'21.60" N	13°13'45.14" E	LEP73	FFS	Marl and clay	Crustaceans bioturbations	sterile	
Carpineto, Pian della Faggeta	41°34'34" N	15°06'53" E	LEP17C	UK	Carbonatic breccia at the top of a lithon	Packstone with Rudist and foraminifera	<i>Rotalispira</i>	Santonian- Campanian
	41°34'34" N	16°06'53" E	LEP17D	C	Fine-grained calcarenite lens	Grainstone-packstone with <i>Amphistegina</i> , <i>Miogypsinids</i> and echinoderm fragments	<i>Miogypsinids</i>	early Miocene
	41°34'34" N	15°06'53" E	LEP17E	C	Microconglomerate lens with carbonatic and crystalline pebbles		sterile	

Sampling Locality	Latitude	Longitude	Sample	Fm	Lithology	Texture and Components	Biomarker	Age Range
	41°34'34" N	15°06'53" E	LEP17F	C	Sandstone with carbonatic e and crystalline clasts		sterile	
	41°34'35" N	18°06'41" E	LEP18B	UK	sStriated carbonate cruston at the top of a lithon	Wackestone with <i>Decastronema</i> , ostracoda, discorbidae	<i>Decastronema</i>	Upper Cretaceous
	41°34'35" N	18°06'41" E	LEP18D	C	Microconglomerate lens with crystalline clasts		<i>Coccolithus pelagicus</i> , <i>Cyclicargolithus abisectus</i> , <i>Cy. floridanus</i> , <i>Reticulofenestra</i> cf. <i>pseudoumbilicus</i>	early Miocene?
	41°34'33" N	19°06'39" E	LEP19A	UK	Rudist rudstone/floatstone at the top of a lithon		rudists	Upper Cretaceous
	41°34'33" N	19°06'39" E	LEP19B	UK	Carbonate breccia	Wackestone with <i>Thaumatoporella</i> , and benthic foraminifera	<i>Nezzazatinella</i> , <i>Rotalispira</i>	Coniacian-Campanian
Patrica, Caccume Mt. north	41°34'46.50" N	13°13'58.92" E	CC20	UK	Limestone	Wackestone with <i>Thaumatoporella</i> , and benthic foraminifera	<i>Accordiella conica</i> , <i>Rotalispira maxima</i>	Santonian Campanian
	41°34'46.50" N	13°13'58.92" E	CC21	UK	Limestone breccia on top	Wackestone with <i>Thaumatoporella</i> , and benthic foraminifera	<i>Nezzazatinella</i> , <i>Rotalispira maxima</i>	Santonian Campanian
	41°34'46.50" N	13°13'58.92" E	CC23	UK	Limestone breccia on top	Wackestone with <i>Thaumatoporella</i> , and benthic foraminifera	<i>Rotalispira maxima</i>	Santonian Campanian
	41°34'39.30" N	13°14'3.01" E	CC24	UK	Cataclastic limestone			Cenomanian?
	41°34'47" N	13°13'59" E	LEP1A	UK	Limestone below unconformity	Benthic foraminifera and small debris of rudist shells fragments	<i>Accordiella conica</i> and <i>Rotalispira maxima</i>	Campanian
	41°34'47" N	13°13'59" E	LEP1B	UK	Dolomitic limestone above unconformity			Upper Cretaceous?
	41°34'47" N	13°13'59" E	LEP1C	UK	Encrusted carbonatic breccia on top	Wackestone with benthic foraminifera, few intraclasts	<i>Rotalispira scarsellai</i>	Santonian-Campanian
	41°34'47" N	13°13'59" E	LEP20	UK	Limestone breccia within Chaotic complex	Wackestone with benthic foraminifera, Cretaceous intraclasts	<i>Rotalispira maxima</i> and <i>Accordiella conica</i>	Campanian
	41°34'32" N	13°14'5" E	LEP68a	C	Clay		<i>Coccolithus pelagicus</i> , <i>C. miopelagicus</i> , <i>Cyclicargolithus abisectus</i> , <i>Cy. floridanus</i> , <i>Discoaster</i> sp., <i>D. berggrenii</i> , <i>D. brouweri</i> , <i>D. deflandrei</i> , <i>D. formosus</i> , <i>D. multiradiatus</i> , <i>D. pentaradiatus</i> , <i>D. quinqueringus</i> , <i>D. variabilis</i> , <i>Helicosphaera recta</i> , <i>H. stalis</i> , <i>H. walberdosfensis</i> , <i>Orthorhabdus rugosus</i> , <i>Reticulofenestra bisecta</i> , <i>R. minuta</i> , <i>R. pseudoumbilicus</i> , <i>Reticulofenestra</i> sp., <i>Sphaenolithus abies</i> , <i>S. ciproensis</i> , <i>S. disbelemnos</i> , <i>S. heteromorphus</i> , <i>S. moriformis</i> , <i>Zygrhablithus bijugatus</i>	Paleocene-Eocene; Oligocene-early Miocene; middle Miocene; upper Tortonian—Messinian?
Giuliano di Roma, Caccume Mt. east	41°34'19" N	13°14'55" E	LEP27B	UK	Limestone below unconformity	Packstone with benthic foraminifera	<i>Rotalispira scarsellai</i>	Upper Turonian-Campanian
	41°34'19" N	13°14'55" E	LEP27C2	UK	Breccia above unconformity			Santonian-Campanian
	41°34'19" N	13°14'55" E	LEP27D	UK	Limestone	Packstone with algae and benthic foraminifera	<i>Thaumatoporella</i> , <i>Rotalispira scarsellai</i> , <i>Rotalispira maxima</i> , <i>Moncharmontia apenninica</i>	Santonian-Campanian
Giuliano di Roma, Caccume Mt. east	41°34'19" N	13°14'55" E	LEP27F	UK	Limestone	Wackestone with benthic foraminifera	<i>Nezzazatinella</i> , <i>Rotalispira</i> , <i>Pseudocyclammina sphaeroidea</i>	Turonian-Santonian
Giuliano di Roma, Caccume Mt. Scoriapane	41°34'14.93" N	13°13'54.82" E	LEP67	C	Clay beneath thrust		sterile	

Sampling Locality	Latitude	Longitude	Sample	Fm	Lithology	Texture and Components	Biomarker	Age Range
Giuliano di Roma, Caccume Mt. west	41°34'40"N	13°13'23"E	LEP69a	C	Clay		<i>Calcidiscus leptoporus</i> , <i>Clarolithus ellipticus</i> , <i>Coccolithus pelagicus</i> , <i>C. miopelagicus</i> , <i>D. berggrenii</i> , <i>D. brouwerii</i> , <i>D. decorus</i> , <i>D. deflandrei</i> , <i>D. multiradiatus</i> , <i>D. pentaradiatus</i> , <i>D. quinquerramus</i> , <i>D. variabilis</i> , <i>Orthorhabdus rugosus</i> , <i>O. striatus</i> , <i>Pontosphaera discopora</i> , <i>P. multipora</i> , <i>Reticulofenestra bisecta</i> , <i>R. minuta</i> , <i>R. pseudoumbilicus</i> , <i>Sphaenolithus abies</i> , <i>S. moriformis</i> , <i>Zygrhablithus bijugatus</i>	Paleocene-Eocene; Oligocene-early Miocene; middle Miocene; upper Tortonian—Messinian?
Giuliano di Roma, Siserno Mt.	41°32'17"N	13°18'02"E	LEP 30	UK	Limestone	Wackestone with Ostracods	ostracods	Campanian?
	41°32'17"N	13°18'02"E	LEP 31	UK	Limestone	Mudstone with Dolomitized intraclasts		Upper Cretaceous
	41°32'17"N	13°18'02"E	LEP 32	UK	Limestone	Wackestone with miliolidae, ostracoda and dolomite crystals	ostracods and miliolids	Campanian
	41°32'17"N	13°18'02"E	LEP 32B	UK	Limestone	Wackestone with miliolidae, ostracoda, discorbidae and porcelaneous foraminifera	ostracods and miliolids	Campanian
Patrica, il Patricano	41°33'4.78"N	13°16'2.89"E	LEP36	UK	Limestone	Wackestone with isorbidae	discorbidae	Campanian
	41°34'17"N	13°15'54"E	LEP39A	UK	Limestone	Wackestone with rudist fragments, miolidae, ostracoda and <i>Thaumatoporella</i>	ostracods and discorbide	Campanian
	41°34'17"N	13°15'54"E	LEP39B	UK	Limestone	Wackestone with ostracods and miliolidae	<i>Rotalispira scarsellai</i> , <i>Accordiella conica</i> ,	Campanian
	41°34'20"N	13°15'55"E	LEP 40A	UK	Limestone	Wackestone/Packstone with ostracods and discorbidae	<i>Thaumatoporella</i> , <i>Nezzazata</i> , <i>Moncharmontia apenninica</i>	Campanian
Giuliano di Roma west	41°33'7"	13°16'10"	LEP70	C	Marl and clay		<i>Coccolithus pelagicus</i> , <i>Reticulofenestra bisecta</i> , <i>R. minuta</i> , <i>Sphenolithus moriformis</i> , <i>Zygrhablithus bijugatus</i>	Paleocene-Tortonian
Frosinone, Le Fornaci cinema	41°37'4.88"N	13°20'26.32"E	LEP71	FFS	Marl and pelite with coal		<i>Coccolithus pelagicus</i> , <i>Cyclicargolithus abisectus</i> , <i>Reticulofenestra bisecta</i> , <i>R. minuta</i> , <i>Pontosphaera sp.</i>	Oligocene-early Miocene; Tortonian?

References

1. Read, J.F. Carbonate platform facies models. *Aapg Bull.* **1985**, *69*, 1–21. [\[CrossRef\]](#)
2. Ford, M.; Stahel, U. The geometry of a deformed carbonate slope-basin transition: The Ventoux-Lure fault zone, SE France. *Tectonics* **1995**, *14*, 1393–1410. [\[CrossRef\]](#)
3. Carminati, E.; Doglioni, C. Alps vs. Apennines: The paradigm of a tectonically asymmetric Earth. *Earth-Sci. Rev.* **2012**, *112*, 67–96. [\[CrossRef\]](#)
4. Davis, D.; Suppe, J.; Dahlen, F.A. Mechanics of fold-and-thrust belts and accretionary wedges. *J. Geophys. Res. Solid Earth* **1983**, *88*, 1153–1172. [\[CrossRef\]](#)
5. Roure, F. Foreland and hinterland basins: What controls their evolution? *Swiss J. Geosci.* **2008**, *101*, 5–29. [\[CrossRef\]](#)
6. Grool, A.R.; Ford, M.; Vergés, J.; Huismans, R.S.; Christophoul, F.; Dielforder, A. Insights into the crustal-scale dynamics of a doubly vergent orogen from a quantitative analysis of its forelands: A case study of the Eastern Pyrenees. *Tectonics* **2018**, *37*, 450–476. [\[CrossRef\]](#)
7. Butler, R.W.; Tavarnelli, E.; Grasso, M. Structural inheritance in mountain belts: An Alpine–Apennine perspective. *J. Struct. Geol.* **2006**, *28*, 1893–1908. [\[CrossRef\]](#)
8. Tavani, S.; Storti, F.; Lacombe, O.; Corradetti, A.; Muñoz, J.A.; Mazzoli, S. A review of deformation pattern templates in foreland basin systems and fold-and-thrust belts: Implications for the state of stress in the frontal regions of thrust wedges. *Earth-Sci. Rev.* **2015**, *14*, 82–104. [\[CrossRef\]](#)
9. Santantonio, M.; Carminati, E. Jurassic rifting evolution of the Apennines and Southern Alps (Italy): Parallels and differences. *Gsa Bull.* **2011**, *123*, 468–484. [\[CrossRef\]](#)

10. Shiner, P.; Beccacini, A.; Mazzoli, S. Thin-skinned versus thick-skinned structural models for Apulian carbonate reservoirs: Constraints from the Val d'Agri Fields, S Apennines, Italy. *Mar. Pet. Geol.* **2004**, *21*, 805–827. [[CrossRef](#)]
11. Livani, M.; Scrocca, D.; Arecco, P.; Doglioni, C. Structural and stratigraphic control on salient and recess development along a thrust belt front: The Northern Apennines (Po Plain, Italy). *J. Geophys. Res. Solid Earth* **2018**, *123*, 4360–4387. [[CrossRef](#)]
12. Cardello, G.L.; Di Vincenzo, G.; Giorgetti, G.; Zwingmann, H.; Mancktelow, N. Initiation and development of the Pennine Basal Thrust (Swiss Alps): A structural and geochronological study of an exhumed megathrust. *J. Struct. Geol.* **2019**, *126*, 338–356. [[CrossRef](#)]
13. Herwegh, M.; Pfiffner, O.-A. Tectono-metamorphic evolution of a nappe stack: A case study of the Swiss Alps. *Tectonophysics* **2005**, *404*, 55–76. [[CrossRef](#)]
14. Festa, A.; Pini, G.A.; Dilek, Y.; Codegone, G. Mélanges and mélange-forming processes: A historical overview and new concepts. *Int. Geol. Rev.* **2010**, *52*, 1040–1105. [[CrossRef](#)]
15. Festa, A.; Dilek, Y.; Pini, G.A.; Codegone, G.; Ogata, K. Mechanisms and processes of stratal disruption and mixing in the development of mélanges and broken formations: Redefining and classifying mélanges. *Tectonophysics* **2012**, *568*, 7–24. [[CrossRef](#)]
16. Ogawa, Y.; Anma, R.; Dilek, Y. *Accretionary Prisms and Convergent Margin Tectonics in the Northwest Pacific Basin*; Springer Science & Business Media: Berlin, Germany, 2011; Volume 8. [[CrossRef](#)]
17. Codegone, G.; Festa, A.; Dilek, Y. Formation of Taconic mélanges and broken formations in the Hamburg Klippe, central Appalachian Orogenic Belt, eastern Pennsylvania. *Tectonophysics* **2012**, *568*, 215–229. [[CrossRef](#)]
18. Ogata, K.; Festa, A.; Pini, G.A.; Pogačnik, Ž.; Lucente, C.C. Substrate deformation and incorporation in sedimentary mélanges (olistostromes): Examples from the northern Apennines (Italy) and northwestern Dinarides (Slovenia). *Gondwana Res.* **2019**, *74*, 101–125. [[CrossRef](#)]
19. Mohn, G.; Manatschal, G.; Masini, E.; Müntener, O. Rift-related inheritance in orogens: A case study from the Austroalpine nappes in Central Alps (SE-Switzerland and N-Italy). *Int. J. Earth Sci.* **2011**, *100*, 937–961. [[CrossRef](#)]
20. Bertok, C.; Martire, L.; Perotti, E.; d'Atri, A.; Piana, F. Kilometre-scale palaeoscarpments as evidence for Cretaceous synsedimentary tectonics in the External Briançonnais Domain (Ligurian Alps, Italy). *Sediment. Geol.* **2012**, *251*, 58–75. [[CrossRef](#)]
21. Cardello, G.L.; Mancktelow, N.S. Cretaceous syn-sedimentary faulting in the Wildhorn Nappe (SW Switzerland). *Swiss J. Geosci.* **2014**, *107*, 223–250. [[CrossRef](#)]
22. Balestro, G.; Festa, A.; Tartarotti, P. Tectonic significance of different block-in-matrix structures in exhumed convergent plate margins: Examples from oceanic and continental HP rocks in Inner Western Alps (northwest Italy). *Int. Geol. Rev.* **2015**, *57*, 581–605. [[CrossRef](#)]
23. Tozer, R.S.J.; Butler, R.W.H.; Corrado, S. Comparing thin-and thick-skinned thrust tectonic models of the Central Apennines, Italy. *Egu Stephan Mueller Spec. Publ. Ser.* **2002**, *1*, 181–194. [[CrossRef](#)]
24. Calabrò, R.A.; Corrado, S.; Di Bucci, D.; Robustini, P.; Tornaghi, M. Thin-skinned vs. thick-skinned tectonics in the Matese Massif, Central–Southern Apennines (Italy). *Tectonophysics* **2003**, *377*, 269–297. [[CrossRef](#)]
25. Tavarnelli, E.; Butler, R.W.H.; Decandia, F.A.; Calamita, F.; Grasso, M.; Alvarez, W.; Renda, P. Implications of fault reactivation and structural inheritance in the Cenozoic tectonic evolution of Italy. *Geol. Italy Spec.* **2004**, *1*, 209–222.
26. Scrocca, D.; Carminati, E.; Doglioni, C. Deep structure of the southern Apennines, Italy: Thin-skinned or thick-skinned? *Tectonics* **2005**, *24*. [[CrossRef](#)]
27. Billi, A.; Barberi, G.; Faccenna, C.; Neri, G.; Pepe, F.; Sulli, A. Tectonics and seismicity of the Tindari Fault System, southern Italy: Crustal deformations at the transition between ongoing contractional and extensional domains located above the edge of a subducting slab. *Tectonics* **2006**, *25*. [[CrossRef](#)]
28. Mazzoli, S.; D'errico, M.; Aldega, L.; Corrado, S.; Invernizzi, C.; Shiner, P.; Zattin, M. Tectonic burial and “young” (<10 Ma) exhumation in the southern Apennines fold-and-thrust belt (Italy). *Geology* **2008**, *36*, 243–246. [[CrossRef](#)]
29. Molli, G.; Menegon, L.; Malasoma, A. Switching deformation mode and mechanisms during subduction of continental crust: A case study from Alpine Corsica. *Solid Earth* **2017**, *8*, 767–788. [[CrossRef](#)]
30. Cardello, G.L.; Doglioni, C. From mesozoic rifting to Apennine orogeny: The gran Sasso range (Italy). *Gondwana Res.* **2015**, *27*, 1307–1334. [[CrossRef](#)]
31. Vitale, S.; Tramparulo, F.D.A.; Ciarcia, S.; Amore, F.O.; Prinzi, E.P.; Laiena, F. The northward tectonic transport in the southern Apennines: Examples from the Capri Island and western Sorrento Peninsula (Italy). *Int. J. Earth Sci.* **2017**, *106*, 97–113. [[CrossRef](#)]
32. Storti, F.; Balsamo, F.; Mozafari, M.; Koopman, A.; Swennen, R.; Taberner, C. Syn-Contractional Overprinting Between Extension and Shortening Along the Montagna Dei Fiori Fault During Plio-Pleistocene Antiformal Stacking at the Central Apennines Thrust Wedge Toe. *Tectonics* **2018**, *37*, 3690–3720. [[CrossRef](#)]
33. Cipriani, A.; Bottini, C. Early Cretaceous tectonic rejuvenation of an Early Jurassic margin in the Central Apennines: The “Mt. Cosce Breccia”. *Sediment. Geol.* **2019**, *387*, 57–74. [[CrossRef](#)]
34. Sabbatino, M.; Vitale, S.; Tavani, S.; Consorti, L.; Corradetti, A.; Cipriani, A.; Arienzo, I.; Parente, M. Constraining the onset of flexural subsidence and peripheral bulge extension in the Miocene foreland of the southern Apennines (Italy) by Sr-isotope stratigraphy. *Sediment. Geol.* **2020**, *401*. [[CrossRef](#)]
35. Cipollari, P.; Cosentino, D. Miocene unconformities in the Central Apennines: Geodynamic significance and sedimentary basin evolution. *Tectonophysics* **1995**, *252*, 375–389. [[CrossRef](#)]

36. Bigi, S.; Milli, S.; Corrado, S.; Casero, P.; Aldega, L.; Botti, F.; Moscatelli, M.; Stanzione, O.; Falcini, F.; Marini, M.; et al. Stratigraphy, structural setting and burial history of the Messinian Laga basin in the context of Apennine foreland basin system. *J. Mediterr. Earth Sci.* **2009**, *1*, 61–84.
37. Vitale, S.; Prinzi, E.P.; Ciarcia, S.; Sabbatino, M.; Tramparulo, F.D.A.; Verazzo, G. Polyphase out-of-sequence thrusting and occurrence of marble detritus within the wedge-top basin deposits in the Mt. Massico (southern Apennines): Insights into the late Miocene tectonic evolution of the central Mediterranean. *Int. J. Earth Sci.* **2019**, *108*, 501–519. [[CrossRef](#)]
38. Vitale, S.; Prinzi, E.P.; Tramparulo, F.D.A.; De Paola, C.; Di Maio, R.; Piegari, E.; Sabbatino, M.; Natale, J.; Notaro, P.; Ciarcia, S. Late Miocene-Early Pliocene Out-of-Sequence Thrusting in the Southern Apennines (Italy). *Geosciences* **2020**, *10*, 301. [[CrossRef](#)]
39. De Capoa, P.; Di Staso, A.; Guerrera, F.; Perrone, V.; Tramontana, M. The extension of the Maghrebian Flysch basin in the Apenninic chain: Paleogeographic and paleotectonic implications. Atti Congr. “Etat des connaissances géologiques des régions nord du Maroc: La Chaîne rifaine dans son cadre Méditerranéen occidental, Rabat (Maroc). *Trav. Inst. Sci. RabatGéogr. Phys.* **2003**, *21*, 77–92.
40. Carboni, F.; Viola, G.; Aldega, L.; van der Lelij, R.; Brozzetti, F.; Barchi, M.R. K-Ar fault gouge dating of Neogene thrusting: The case of the siliciclastic deposits of the Trasimeno Tectonic Wedge (Northern Apennines, Italy). *Ital. J. Geosci.* **2020**, *139*, 300–308. [[CrossRef](#)]
41. Curzi, M.; Aldega, L.; Bernasconi, S.M.; Berra, F.; Billi, A.; Boschi, C.; Carminati, E. Architecture and evolution of an extensionally-inverted thrust (Mt. Tancia Thrust, Central Apennines): Geological, structural, geochemical, and K–Ar geochronological constraints. *J. Struct. Geol.* **2020**, 104059. [[CrossRef](#)]
42. Curzi, M.; Billi, A.; Carminati, E.; Rossetti, F.; Albert, R.; Aldega, L.; Cardello, G.L.; Conti, A.; Gerdes, A.; Smeraglia, L.; et al. Disproving the Presence of Paleozoic-Triassic Metamorphic Rocks on the Island of Zannone (Central Italy): Implications for the Early Stages of the Tyrrhenian–Apennines Tectonic Evolution. *Tectonics* **2020**, *39*, e2020TC006296. [[CrossRef](#)]
43. Smeraglia, L.; Aldega, L.; Billi, A.; Carminati, E.; Di Fiore, F.; Gerdes, A.; Richard, A.; Rossetti, F.; Vignaroli, G. Development of an intrawedge tectonic mélange by out-of-sequence thrusting, buttressing, and intraformational rheological contrast, Mt. Massico ridge, Apennines, Italy. *Tectonics* **2019**, *38*, 1223–1249. [[CrossRef](#)]
44. Vitale, S.; Ciarcia, S. Tectono-stratigraphic and kinematic evolution of the southern Apennines/Calabria–Peloritani Terrane system (Italy). *Tectonophysics* **2013**, *583*, 164–182. [[CrossRef](#)]
45. Cardello, G.L.; Consorti, L.; Palladino, D.M.; Carminati, E.; Carlini, M.; Doglioni, C. Tectonically controlled carbonate-seated maar-diatreme volcanoes: The case of the Volsci Volcanic Field, central Italy. *J. Geodyn.* **2020**, *139*, 101763. [[CrossRef](#)]
46. Roure, F.; Casero, P.; Vially, R. Growth processes and mélange formation in the southern Apennines accretionary wedge. *Earth Planet. Sci. Lett.* **1991**, *102*, 395–412. [[CrossRef](#)]
47. Molli, G. Northern Apennine–Corsica orogenic system: An updated overview. *Geol. Soc. Lond. Spec. Publ.* **2008**, *298*, 413–442. [[CrossRef](#)]
48. Rosenbaum, G.; Gasparon, M.; Lucente, F.P.; Peccerillo, A.; Miller, M.S. Kinematics of slab tear faults during subduction segmentation and implications for Italian magmatism. *Tectonics* **2008**, *27*. [[CrossRef](#)]
49. Carminati, E.; Fabbi, S.; Santantonio, M. Slab bending, syn-subduction normal faulting, and out-of-sequence thrusting in the Central Apennines. *Tectonics* **2014**, *33*, 530–551. [[CrossRef](#)]
50. Faccenna, C.; Becker, T.W.; Miller, M.S.; Serpelloni, E.; Willett, S.D. Isostasy, dynamic topography, and the elevation of the Apennines of Italy. *Earth Planet. Sci. Lett.* **2014**, *407*, 163–174. [[CrossRef](#)]
51. Boccaletti, M.; Guazzone, G. Remnant arcs and marginal basins in the Cainozoic development of the Mediterranean. *Nature* **1974**, *252*, 18–21. [[CrossRef](#)]
52. Malinverno, A.; Ryan, W.B. Extension in the Tyrrhenian Sea and shortening in the Apennines as result of arc migration driven by sinking of the lithosphere. *Tectonics* **1986**, *5*, 227–245. [[CrossRef](#)]
53. Royden, L.; Patacca, E.; Scandone, P. Segmentation and configuration of subducted lithosphere in Italy: An important control on thrust-belt and foredeep-basin evolution. *Geology* **1987**, *15*, 714–717. [[CrossRef](#)]
54. Doglioni, C. A proposal for the kinematic modelling of W-dipping subductions-possible applications to the Tyrrhenian–Apennines system. *Terra Nova* **1991**, *3*, 423–434. [[CrossRef](#)]
55. Jolivet, L.; Faccenna, C. Mediterranean extension and the Africa–Eurasia collision. *Tectonics* **2000**, *19*, 1095–1106. [[CrossRef](#)]
56. Van Hinsbergen, D.J.; Torsvik, T.H.; Schmid, S.M.; Mañenco, L.C.; Maffione, M.; Vissers, R.L.; Gürer, D.; Spakman, W. Orogenic architecture of the Mediterranean region and kinematic reconstruction of its tectonic evolution since the Triassic. *Gondwana Res.* **2020**, *81*, 79–229. [[CrossRef](#)]
57. Sartori, R.; Torelli, L.; Zitellini, N.; Carrara, G.; Magaldi, M.; Mussoni, P. Crustal features along a W–E Tyrrhenian transect from Sardinia to Campania margins (Central Mediterranean). *Tectonophysics* **2004**, *383*, 171–192. [[CrossRef](#)]
58. Acocella, V.; Funicello, R. Transverse systems along the extensional Tyrrhenian margin of central Italy and their influence on volcanism. *Tectonics* **2006**, *25*. [[CrossRef](#)]
59. Beaudoin, A.; Augier, R.; Jolivet, L.; Jourdon, A.; Raimbourg, H.; Scaillet, S.; Cardello, G.L. Deformation behavior of continental crust during subduction and exhumation: Strain distribution over the Tenda massif (Alpine Corsica, France). *Tectonophysics* **2017**, *705*, 12–32. [[CrossRef](#)]
60. Locardi, E. The origin of the Apenninic arcs. *Tectonophysics* **1988**, *146*, 105–123. [[CrossRef](#)]
61. Pizzi, A.; Galadini, F. Pre-existing cross-structures and active fault segmentation in the northern-central Apennines (Italy). *Tectonophysics* **2009**, *476*, 304–319. [[CrossRef](#)]

62. Castellarin, A.; Colacicchi, R.; Praturlon, A. Fasi distensive, trascorrenze e sovrascorrimenti lungo la <<Linea Ancona-Anzio>>, dal Lias Medio al Pliocene. *Geol. Romana* **1978**, *17*, 161–189.
63. Centamore, E.; Di Manna, P.; Rossi, D. Kinematic evolution of the Volsci Range: A new overview. *Ital. J. Geosci.* **2007**, *126*, 159–172.
64. Centamore, E.; Dramis, F.; Di Manna, P.; Fumanti, F.; Milli, S.; Rossi, D.; Palombo, M.R.; Palladino, D.M.; Trigila, R.; Zanon, V.; et al. Note illustrative del Foglio 402 Ceccano. In *Carta Geol. D'italia 1:50.000. Serv. Geol. D'italia (ISPRA)*; Istituto Superiore per la Protezione e la Ricerca Ambientale: Rome, Italy, 2010.
65. Fazzini, P.; Gelmini, R.; Mantovani, P.; Pellegrini, M. Geologia dei Monti della Tolfa (Lazio settentrionale; prov. di Viterbo e Roma). *Mem. Soc. Geol. Ital.* **1972**, *11*, 65–144.
66. Parotto, M.; De Rita, D.; Giordano, G.; Cecili, A.; Chiocci, F.L.; La Monica, G.B. Note illustrative del Foglio 187 Albano Laziale. In *Carta Geol. D'italia 1:50.000. Serv. Geol. D'italia (ISPRA)*; Istituto Superiore per la Protezione e la Ricerca Ambientale: Rome, Italy, 2009.
67. Ogniben, L. Schema Introduttivo alla Geologia del confine Calabro-Lucano. *Mem. Soc. Geol. Ital.* **1969**, *8*, 453–763.
68. Acocella, V.; Faccenna, C.; Funiello, R. Elementi strutturali della media Valle Latina. *Boll. Soc. Geol. Ital.* **1996**, *115*, 501–518.
69. Selli, R. Sulla trasgressione del Miocene nell'Italia meridionale. *Museo Geologico Giovanni Capellini* **1957**, *2*, 1–54.
70. De Blasio, I.; Lima, A.; Perrone, V.; Russo, M. Nuove vedute sui depositi miocenici della Penisola Sorrentina. *Boll. Soc. Geol. Ital.* **1981**, *100*, 55–70.
71. Accordi, B. La componente traslativa nella tettonica dell'Appennino laziale-abruzzese. *Geol. Romana* **1966**, *5*, 355–406.
72. Cosentino, D.; Cipollari, P.; Di Donato, V.; Sgrosso, I.; Sgrosso, M. The Volsci Range in the kinematic evolution of the northern and southern Apennine orogenic system. *Boll. Della Soc. Geol. Ital.* **2002**, *121*, 209–218.
73. Devoto, G. Note geologiche sul settore centrale dei Monti Simbruini ed Ernici (Lazio nord-orientale). *Boll. Soc. Nat. Napoli* **1967**, *76*, 1–112.
74. Fabbi, S.; Santantonio, M. First report of a Messinian coralgial facies in a terrigenous setting of Central Apennines (Italy) and its palaeogeographic significance. *Geol. J.* **2019**, *54*, 1756–1768. [[CrossRef](#)]
75. Dondi, L.; Papetti, I.; Tedeschi, D. Stratigrafia del pozzo Trevi 1 (Lazio). *Geol. Romana* **1966**, *5*, 249–262.
76. Cavinato, G.; Cerisola, R.; Sirna, M. Strutture compressive pellicolari e tettonica distensiva nei Monti Ernici sudoccidentali (Appennino centrale). *Mem. Sgi* **1990**, *45*, 539–553.
77. Cavinato, G.P.; Parotto, M.; Sirna, M. Geological summary of the Central Apennines. Four decades later. *RendOnline Soc. Geol. Ital.* **2012**, *23*, 31–44.
78. Brozzetti, F.; Cerritelli, F.; Cirillo, D.; Agostini, S.; Lavecchia, G. The Roccamariano Conglomerate (Maiella Tectonic Unit) in the frame of the Abruzzo early Pliocene Foreland Basin System: Stratigraphic and structural implications. *Ital. J. Geosci.* **2020**, *139*, 266–286. [[CrossRef](#)]
79. Accordi, G.; Carbone, F. Sequenze carbonatiche meso-cenozoiche. In *Note Illustrative della Carta delle Litofacies del Lazio-Abruzzo ed Aree Limitrofe*; Consiglio Nazionale delle Ricerche: Rome, Italy, 1988; pp. 11–92.
80. Civitelli, G.; Brandano, M. Atlante delle litofacies e modello deposizionale dei Calcari a Briozoi e Litotamni nella Piattaforma carbonatica laziale-abruzzese. *Boll. Della Soc. Geol. Ital.* **2005**, *124*, 611.
81. Cosentino, D.; Cipollari, P.; Marsili, P.; Scrocca, D. Geology of the central Apennines: A regional review. *J. Virtual Explor.* **2010**, *36*, 1–37. [[CrossRef](#)]
82. Consorti, L.; Frija, G.; Caus, E. Rotaloidean foraminifera from the Late Cretaceous carbonates of Central and Southern Italy. *Cretac. Res.* **2017**, *70*, 226–243. [[CrossRef](#)]
83. Romano, M.; Manni, R.; Venditti, E.; Nicosia, U.; Cipriani, A. First occurrence of a Tylosaurinae mosasaur from the Turonian of the Central Apennines, Italy. *Cretac. Res.* **2019**, *96*, 196–209. [[CrossRef](#)]
84. Angelucci, A.; Devoto, G. Geologia del Monte Caccume. *Geol. Romana* **1966**, *5*, 177–196.
85. Casero, P. Structural setting of petroleum exploration plays in Italy. In *Special Volume of the Italian Geological Society for the IGC 32 Florence-2004*; Crescenti, U., d'Offizi, S., Merlino, S., Sacchi, L., Eds.; Italian Geological Society: Rome, Italy, 2004; pp. 189–199.
86. Sani, F.; Del Ventisette, C.; Montanari, D.; Coli, M.; Nafissi, P.; Piazzini, A. Tectonic evolution of the internal sector of the Central Apennines, Italy. *Mar. Pet. Geol.* **2004**, *21*, 1235–1254. [[CrossRef](#)]
87. Pasquali, V.; Castorina, F.; Cipollari, P.; Cosentino, D.; Lo Mastro, S. I depositi tardo-orogenici della Valle Latina meridionale: Stratigrafia e implicazioni cinematiche per l'evoluzione dell'Appennino centrale. *Boll. Soc. Geol. Ital.* **2007**, *126*, 101–118.
88. Parotto, M.; Tallini, M. Geometry and kinematics of the Montelanico-Carpineto Backthrust (Lepini Mts., Latium) in the hanging wall of the early Messinian thrust front of the central Apennines: Implications for the Apennine chain building. *Ital. J. Geosci.* **2013**, *132*, 274–289. [[CrossRef](#)]
89. Delchiaro, M.; Fioramonti, V.; Della Seta, M.; Cavinato, G.P.; Mattei, M. Fluvial inverse modelling for inferring the timing of Quaternary uplift in the Simbruini range (Central Apennines, Italy). In *Proceedings of the Geomorphometry 2020 Conference*; Alvioli, M., Marchesini, I., Melelli, L., Guth, P., Eds.; Consiglio Nazionale delle Ricerche: Rome, Italy, 2020. [[CrossRef](#)]
90. Boni, C.; Bono, P.; Calderoni, G.; Lombardi, S.; Turi, B. Indagine idrogeologica e geochemica sui rapporti tra ciclo carsico e circuito idrotermale nella Pianura Pontina. *Geol. Appl. E Idrogeol.* **1980**, *15*, 204–247.
91. Marra, F.; Bahain, J.-J.; Jicha, B.R.; Nomade, S.; Palladino, D.M.; Pereira, A.; Tolomei, C.; Voinchet, P.; Anzidei, M.; Aureli, D.; et al. Reconstruction of the MIS 5.5, 5.3 and 5.1 coastal terraces in Latium (central Italy): A re-evaluation of the sea-level history in the Mediterranean Sea during the last interglacial. *Quat. Int.* **2019**, *525*, 54–77. [[CrossRef](#)]

92. Marra, F.; Cardello, G.L.; Gaeta, M.; Jicha, B.; Montone, P.; Niespolo, E.M.; Nomade, S.; Palladino, D.M.; Pereira, A.; De Luca, G.; et al. The Volsci Volcanic Field (central Italy): An open window on continental subduction processes. *Int. J. Earth Sci.* **2021**. [[CrossRef](#)]
93. Cocozza, T.; Praturlon, A. Note geologiche sul colle Cantocchio (Lepini sud-occidentali, Lazio). *Geol. Rom* **1966**, *5*, 323–334.
94. Cosentino, D.; Cipollari, P.; Pipponzi, G. Il sistema orogenico dell'Appennino centrale: Vincoli stratigrafici e cronologia della migrazione. Evoluzione cinematica del sistema orogenico dell'Appennino centro-meridionale: Caratterizzazione stratigrafico-strutturale dei bacini sintettonici. In *Studi Geologici Camerti - Convegno-escursione COFIN '99*; Numero Speciale; Cipollari, P., Cosentino, D., Eds.; Università degli Studi di Camerino: Camerino, Italy, 2003; pp. 85–99.
95. Bown, P.R.; Young, J.R. Techniques. In *Calcareous Nannofossil Biostratigraphy*; Bown, P.R., Ed.; Springer: Dordrecht, The Netherlands, 1998; pp. 16–28.
96. Chiocchini, M.; Mancinelli, A. Microbiostratigrafia del Mesozoico in facies di piattaforma carbontica dei Monti Aurunci (Lazio Meridionale). *Studi Geol. Camerti* **1977**, *3*, 109–152.
97. Brandano, M.; Giannini, E.; Schiavinotto, F.; Varrubbi, V. Miogypsina globulina (Michelotti) from Lower Miocene Villa, S. Lucia section (M. te Cairo, Central Apennines). *Geol. Romana* **2007**, *40*, 119–127.
98. Chiocchini, M.; Pampaloni, M.L.; Pichezzi, R.M. Microfacies and microfossils of the Mesozoic carbonate successions of Latium and Abruzzi (Central Italy). In *Memorie per Servire alla Descrizione della Carta Geologica D'Italia (ISPRA) Dipartimento Difesa del Suolo*; Istituto Superiore per la Protezione e la Ricerca Ambientale: Rome, Italy, 2012; Volume 17, p. 269.
99. Martini, E. Standard Tertiary and Quaternary calcareous nannoplankton zonation, in: Proceedings of the Second Planktonic Conference, Roma 1970. *Tecnoscienza* **1971**, *2*, 739–785.
100. Okada, H.; Bukry, D. Supplementary modification and introduction of code numbers to the low-latitude coccolith biostratigraphic zonation (Bukry, 1973; 1975). *Marine Micropaleontology* **1980**, *5*, 321–325. [[CrossRef](#)]
101. Backman, J.; Raffi, I.; Rio, D.; Fornaciari, E. Biozonation and biochronology of Miocene through Pleistocene calcareous nannofossils from low and middle latitudes. *Newsl. Stratigr.* **2012**, *47*, 131–181. [[CrossRef](#)]
102. Accordi, B.; Angelucci, A.; Sirna, G. Note illustrative della Carta Geologica d'Italia alla scala 1:100.000. Foglio 159 (Frosinone) e 160 (Cassino). In *Servizio Geologico d'Italia (ISPRA), Roma*; Istituto Superiore per la Protezione e la Ricerca Ambientale: Rome, Italy, 1967.
103. Alberti, A.; Bergomi, C.; Catenacci, V.; Centamore, E.; Cestar, G.; Chiocchini, M.; Chiocchini, U.; Manganelli, V.; Molinari-Paganelli, V.; Panseril-Crescenzi, C.; et al. Note illustrative del Foglio 389 Anagni. In *Carta Geol. D'Italia 1:50.000. Serv. Geol. D'Italia (ISPRA)*; Istituto Superiore per la Protezione e la Ricerca Ambientale: Rome, Italy, 1975.
104. Ortner, H.; Retier, F.; Acs, P. Easy handling tectonic data: The programs VB for Mac and Tectonics FP for windows. *Comput. Geosci.* **2002**. [[CrossRef](#)]
105. Novarese, V. Il Miocene della Valle Latina. *Boll. Del Reg. Uff. Geol. D'Italia. Col. Roma* **1943**, *68*, 29–48.
106. Novarese, V. I terreni petroliferi della Valle Latina. *Boll. Soc. Geol. Ital.* **1923**, *42*, 347–367.
107. Carboni, S.; Lombardi, L. Su alcuni affioramenti in facies di flysch della Valle Latina. *Bol. Soc. Geol. Ital.* **1956**, *75*, 109–113.
108. Bally, A.W.; Burbi, L.; Cooper, C.; Ghelardoni, R. Balanced sections and seismic reflection profiles across the Central Apennines. *Mem. Soc. Geol. Ital.* **1986**, *35*, 257–310.
109. Cassinis, R.; Scarascia, S.; Lozej, A. The deep crustal structure of Italy and surrounding areas from seismic refraction data; a new synthesis. *Boll. Soc. Geol. Ital.* **2003**, *122*, 365–376.
110. Mirabella, F.; Barchi, M.R.; Lupattelli, A. Seismic reflection data in the Umbria Marche Region: Limits and capabilities to unravel the subsurface structure in a seismically active area. *Ann. Geophys.* **2008**, *51*. [[CrossRef](#)]
111. Chiocchini, M.; Mancinelli, A. Sivasella monolateralis Sirel and Gunduz, 1978 (Foraminiferida) in the Maastrichtian of Latium (Italy). *Rev. Micropaleontol.* **2001**, *44*, 267–277. [[CrossRef](#)]
112. Vecchio, E.; Barattolo, F.; Hottinger, L. Alveolina horizons in the Trentinara Formation (Southern Apennines, Italy): Stratigraphic and paleogeographic implication. *Riv. Ital. Paleontol. E Stratigr.* **2007**, *113*, 21–42. [[CrossRef](#)]
113. Romano, A.; Urgera, A. Geologia del Paleogene dei Monti Aurunci orientali (Lazio meridionale). *Studi Geol. Camerti* **1995**, *13*, 29–38.
114. Angelucci, A.; Devoto, G.; Farinacci, A. Le "argille caotiche" di Colle Cavallaro a est di Castro dei Volsci (Frosinone). *Geol. Romana* **1963**, *2*, 305–329.
115. Bergomi, C.; Catenacci, V.; Cestari, G.; Manfredini, M.; Manganelli, V. Note illustrative della Carta Geologica d'Italia, F° 171. In *Gaeta. Servizio Geologico d'Italia, Napoli*; Istituto Superiore per la Protezione e la Ricerca Ambientale (ISPRA): Rome, Italy, 1969.
116. Putignano, M.L.; Ungaro, A. Considerazioni sulla provenienza delle intercalazioni carbonatiche nella successione terrigena Messiniana nella Valle dell'Ausente (Appennino centro-meridionale). *Mem. Soc. Geol. Ital.* **1996**, *51*, 351–362.
117. Angelucci, A. Tectonic marks on pebbles of Middle Latina Valley (Central Italy). *Geol. Romana* **1966**, *5*, 313–322.
118. Vitale, S.; Amore, O.F.; Ciarcia, S.; Fedele, L.; Grifa, C.; Prinzi, E.P.; Tavani, S.; Tramparulo, F.D.A. Structural, stratigraphic, and petrological clues for a Cretaceous–Paleogene abortive rift in the southern Adria domain (southern Apennines, Italy). *Geol. J.* **2017**, *53*, 660–681. [[CrossRef](#)]
119. Brandano, M. Tropical/subtropical inner ramp facies in Lower Miocene «Calcari a Briozoi e Litotamni» of the Monte Lungo Area (Cassino Plain, Central Apennines, Italy). *Boll. Della Soc. Geol. Ital.* **2003**, *122*, 85–98.
120. Lombardi, L. Il pozzo Fogliano nei pressi di Latina e la paleogeografia dell'area. *Boll. Soc. Geol. Ital.* **1968**, *87*, 13–18.
121. Corda, L.; Madonna, S.; Mariotti, G. Late Cretaceous to early Miocene evolution of the Southern Prenestini Mountains (Central Apennines): From fault-block platforms to carbonate ramp. *J. Mediterr. Earth Sci.* **2020**, *12*, 15–31. [[CrossRef](#)]

122. Funiciello, R.; Giordano, G.; Capelli, G.; De Benedetti, A.; Del Monaco, F.; Mazza, R.; Tallini, M. Note illustrative del Foglio 388 Velletri. Carta Geologica 1:50.000. In *Serv. Geol. D'Italia*; Istituto Superiore per la Protezione e la Ricerca Ambientale (ISPRA): Rome, Italy, 2018.
123. Beneo, E. Dalla Valle Latina a Carpineto Romano. *Boll. Soc. Geol. Ital.* **1950**, *69*, 600–601.
124. Fagereng, Å.; Sibson, R.H. Melange rheology and seismic style. *Geology* **2010**, *38*, 751–754. [[CrossRef](#)]
125. Festa, A.; Ogata, K.; Pini, G.A.; Dilek, Y.; Alonso, J.L. Origin and significance of olistostromes in the evolution of orogenic belts: A global synthesis. *Gondwana Res.* **2016**, *39*, 180–203. [[CrossRef](#)]
126. Corrado, S.; Aldega, L.; Di Leo, P.; Giampaolo, C.; Invernizzi, C.; Mazzoli, S.; Zattin, M. Thermal maturity of the axial zone of the southern Apennines fold-and-thrust belt (Italy) from multiple organic and inorganic indicators. *Terra Nova* **2005**, *17*, 56–65. [[CrossRef](#)]
127. Carlini, M.; Artoni, A.; Aldega, L.; Balestrieri, M.L.; Corrado, S.; Vescovi, P.; Bernini, M.; Torelli, L. Exhumation and reshaping of far-travelled/allochthonous tectonic units in mountain belts. New insights for the relationships between shortening and coeval extension in the western Northern Apennines (Italy). *Tectonophysics* **2013**, *608*, 267–287. [[CrossRef](#)]
128. Catalano, R.; Valenti, V.; Albanese, C.; Accaino, F.; Sulli, A.; Tinivella, U.; Morticelli, M.G.; Zanolta, C.; Giustiniani, M. Sicily's fold-thrust belt and slab roll-back: The SI. RI. PRO. seismic crustal transect. *J. Geol. Soc.* **2013**, *170*, 451–464. [[CrossRef](#)]
129. Angelucci, A.; Bellotti, P.; Valeri, P. Analisi di facies dei sedimenti terrigeni tortoniani nella zona di Frosinone. *Geol. Romana* **1979**, *18*, 127–135.
130. Critelli, S.; Le Pera, E.; Galluzzo, F.; Milli, S.; Moscatelli, M.; Perrotta, S.; Santantonio, M. Interpreting siliciclastic-carbonate detrital modes in foreland basin systems: An example from Upper Miocene arenites of the central Apennines, Italy. *Spec. Pap. Geol. Soc. Am.* **2007**, *420*, 107. [[CrossRef](#)]
131. Casciano, C.I.; Patacci, M.; Longhitano, S.G.; Tropeano, M.; Mccaffrey, W.D.; Di Celma, C. Multi-scale analysis of a migrating submarine channel system in a tectonically-confined basin: The Miocene Gorgoglione Flysch Formation, southern Italy. *Sedimentology* **2019**, *66*, 205–240. [[CrossRef](#)]
132. Cipollari, P.; Cosentino, D.; Pipponzi, G. Il sistema orogenico dell'Appennino centrale: Vincoli stratigrafici e cronologia della migrazione. *Studi Geol. Camerti* **2003**, 87–101. [[CrossRef](#)]
133. Smeraglia, L.; Aldega, L.; Bernasconi, S.M.; Billi, A.; Boschi, C.; Caracausi, A.; Carminati, E.; Franchini, S.; Rizzo, A.L.; Rossetti, F.; et al. The role of trapped fluids during the development and deformation of a carbonate/shale intra-wedge tectonic mélange (Mt. Massico, Southern Apennines, Italy). *J. Struct. Geol.* **2020**, *138*. [[CrossRef](#)]
134. Artoni, A.; Bernini, M.; Papani, G.; Rizzini, F.; Barbacini, G.; Rossi, M.; Rogledi, S.; Ghielmi, M. Mass-transport deposits in confined wedge-top basins: Surficial processes shaping the messinian orogenic wedge of Northern Apennine of Italy. *Ital. J. Geosci.* **2010**, *129*, 101–118. [[CrossRef](#)]
135. Butler, R.W.H. Thrust sequences. *J. Geol. Soc.* **1987**, *144*, 619–634. [[CrossRef](#)]
136. Doglioni, C.; Harabaglia, P.; Merlini, S.; Mongelli, F.; Peccerillo, A.T.; Piromallo, C. Orogens and slabs vs. their direction of subduction. *Earth-Sci. Rev.* **1999**, *45*, 167–208. [[CrossRef](#)]
137. Roveri, M.; Bassetti, M.A.; Lucchi, F.R. The Mediterranean Messinian salinity crisis: An Apennine foredeep perspective. *Sediment. Geol.* **2001**, *140*, 201–214. [[CrossRef](#)]
138. Jolivet, L.; Augier, R.; Robin, C.; Suc, J.P.; Rouchy, J.M. Lithospheric-scale geodynamic context of the Messinian salinity crisis. *Sediment. Geol.* **2006**, *188*, 9–33. [[CrossRef](#)]
139. Roveri, M.; Flecker, R.; Krijgsman, W.; Lofi, J.; Lugli, S.; Manzi, V.; Sierro, F.J.; Bertini, A.; Camerlenghi, A.; De Lange, G.; et al. The Messinian salinity crisis: Past and future of a great challenge for marine sciences. *Mar. Geol.* **2014**, *349*, 113–125. [[CrossRef](#)]
140. Andreotto, F.; Aloisi, G.; Raad, F.; Heida, H.; Flecker, R.; Agiadi, K.; Lofi, J.; Blondel, S.; Bulian, F.; Camerlenghi, A.; et al. Freshening of the Mediterranean Salt Giant: Controversies and certainties around the terminal (Upper Gypsum and Lago-Mare) phases of the Messinian Salinity Crisis. *Earth-Sci. Rev.* **2021**, *216*, 103577. [[CrossRef](#)]
141. Tavarnelli, E. The effects of pre-existing normal faults on thrust ramp development: An example from the northern Apennines, Italy. *Geol. Rundsch.* **1996**, *85*, 363–371. [[CrossRef](#)]
142. Patacca, E.; Scandone, P.; Di Luzio, E.; Cavinato, G.P.; Parotto, M. Structural architecture of the central Apennines: Interpretation of the CROP 11 seismic profile from the Adriatic coast to the orographic divide. *Tectonics* **2008**, *27*. [[CrossRef](#)]
143. Scisciani, V. Styles of positive inversion tectonics in the Central Apennines and in the Adriatic foreland: Implications for the evolution of the Apennine chain (Italy). *J. Struct. Geol.* **2009**, *31*, 1276–1294. [[CrossRef](#)]
144. Turienzo, M.; Sánchez, N.; Dimieri, L.; Lebinson, F.; Araujo, V. Tectonic repetitions of the Early Cretaceous Agrio Formation in the Chos Malal fold-and-thrust belt, Neuquén basin, Argentina: Geometry, kinematics and structural implications for Andean building. *J. South Am. Earth Sci.* **2014**, *53*, 1–19. [[CrossRef](#)]
145. Schori, M.; Mosar, J.; Schreurs, G. Multiple detachments during thin-skinned deformation of the Swiss Central Jura: A kinematic model across the Chasseral. *Swiss J. Geosci.* **2015**, *108*, 327–343. [[CrossRef](#)]
146. Milia, A.; Torrente, M.M. Tectono-stratigraphic signature of a rapid multistage subsiding rift basin in the Tyrrhenian-Apennine hinge zone (Italy): A possible interaction of upper plate with subducting slab. *J. Geodyn.* **2015**, *86*, 42–60. [[CrossRef](#)]
147. Farinacci, A. Breccias and laminated dolomites of the Gavignano exposure. *Geol. Romana* **1965**, *4*, 129–144.
148. Civitelli, G.; Funiciello, R.; Lombardi, S. Alcune considerazioni sulla genesi della «Pietra Paesina». *Geol. Romana* **1970**, *9*, 195–204.

-
149. Angrisani, A.C.; Calcaterra, D.; Cappelletti, P.; Colella, A.; Parente, M.; Prikryl, R.; de'Gennaro, M. Geological features, technological characterization and weathering phenomena of the Miocene Bryozoan and Lithothamnion limestones (central-southern Italy). *Ital. J. Geosci.* **2011**, *130*, 75–92.
 150. Cipollari, P.; Cosentino, D. Considerazioni sulla strutturazione della Catena dei Monti Aurunci: Vincoli stratigrafici. *Studi Geol. Camerti* **1991**, *2*, 151–156.